博 士 学 位 論 文

Doctoral Dissertation

Numerical modelling of groundwater pollution under

remediation processes at an illegal waste dumping site

(廃棄物不法投棄サイトでの修復過程における地下水汚染

の数値モデリング）

東北大学大学院環境科学研究科
Graduate School of Environmental Studies, Tohoku University

先進社会環境学専攻

専攻 major／
コース course

学籍番号 Student ID No.	C0GD1508
氏　名 Name	Thatthep Pongritsakda

指　導　教　員 Supervisor at Tohoku Univ.	Prof. Noriaki Watanabe	
研　究　指　導　教　員 Research Advisor at Tohoku Univ.	Assist. Prof. Jiajie Wang	
審　査　委　員 (○印は主査) Dissertation Committee Members Name marked with "○" is the Chief Examiner	○　Prof. Noriaki Watanabe	
	1　Prof. Chihiro Inoue	2　Visiting Prof. Takeshi Komai
	3　Assist. Prof. Jiajie Wang	4
	5	6

Table of Contents

Chapter 1 Introduction

1.1 Illegal waste dumping sites

Rapid urbanization has given rise to numerous environmental challenges, one of which is the escalating problem of illegal dumping. This issue has increasingly serious implications for the livability and sustainability of our communities, particularly in developing countries (Niyobuhungiro et al., 2021; Otwong et al., 2021; da Pez et al., 2020; Vrigheid et al., 2017). Additionally, uncontrolled disposal, mismanagement, and some negative legislative and political are the problems that accelerate the occurring of illegal waste dumping sites (Ferronato et al., 2017 and 2019; Velis and Cook, 2019).

In contemporary times, the issue of illegal waste dumping sites remains a significant concern, prompting investigations into the associated risks to human health and the environment. For instance, Bangani et al. (2023) examined the impact of illegal waste dumping on river water quality in a region of South Africa. In Israel, the focus has been on the illegal dumping of construction and demolition waste, with efforts aimed at evaluating the effectiveness of environmental laws and enforcement policies in tackling this problem (Seror and Portnov, 2020). Likewise, in Poland, researchers have conducted studies to comprehend the transport behavior of contaminants originating from illegal waste dumping sites situated in natural protected areas (Jakiel et al., 2019). These cases underscore the global nature of this issue and the continuous endeavors made to address the challenges presented by illegal waste dumping.

Illegal dumping sites often harbor multiple, unidentified sources of contamination, in addition the subsurface geology remains uncertain (Allen et al., 2001; Ritter et al., 2002). This complexity adds to the challenge of understanding the spreading behaviors of contaminants in groundwater. Various approaches have been employed to predict the transport of pollutants in groundwater from illegal dumpsites. These approaches include monitoring the dumpsites, identifying scavenger accumulations on the land, and utilizing aerial photography (Navarro et al., 2016; Đidelija et al., 2022; Karimi et al., 2022). However, owing to the intricate nature of illegal dumping sites, relying solely on monitoring techniques is insufficient for assessing the spatial spread of contamination and predicting future contamination.

1.2 Numerical modeling and its challenges

Simulation based on numerical modeling offers a potentially effective method for interpreting and predicting the behavior of contamination. Through simulations based on numerical modeling, it becomes possible to better understand how contaminants disperse in groundwater within illegal dumping sites (Hem

et al., 2013; Banejad et al., 2014). This approach enables a more comprehensive evaluation of the contamination's spatial extent and the sufficient prediction results for potential future contamination.

Recently, some studies reported that numerical modeling, based on monitoring data of piezometric head and contaminant concentrations, can help identify contamination sources and determine the distribution of hydraulic conductivity (Xu et al., 2021; Xing et al., 2021). Furthermore, the research conducted by Shen et al. (2023) utilized numerical modeling in conjunction with laboratory experiment results to investigate the transport behavior of pollutants. In addition, Saadatpour et al. (2023) conducted studies specifically focused on assessing the efficiency of remediation methods on groundwater pollutants using numerical modeling. Hem et al. (2013) proposed a numerical modeling process for predicting the distribution of 1,4-dioxane in an illegal waste dumping site, with validation of the groundwater flow. They suggested that numerical modeling provides more precise contaminant prediction compared to conventional monitoring approaches.

However, there are also challenges in applying numerical modeling to pollutant transport in illegal dumping sites. To prevent the spread of contaminants beyond illegal dumping sites, a range of remediation measures are being implemented. These measures include the construction of impermeable walls, groundwater pumping, chemical oxidation techniques, activated carbon techniques, and bioremediation (U.S. EPA 2006 and 2018). Moreover, the effectiveness of these costly remediation measures has been questioned owing to a lack of sufficient knowledge of the spreading behaviors of contaminants (O'Connor et al., 2019; Smith et al., 2021). For example, the pumping process has been found to significantly impact the distribution of hydraulic gradients, potentially promoting the spread of contaminants (Atlabachew et al., 2018). This suggests that the pumping process may inadvertently exacerbate the flow of contaminants, raising concerns about its effectiveness. To address these uncertainties and improve the planning of remediation measures, it is crucial to develop an efficient modeling procedure for predicting the spread of contamination. Such a modeling procedure would provide valuable insights into the behavior of contaminants, allowing for more effective and targeted remediation strategies.

Another challenge lies in the disparities between the conditions assumed for modeling and the actual situation encountered in previous modeling processes. While earlier studies typically employed single constant source conditions (Hem et al., 2013) for modeling, the reality is that sources are unknown, multiple and dynamic. The behavior of contaminant dispersion can vary based on the conditions of these sources and the remediation measures being implemented. Furthermore, the impact of remediation on the groundwater flow field remains uncertain and necessitates clarification prior to conducting an accurate prediction process.

However, it should be noted that although recent research has made advancements in addressing multiple source conditions through reverse calculation using a geostatistical approach (Takai et al., 2022),

and others have conducted numerical modeling studies considering multiple sources and the effects of remediation (Shao et al., 2022), both studies assume known source locations. This assumption fails to accurately reflect the complex reality of unknown and multiple source conditions typically encountered in illegal waste dumping sites. Therefore, this study aims to develop a modeling process that accounts for the unknown multiple and non-stationary nature of contamination sources and the dynamic hydraulic gradients arising from remediation activities in illegal landfills.

1.3 Ideal modeling process proposal

To gain a comprehensive understanding of the transport behavior of groundwater pollutants in an illegal waste dumping site, an ideal approach was proposed, as depicted in Figure 1-1. In the proposed modeling process, the hydrogeological conditions were simplified to a homogeneous aquifer condition. The assumption of a homogeneous aquifer condition allows for easier modeling and a better understanding of the actual transport behavior of groundwater pollutants. It enables the development of a conceptual model that can be easily implemented in numerical simulations and provides insights into the general behavior of pollutants within the site. While the homogeneous aquifer assumption simplifies the modeling process, it is important to note that in reality, illegal waste dumping sites often exhibit complex hydrogeological conditions, with a heterogeneity and non-uniformity in aquifer properties. To account for the complexities of non-stationary and multiple pollution sources in illegal waste dumping sites, additional considerations and refinements will be made in future studies. These may include incorporating more detailed site-specific data, such as hydrogeological properties, source characteristics, and temporal variations, to improve the accuracy of the modeling results.
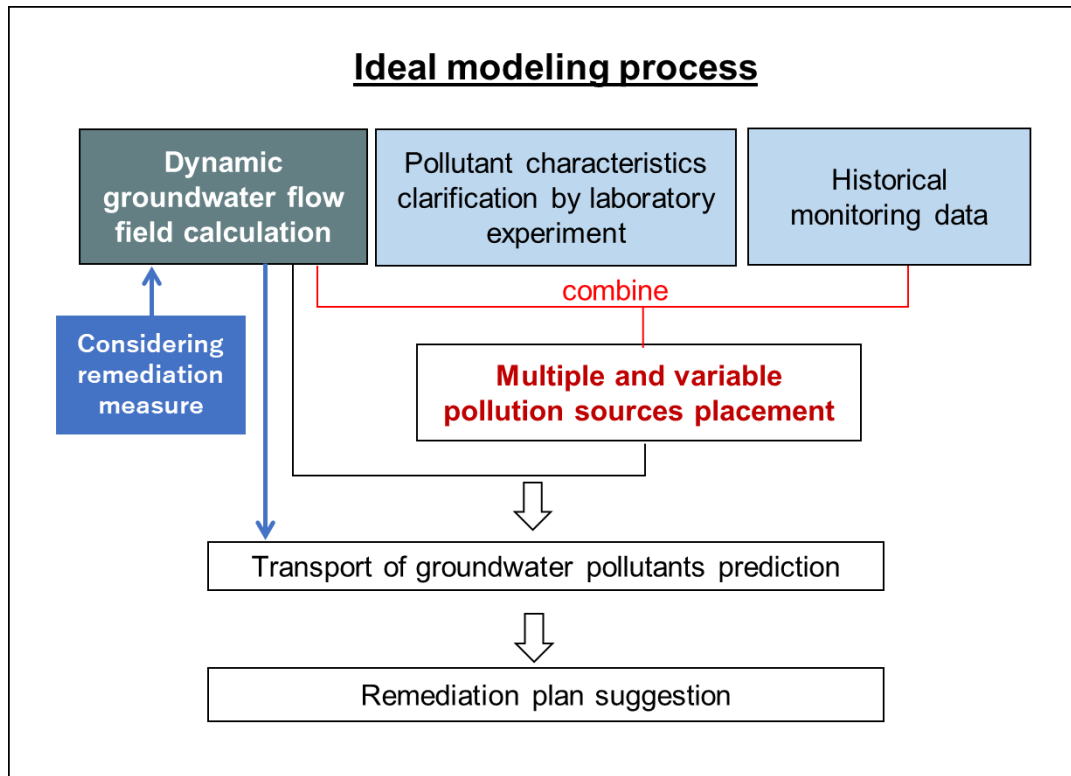
Ideal modeling process

| Dynamic groundwater flow field calculation | Pollutant characteristics clarification by laboratory experiment | Historical monitoring data |

Considering remediation measure

combine

Multiple and variable pollution sources placement

Transport of groundwater pollutants prediction

Remediation plan suggestion

Figure 1-1 Flowchart of ideal modeling process for pollution prediction in an illegal waste dumping site

The modeling process incorporates three crucial components: (1) calculation of the dynamic groundwater flow field, (2) elucidation of pollutant characteristics through laboratory experiments, and (3) analysis of historical monitoring data. The objective of this ideal modeling process is to refine the numerical model by utilizing reliable parameters to establish an effective model capable of examining the multiple and variable pollution sources found in illegal waste dumping sites. Although this approach provides valuable insights into pollutant characteristics and historical data, the effects of remediation in complex hydrogeological conditions remain unknown and may lead to unforeseen outcomes in the transport behavior of groundwater pollutants in such sites.

1.4 Objectives and Thesis Structure

This study aims to establish an effective numerical modeling process for groundwater pollution prediction and remediation plan making, by considering multiple non-stationary pollution sources and the impacts of remediation measures under dynamic environmental conditions. A representative illegal dumping site located in Iwate and Aomori prefectures in Japan was used to develop the modeling process. The site has been subject to severe pollution by volatile organic compounds (VOCs) and chlorinated solvents since 1991 (as reported in Iguro et al., 2012). Of particular concern is the presence of 1,4-dioxane,

which was included in Japan's environmental standards list of pollutants in 2009 with a limit concentration of 0.05 mg/L. Since then, higher concentrations of 1,4-dioxane have been detected in the groundwater across a wide area within the site. The significant spreading of 1,4-dioxane is attributed to its characteristics, including high solubility, low adsorption in soil particles, and strong resistance to spontaneous biodegradation (U.S. EPA 2017; Otto et al., 2007). Similar to other VOCs, 1,4-dioxane is believed to have multiple sources of contamination within the site, as indicated by monitoring data.

Chapter 2 focuses on the setup of the initial and boundary conditions for a numerical modeling approach that incorporates the effects of remediation measures on the groundwater flow field. These measures, namely pumping operations and the installation of impermeable walls, are analyzed to determine their influence on the groundwater flow field and transport behavior of pollutants within the illegal waste dumping site. The historical remediation measures are examined to clarify their specific impacts on the groundwater flow field and transport behaviors.

In Chapter 3, the established numerical modeling approach is utilized for the simulation of 1,4-dioxane concentration levels in each monitoring well. This process takes into account multiple and non-stationary pollution source conditions. The location of each pollution source is considered based on the groundwater flow field established in Chapter 2, and the reproduction results are verified using historical monitoring data. In this chapter, we reproduce the distribution of 1,4-dioxane groundwater pollutant throughout the entire area of the illegal waste dumping site.

In the final chapter, the successfully predicted results obtained in Chapter 3 are used to evaluate the existing remediation measures. While the evaluation results indicate that the previous remediation measures were effective in addressing the pollution situation in the illegal waste dumping site, there is a belief that certain aspects of the remediation measures can be improved, including both pumping operation and overall remediation strategies. The author thus proposed improved pumping plans using the modeling developed.

Part of the research results has been published in (Pongritsakda et al., 2021; Pongritsakda et al., 2022), which will be used in Chapters 2, 3 and 4.

Chapter 2 Groundwater flow field calculation for model setup

2.1 Target illegal waste dumping site

The target illegal dumping site in this study (Figure 2-1) is located on a gently undulating plateau about 450 m above sea level between Aomori prefecture and Iwate prefecture, Japan. In 1991, industrial waste composting business was started by a company at the site. However, owing to foul odors and sewage runoff detected in 1999, this site was found to be an illegal dumping site. The dumping site covers a total area of 27 ha, with 11 ha on the Aomori side and 16 ha on the Iwate side. The illegally dumped wastes mainly consisted of cinders, sludge, waste oil, and refuse-derived fuel (RDF), and the total amount was estimated to be more than 1 million m^3 (270,000 m^3 on the Iwate side and 790,000 m^3 on the Aomori side). Especially on the Iwate side, the soil and groundwater are contaminated in large parts by barrels of used oil. Both prefectures started restoration and remediation measures since 1999.
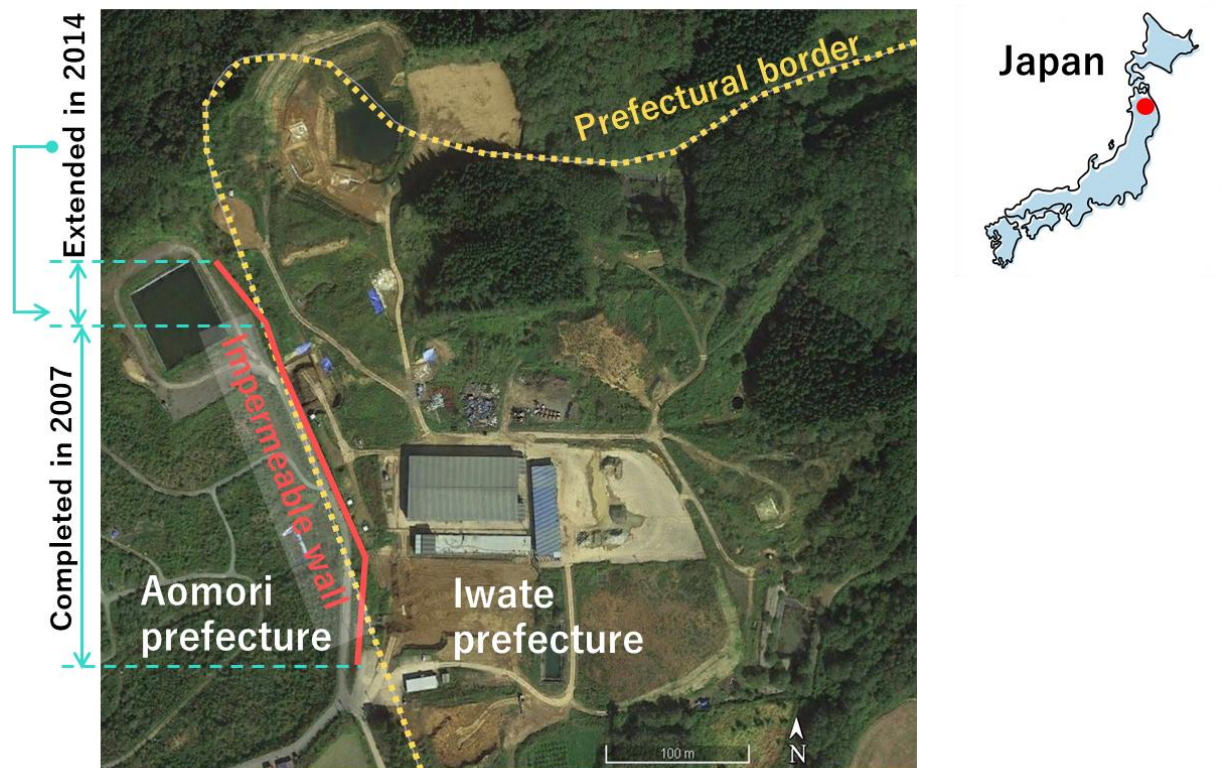

Figure 2-1 Topography map of illegal waste dumping site, Iwate prefecture, Japan

The history of remediation measures at the Iwate prefecture site is shown in Table 2-1. Following the start of the removal of waste in 2001, groundwater levels were measured to understand the groundwater

flow direction distribution at the site. The location of the groundwater table was confirmed to be at a depth of approximately 7–8 m below the ground surface, and the thickness of the aquifer was up to a dozen meters. On the Iwate prefecture site, the highest elevation is on the northwest side, about 460 m, and gradually decreases toward the southwest, southeast, and northwest sides, with a difference of about 40 m within site, as shown in Figure 2-2, groundwater thus correspondingly flows toward the same directions. To prevent the contamination from spreading to Aomori Prefecture, an impermeable wall was built on the prefectural border in March 2007 and pumping of water from four wells near the wall began in September 2007.

Table 2-1. History of remediation measures at the illegal dumping site.

| Year. Month	Event
1990.01	Start of industrial waste composting business
1999	Detection of foul odors and sewage runoff and discovery of illegal dumping
2001	Start of removal of waste
2001-2002	Survey of groundwater level for whole area for understanding of the distribution of groundwater flow direction
2004-2013	Start of removal of waste (Aomori prefecture)
2005.06	Operation of wastewater treatment facility (Aomori prefecture)
2006.09	Installation of impermeable wall at the site boundary on Aomori prefectural side (Aomori prefecture)
2007.03	Installation of impermeable wall at the prefectural boundary
2007.09	Operation of wastewater treatment facility
	Start of pumping water as a remediation measure at four wells near the impermeable wall
2009.07-2009.12	Treatment of pumping aeration in N area
2009	Add of 1,4-dioxane to a new environmental criteria item
2010	Survey of 1,4-dioxane contamination
2013.04	Start of remediation measure for 1,4-dioxane contamination by pumping groundwater in the entire site
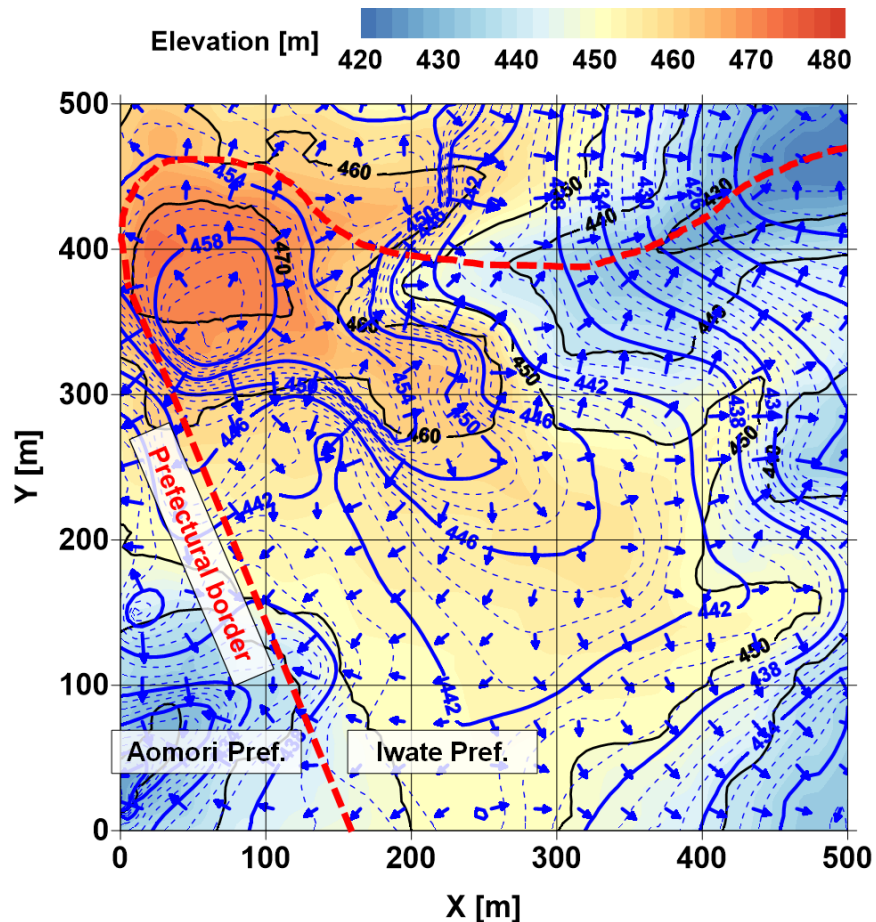
Figure 2-2 Elevation contour of dumping site and potential groundwater flow; red dashed line shows the boundary between two prefectures, black line show the elevation contour, blue line show the reproduced groundwater distribution based on the survey from 2001 to 2002.

Figure 2-3 shows the areas where VOC concentrations exceeded soil and groundwater standards in July 2010, as well as the areas where remedial action had been taken by November 2012. We can see that surface contamination from waste dumping had occurred in several places on the site. Since 2001, the Iwate site has been divided into 16 remediation areas where waste and contaminated soils are being removed, bioremediated, and groundwater pumped out. In particular, in the N area, where VOCs contamination was confirmed to be several dozen times higher than the environmental standard, groundwater pumping and aeration treatment was conducted from July to December 2009, prior to being done in other areas, with a total of 29,124 m^3 of water pumped out. Waste removal was completed in March 2014 and it is believed that the inflow of contaminants from the surface soil into the aquifer has largely slowed since then. In 2009, as soon as 1,4-dioxane was included as a new environmental criterion, an investigation of 1,4-dioxane

contamination was carried out at the site. The results show that 1,4-dioxane concentrations in groundwater exceeded the standard (0.05 mg/L) by a wide margin. In April 2013, remediation measures were started by pumping out water in the entire area.
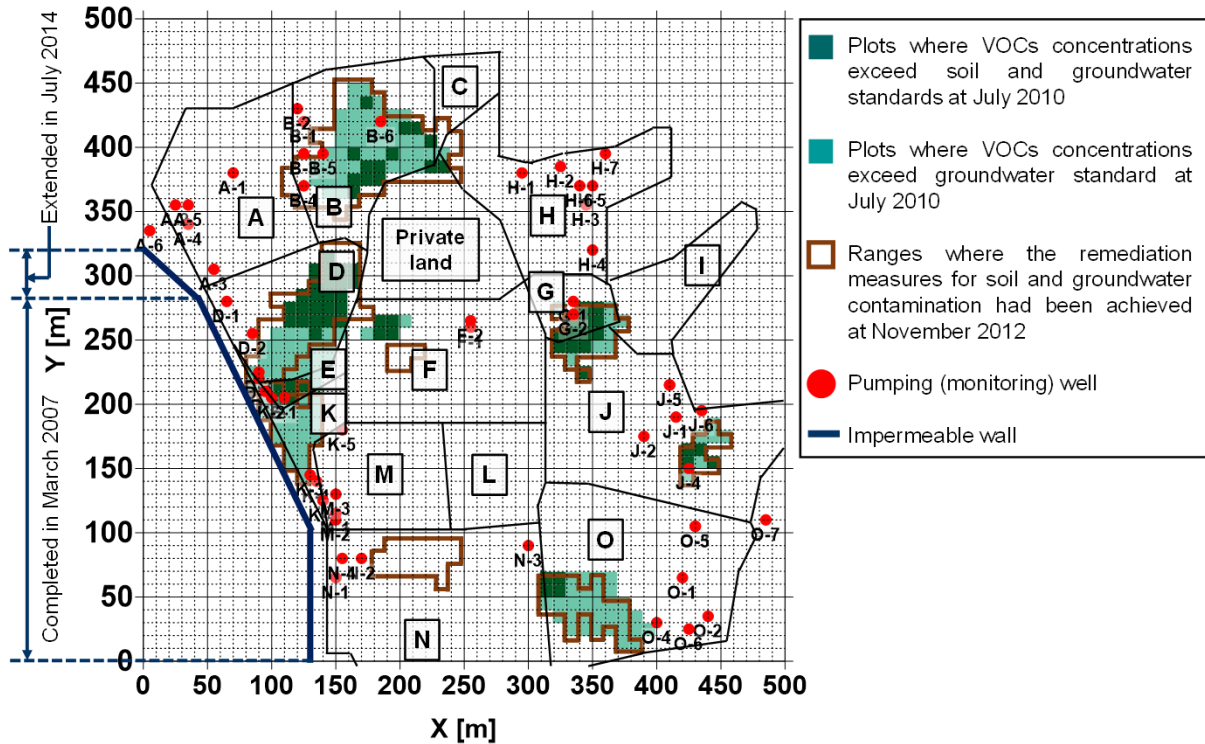

Figure 2-3 Areas where VOCs concentrations exceeded soil and groundwater standards in July 2010 and the areas where remediation measures were implemented until November 2012.

The distribution of 1,4-dioxane concentrations in groundwater at the site in April 2013 and April 2021 are compared in Figure 2-4. Similar to other volatile organic compounds, 1,4-dioxane is assumed to have multiple sources of contamination at the site. From 2013 to 2021, a significant spread from Area B to the area along the impermeable wall was observed. This distribution might have resulted from the preventing of contamination from spreading owing to changes in groundwater flow direction due to the installing of the impermeable wall and pumping operation. At the western boundary of area A and between areas A and B, a high concentration of 1,4-dioxane was observed in 2013. Intensive remediation measures were therefore taken, including the removal of contaminated soil and the installation of water collection ponds. In July 2014, the impermeable wall was extended to prevent further spread of contamination to the Aomori Prefecture side. Remediation work at the site was extended until 2022, because 1,4-dioxane levels in some areas still exceeded the standard by 2021.
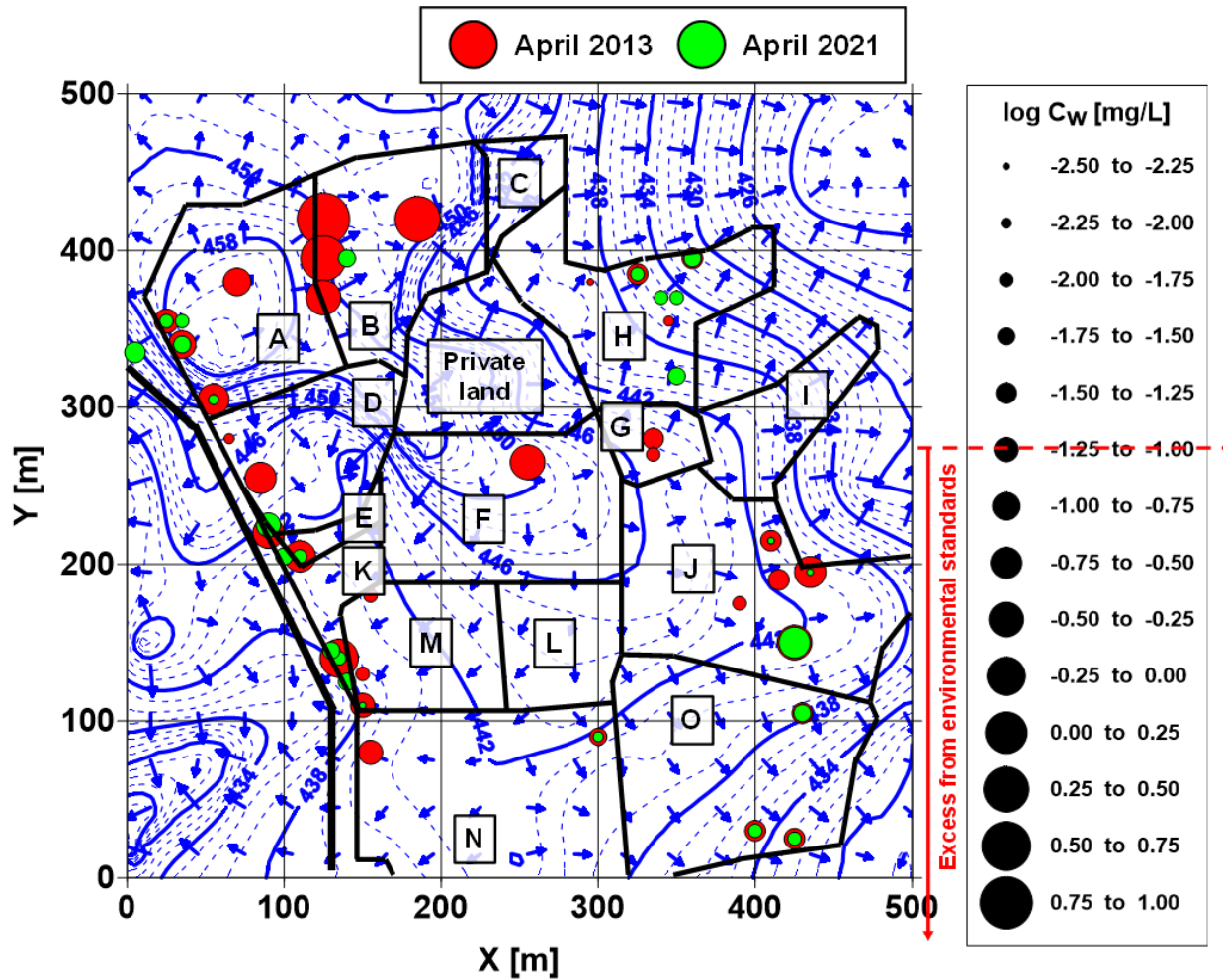
Figure 2-4 Comparison between concentration level of 1,4-dioxane in each pumping well in April 2013 and 2021.

This chapter focuses on the setup of the initial and boundary conditions for a numerical modeling approach that incorporates the effects of remediation measures on the groundwater flow field. These measures, namely pumping operations and the installation of impermeable walls, are analyzed to determine their influence on the groundwater flow field and transport behavior of pollutants within the illegal waste dumping site. The impacts of historical remediation measures on the groundwater flow field and transport behaviors are clarified.

2.2 Methodology

2.2.1 Set initial conditions and governing equation

A single-cell aquifer model with saturated condition using the implicit pressure, explicit saturation (IMPES) simulation method was applied. According to a survey of the geological structure of the illegal waste dumping site, as shown in Figure 2-5, sandy loam is assumed as the major soil type of aquifer.

1,4-dioxane is selected as the representative pollutant in the model. The reasons are as follows: 1) 1,4-dioxane falls within the criteria of environmental pollutants of concern, 2) historical monitoring data are available for this substance in the target area, 3) previous remediation measures have specifically aimed at eliminating this pollutant from the site, thereby providing valuable information for analysis.

1-3) waste and cover soil
4) Pyroclastic deposit
5-8) pyroclastic flow deposit corresponding to aquifer
9) Tuff breccia corresponding to impermeable layer
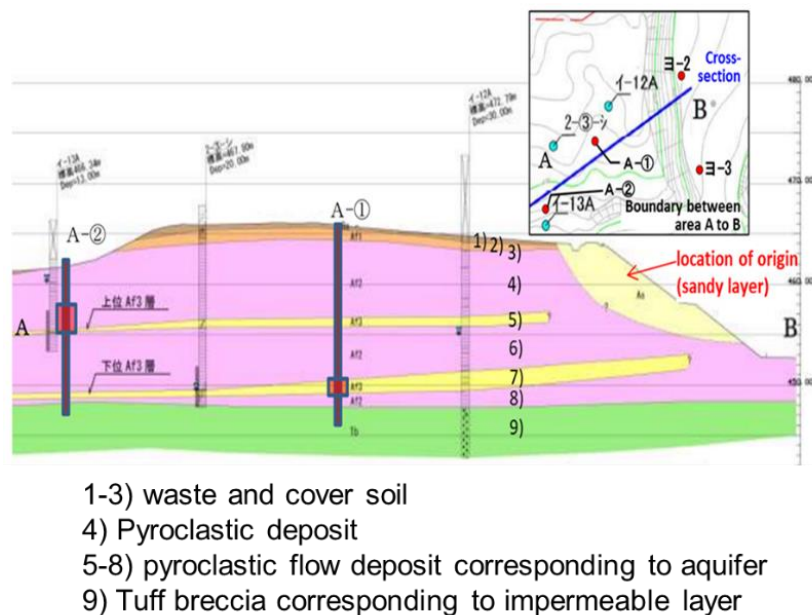
Figure 2-5 geological structure of illegal waste dumping site

Based on the site remedial actions described in Section 2.1, the development of a numerical model is proposed to predict future contamination and quantify the effects of building impermeable walls and pumping operations. It should be noted that, although considering the migration of 1,4-dioxane from the unsaturated layer (surface soil) to the aquifer can improve the modeling accuracy, the various remediation measures conducted in this area had changed the soil conditions and made modeling of the unsaturated layer difficult. Therefore, only migration within the aquifer is considered in the development of the model. It is assumed that 1,4-dioxane contamination and dispersion in the aquifer 1) began after January 1991, when

the company (mentioned in subsection 2.1) began operations, and 2) inflow was generally terminated by the removal of waste and contaminated soil. Based on the situation of surface contamination and actual results of remediation, a certain amount of 1,4-dioxane flowing into the aquifer was defined as a boundary condition, and numerical simulations were performed for the horizontal two-dimensional x-y aquifer. In addition, the biodegradability of 1,4-dioxane in the environment is not considered in this study because it was reported to be very low (U.S. EPA 2017; Otto et al., 2007).

As mentioned earlier, only the liquid phase, consisting of water and 1,4-dioxane, is considered in the mass balance modeling in this study. Although 1,4-dioxane is highly miscible with water, its undiluted solution can also be considered as non-aqueous phase liquid (NAPL). The coupled analysis for advection and dispersion of 1,4-dioxane dissolved in the water phase and its adsorption on soil particles in the NAPL-water two-phase system can be used to predict the spatiotemporal distribution of 1,4-dioxane in the aquifer. The flux of each phase generally follows the Darcy's law. The equations for mass conservation in the numerical model consist of two phases (NAPL and water), a 1,4-dioxane component in the NAPL phase, and two components, 1,4-dioxane and water, in the water phase, and are given as follows.

NAPL phase:

$$\nabla \cdot \left(\alpha \frac{K k_{rn}}{\mu_n} \rho_n \nabla \Phi_n \right) = \frac{\partial (\phi \rho_n S_n)}{\partial t}$$

(2-1)

Water phase：

$$\nabla \cdot \left(\alpha \frac{K k_{rw}}{\mu_w} \rho_w \nabla \Phi_w \right) + \alpha \left(q_{wi} - q_{wp} \right) = \frac{\partial (\phi \rho_w S_w)}{\partial t}$$

(2-2)

Components in the NAPL phase (k=1)：

$$\nabla \cdot \left(\alpha y_{n,1} \frac{K k_{rn}}{\mu_n} \rho_n \nabla \Phi_n \right) = \frac{\partial (y_{n,1} \phi \rho_n S_n)}{\partial t}$$

(2-3)

Components in the water phase (k=1 ~ 2)：

$$\nabla \cdot \left(\alpha x_{w,k} \frac{K k_{rw}}{\mu_w} \rho_w \nabla \Phi_w \right) + \nabla \cdot \left[\alpha D_{w,k} \nabla \left(x_{w,k} \phi \rho_w S_w \right) \right]$$

$$+ \alpha \left(-R_{A,k} \right) + \alpha \left(q_{nwi,k} - x_{w,k} q_{wp} \right) = \frac{\partial (x_{w,k} \phi \rho_w S_w)}{\partial t}$$

(2-4)

where $\boldsymbol{\alpha}$: dimensional constant, $\boldsymbol{K}$: absolute permeability [m^2], $\boldsymbol{k_{rn}}$: relative permeability to the NAPL phase [-], $\boldsymbol{k_{rw}}$: relative permeability to the water phase [-], $\boldsymbol{\mu_n}$: viscosity of the NAPL phase[Pa·s], $\boldsymbol{\mu_w}$:

viscosity of the water phase [Pa·s], ρ_n: molar density of the NAPL phase [kmol/m³], ρ_w: molar density of the water phase [kmol/m³], Φ_n: flow potential of the NAPL phase [Pa], Φ_w: flow potential of water phase [Pa], q_{wi}: water inflow rate [kmol/m³/sec], q_{wp}: water outflow rate [kmol/m³/sec], S_n : NAPL saturation [-], S_w: water saturation [-], ϕ : porosity [-], $y_{n,k}$: mole fraction of component k in water phase [-], $x_{w,k}$:: mole fraction component k in water phase [-], $R_{A,k}$: attenuation rate of component k [kmol/m3/sec], $q_{nwi,k}$: inflow rate of component k [kmol/m³/sec], $D_{w,k}$: dispersion coefficient of the component k in the water phase [m²/s]; t : time [sec].

The equation for the saturation, which represents the volume fraction of fluid in the pore space, is as follows :

$$S_n + S_w = 1 \tag{2-5}$$

On the other hand, the subscripts in Equation (2-3) represent the component numbers corresponding to =1: 1,4-dioxane and =2: water, respectively. The sum of the mole fractions of each phase is always 1, because the NAPL phase is a 1,4-dioxane-only one-component system.

$$y_{n,1} = 1 \tag{2-6}$$

Because the water phase consists of two components, dissolved 1,4-dioxane, and water, the sum of the two is expressed by the following equation

$$x_{w,1} + x_{w,2} = 1 \tag{2-7}$$

In this model, the pressure P_n at the flow potential of the NAPL phase Φ_n ($\nabla\Phi_n = \nabla P_n - M_n \rho_n g$) is treated as the system pressure P, considering the effect of capillary pressure on the water phase. Hence, there are four basic variables: pressure (P), S_w (or S_n), $x_{w,1}$ and $y_{n,1}$. To solve the numerical model, we first, discretize each mass conservation equation using the finite difference method, and then apply the IMPES method to calculate P, S_w, $x_{w,1}$ and $y_{n,1}$ at each position. Next, assuming that the time steps in the flow calculation are long enough to reach equilibrium for elution and adsorption among the NAPL phase, water phase, and soil particles, and that equilibrium is established instantaneously, the mole fraction and the amount of adsorption $x_{s,1}$ are updated within the same time step. As a result, the mass balance equation does not include a term for adsorption. For the formulation of various parameters, such as relative permeability, see the separate paper by the authors (Pongritsakda et al., 2021).

2.2.2. Treatment of Elution and Adsorption in a Numerical Model

13

Soil particle adsorption is an important process that affects the spatial and temporal distribution of contaminants in soil and groundwater. To understand the effects of soil adsorption and incorporate it into numerical modeling, the authors conducted soil adsorption experiments with a solution of 1,4-dioxane, varying concentrations over several stages and five types of soils (black-box soil, Kanto loam, sandy soil, Kanuma soil, and red ball soil) (Nakamura et al., 2018).

The relationship between the equilibrium concentration in the water phase and the amount of adsorption is shown in Figure 2-6. A similar trend was observed for all soil types, with the amounts of adsorption approximately 0.2, 1.2, and 2.5 mg/kg for equilibrium concentrations of 0.1, 1.0 mg/L, and 10 mg/L, respectively. These results suggest that 1,4-dioxane adsorption by soil follows the Langmuir adsorption model, adsorption coefficient (equilibrium constant ratio) $K_{d,1}$ [m^3/kg] and saturated adsorption $x_{s,sat,1}$ [kmol/kg] were obtained as 7.88×10^4 m^3/kg and 3.21×10^{-8} kmol/kg (=2.83 mg/kg), respectively. The calculation is shown in Eq. (2-8), where $x_{w,1}$ is the mole fraction of 1,4-dioxane in the water phase and $x_{s,1}$ is the amount of adsorption on the soil particles [kmol/kg].

$$x_{s,1} = \frac{K_{d,1} x_{s,sat,1} \rho_w x_{w,1}}{1 + K_{d,1} \rho_w x_{w,1}}$$

(2-8)

Although the adsorption of 1,4-dioxane to soil is generally described as extremely low (Inoue et al., 2016; Pugazhendi et al., 2015), our experimental results indicate that it is still estimated to be many times higher than the number of moles dissolved in the water phase that is transformed.
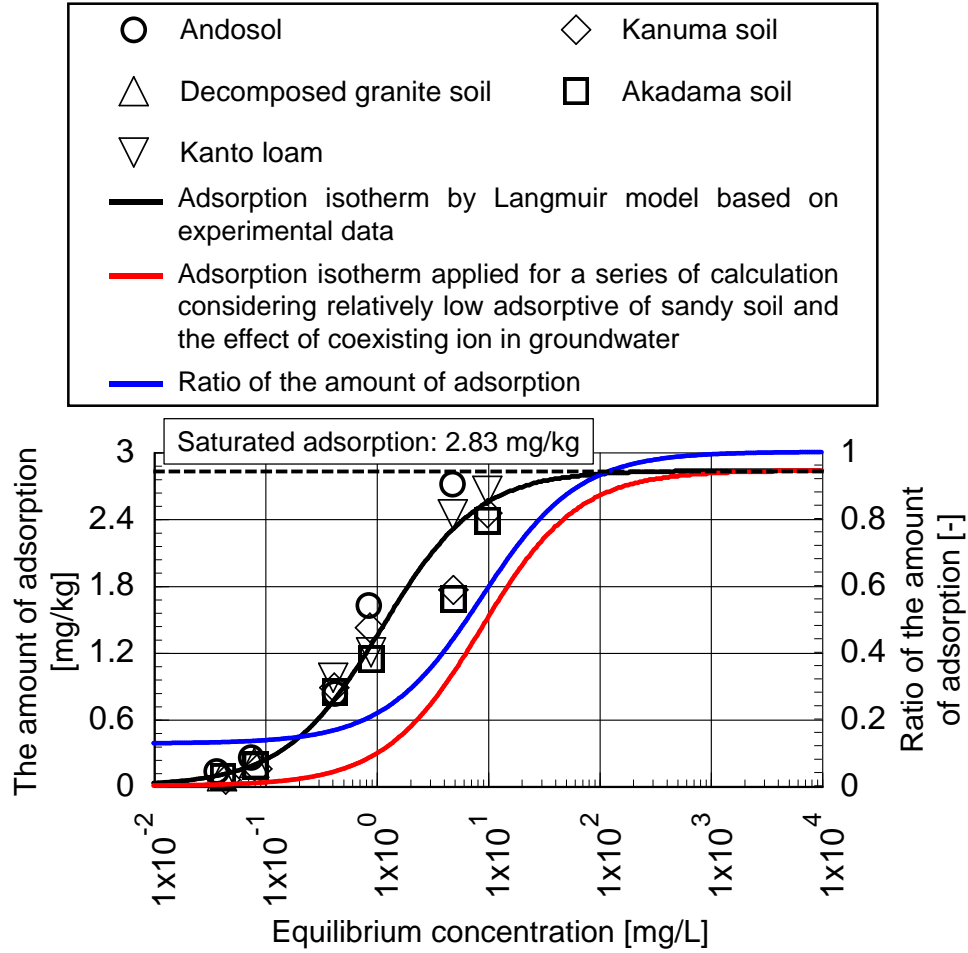
Figure 2-6. The relationship between the equilibrium concentration in the water phase and the amount of adsorption.

However, it can be assumed that the actual adsorption of 1,4-dioxane at this site is relatively low because the main soil type in the aquifer is sandy soil, which has low organic content and a relatively small specific surface area [Hartmann and Lesturgez 2005; Huang et al., 2020]. In addition, the coexisting ionic components and solutes in groundwater may also affect the adsorption of 1,4-dioxane. Therefore, in this study, the adsorption isotherm shown by the red line in Figure 2-6 was applied with the assumption of a theoretical value of 1.00×10^4 m^3/kg for $K_{d,1}$ instead of 7.88×10^4 m^3/kg. Correspondingly, the adsorption ratios to the original isotherm are estimated to be approximately 0.14, 0.22, and 0.59 for equilibrium concentrations of 0.1, 1, 10 mg/L, respectively (blue lines in Figure 2-6). The validity of the assumption will be verified in the results and discussion part.

As mentioned above, the mole fractions of 1,4-dioxane ($x_{w,1}$, $y_{n,1}$) in the NAPL and water phases at each location will first be calculated using the advection and dispersion equations shown in Eqs. (2-1 to

15

2-3) and (2-4). Thereafter, $x_{w,1}$, $y_{n,1}$ and $x_{s,1}$ values are updated within the same time step, based on the octanol-water partition coefficient $K_{ow,1}$ [m³/m³] and $K_{d,1}$ according to the following process. First, when the analysis block lengths in each direction are Δx, Δy, and Δz, respectively, the total number of moles of 1,4-dioxane per block, $N_{mol,1}$ [kmol] can be calculated by Eq. (2-9).

$$N_{mol,1} = \left[y_{n,1}\phi\rho_n S_n + x_{w,1}\phi\rho_w S_w + x_{s,1}(1-\phi)\rho_s \right] \Delta x \Delta y \Delta z$$

(2-9)

Because the molar fraction ($y_{n,1}$, $x_{w,1}$) can be converted to the concentration in each phase [kmol/m³] by multiplying by the molar density (ρ_n, ρ_w), the elution equilibrium between the NAPL and water phases is calculated by applying $K_{ow,1}$ and the following formula.

$$\rho_n y_{n,1} = K_{ow,1}\rho_w x_{w,1}$$

(2-10)

Furthermore, $x_{s,1}$ is expressed as a function of $x_{w,1}$ in Eq. 2-8. If substituting Eqs. 2-8 and 2-10 into Eq. 2-9, the following nonlinear equation for $x_{w,1}$ is obtained.

$$\phi\rho_w \left(K_{ow,1}S_n + S_w \right) x_{w,1}\left(1 + K_{d,1}\rho_w x_{w,1}\right)$$
$$+K_{d,1}x_{s,sat,1}\rho_w x_{w,1}(1-\phi)\rho_s - \frac{N_{mol,1}\left(1 + K_{d,1}\rho_w x_{w,1}\right)}{\Delta x \Delta y \Delta z} = 0$$

(2-11)

For Eq. 2-11, the solution for $x_{w,1}$ obtained by applying the Newton-Raphson method corresponds to the value where the effects of elution and adsorption are considered. The updated $x_{w,1}$ is then used to update $y_{n,1}$ and $x_{s,1}$ according to Eqs. 2-8 and 2-10.

2.3. Analytical Mesh Zone and Boundary Conditions

2.3.1. Modeling Area and Parameters of the Aquifer

The analytical mesh zone and associated aquifer parameters are shown in Table 2-2. The constructed area for modeling spans the entire site of illegal dumping in Iwate Prefecture, including the boundary area, with a size of 500×500 m. The mass conservation equations are shown in Eqs. 2-1 to 2-4 are discretized in a two-dimensional x-y coordinate system, neglecting the effect of gravity. The lengths of the blocks in the x- and y-directions, Δx, and Δy, were set equal to 5 m, and a total of 10,000 blocks were set. The aquifer thickness was set at 5 m, and the temperature was constant at 15 °C. The hydraulic conductivity value of the aquifer was set at 5.06×10^{-6} m/sec, in accordance with the simulation study by Iguro et al. Thus, the absolute permeability value is calculated to be 5.88×10^{-1} μm², based on the mass conservation equation. The porosity value was set to 0.30, according to Iguro et al.

In addition, as described in Section 2.1, an impermeable wall was constructed at the prefectural boundary in March 2007 to prevent the spread of contamination to the Aomori Prefecture side, and an extension of the wall was built in July 2014. In the numerical analysis regarding the installation of the impermeable wall, the permeability values at the blocks corresponding to the impermeable wall and at the wall sides of the blocks adjacent to the impermeable wall were updated at these two dates. According to the hydraulic conductivity values for vertical impermeable wall construction and the experimental results reported by Koizumi et al., 1.00×10^{-8} m/sec was used as the hydraulic conductivity (absolute permeability value of 1.16×10^{-3} mm^2) for the impermeable wall. Furthermore, the porosity value was updated for the block associated with the impermeable wall, and the updated value was set to 0.01, considering the stability of the calculation in the vicinity of the impermeable wall.

Table 2-2. The analytical mesh zone and related parameters of the aquifer.

Parameter	Value
Distance in x-direction [m]	500
Distance in y-direction [m]	500
Block length in x-direction [m]	5
Block length in y-direction [m]	5
Thickness of aquifer [m]	5
Temperature in aquifer [°C]	5
Hydraulic conductivity in x-direction [m/sec]	5.06×10^{-6}
Hydraulic conductivity in y-direction [m/sec]	5.06×10^{-6}
Porosity [-]	0.300
Hydraulic conductivity of impermeable wall [m/sec]	1.00×10^{-8}

2.3.2 Lateral boundary and initial groundwater level distribution

The lateral side of the 2-D analysis area was treated as an open boundary and, according to the advection and dispersion according to Eq. 2-4, the outflow of 1,4-dioxane due to pressure and concentration gradients at the boundary and the dilution effects from groundwater inflow from outside due to the decrease in the hydraulic head at the site resulting from pumping were considered. The establishment of the lateral boundary pressure P_b [Pa] and the initial groundwater level distribution are described below.

Surveys of groundwater levels conducted in 2001-2002 produced the three-dimensional groundwater level distribution shown in Figure 2-2. However, because this numerical model considers only a two-

dimensional horizontal water body, it is necessary to reproduce the measured groundwater level distribution in this two-dimensional analysis domain in a quasi-three-dimensional manner. In a normal two-dimensional horizontal flow simulation, the groundwater level is only defined as a boundary condition at the boundaries. The groundwater level distribution inside the area is defined only by these boundary values as long as fluctuations due to pumping or water injection will not be accompanied. Therefore, it is not easy to reproduce the condition in which the groundwater level is higher than the boundary in the present simulation, and the difference from the measured value may be extremely large. On the other hand, the distribution of the groundwater level shown in Figure 2-2 corresponds to the initial condition before the installation of the impermeable wall and the implementation of the pump remediation measures. To make the distribution of groundwater level in the 2-D domain closer to the measured values, we applied the latter to the groundwater levels at the boundaries and defined the virtual inflow of water into each block to simulate groundwater recharge due to rainfall. Preliminary simulations were performed to determine the initial distribution of groundwater levels by adjusting the inflow rate and locations and comparing them to Figure 2-2.

To set the lateral boundary pressure P_b, the minimum value of groundwater table height GL_{min} [m] is first calculated by subtracting GL from EL based on each distribution of EL [m] and groundwater level GL [m] at each boundary (x=0 m, x=500 m, y=0 m and y=500 m). The notation GL_{min} is the reference height (that is, the potential hydraulic head of zero) and P_b, the value obtained according to the following equation, is applied as a boundary condition.

$$P_b = P_s + M_w \rho_{w0} g \left(EL + GL - GL_{min} \right)$$

(2-12)

where P_s is reference pressure (atmospheric pressure) [Pa] (=101,325), M_w is molar weight of water [kg/kmol], g is gravitational acceleration [m^2/sec] and ρ_{w0} is molar density of water in standard state [kmol/m^3].

For introduction of the virtual water inflow rate into each block q_{wi} [kmol/m^3/sec] into Eq. 2-2, the inflow rate Q_{wi} [m^3/day] is multiplied by ρ_{w0} and divided by Δx, Δy, and the aquifer thickness Δz, as shown in Eq. 2-13.

$$q_{wi} = \frac{Q_{wi} \rho_{w0}}{60 \times 60 \times 24 \times \Delta x \Delta y \Delta z}$$

(2-13)

The groundwater level distribution obtained after several trials is shown in Figure 2-7. Along the watershed that crosses from the northwest to the southeast side, the Q_{wi} values (contour plot) were set to

decrease stepwise as the elevation decreases, with a width of 45 m and a range of $1.67\times10^{-1}\sim5.84\times10^{-1}$ m^3/day. Furthermore, to reproduce the local groundwater flow direction in each area, Q_{wi} values of 5.84×10^{-1}, 1.67×10^{-1} and 3.34×10^{-1} m^3/day were set for the north side of B area, east side of I area, and east side of J area, respectively. The figure shows that the groundwater level distribution and flow direction generally correspond with the measured data. However, there are some differences in the local flow direction compared with that in Figure 2-2, due to the smoothness of the groundwater level change. With the assumption that the Q_{wi} values at each location are maintained after the start of remediation measures and that the groundwater level at the boundary does not fluctuate, the P_b values based on Equation (2-12) were also considered unchanged throughout the simulations.
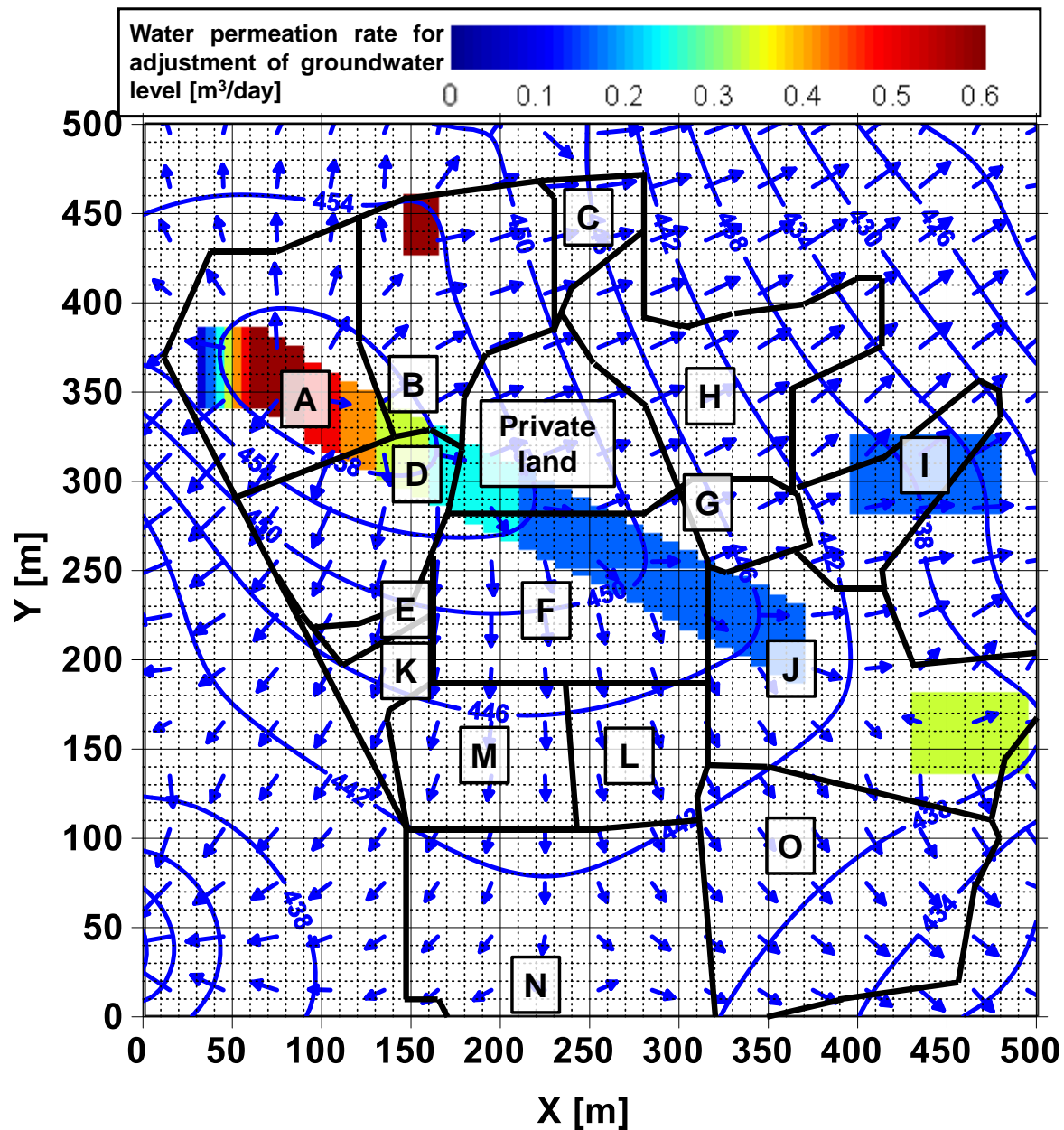
Figure 2-7. Adjustment of calculated value for groundwater levels of by considering virtual water permeation.

2.3.3 Treatment of direct inflow of 1,4-dioxane to aquifers in numerical analysis

As shown in Figure 2-3, the site is characterized by the presence and area-wide spread of surface contamination due to waste deposition. In this numerical model, by placing several sources of 1,4-dioxane contamination in the area and setting boundary conditions, the spread of contamination from the surface soil

into the aquifer is presented. In this case, it is necessary to determine the amount of 1,4-dioxane inflow $Q_{nwi,1}$ [kg], area A_{cs} [m^2], inflow start time ST [years before], and inflow end time ET [years after] for each contamination source. Because the number of blocks at each contamination source is represented by $A_{cs}/(\Delta x \Delta y)$, if dividing $Q_{nwi,1}$ by $A_{cs}/(\Delta x \Delta y)$, the molar weight of 1,4-dioxane $M_{c,1}$ [kg/kmol], the inflow period $(ET - ST) \times 365 \times 24 \times 60 \times 60$ [sec] and $(\Delta x \Delta y \Delta z)$, it is possible to calculate the 1,4-dioxane inflow rate $q_{nwi,1}$ [kmol/m^3/sec] into each block as contamination source.

$$q_{\mathrm{nwi},1} = \frac{Q_{\mathrm{nwi},1}}{M_{c,1} A_{\mathrm{cs}} \Delta z \cdot \left[\left(ET - ST \right) \times 365 \times 24 \times 60 \times 60 \right]}$$

(2-14)

Note that calculation parameters $Q_{nwi,1}$, A_{cs} [m^2], ST and ET were changed to reproduce the spatiotemporal changes in 1,4-dioxane concentration with the impermeable wall installation and pumping operation at the site.

2.3.4 Treatment of Pumping

The water pumping remediation measure at this site started in August 2007 with the installation of four pumping wells at D-4 (x=90m, y=220m), D-5 (x=95m, y=210m), M-2 (x=150m, y=110m) and M-3 (x=150m, y=130m) after the impermeable wall was constructed. At that time, the pumping rates at each well were reported as D-4: 5.9 m^3/day, D-5: 2.3 m^3/day, M-2: 6.4 m^3/day, and M-3: 41.3 m^3/day, respectively. In the N area, pumping aeration treatment was conducted from July to December 2009 with a total pumping capacity of 29,124 m^3. In addition, in the area where 1,4-dioxane concentration exceeds the environmental standard, a total of 38 pumping wells have been newly installed, and the remediation of 1,4-dioxane concentration by pumping had been started in earnest as of April 2013. Although there are no sufficient published data on pumping rates for individual wells, monthly changes in pumping rates for the entire area from April 2013 to September 2015 and cumulative pumping volumes for each area, except the M and N areas, over the two years from 2013 to 2015 are reported, as shown in Figure 2-8 and Table 2-3. In this case, the average monthly pumping, except for the M and N areas, is calculated to be 1,609 m^3/month, and the cumulative total pumping in the entire area from April 2013 to September 2015 is 163,913 m^3. Thus, the average monthly pumping in the M and N areas is estimated to be 3,855 m^3/month.
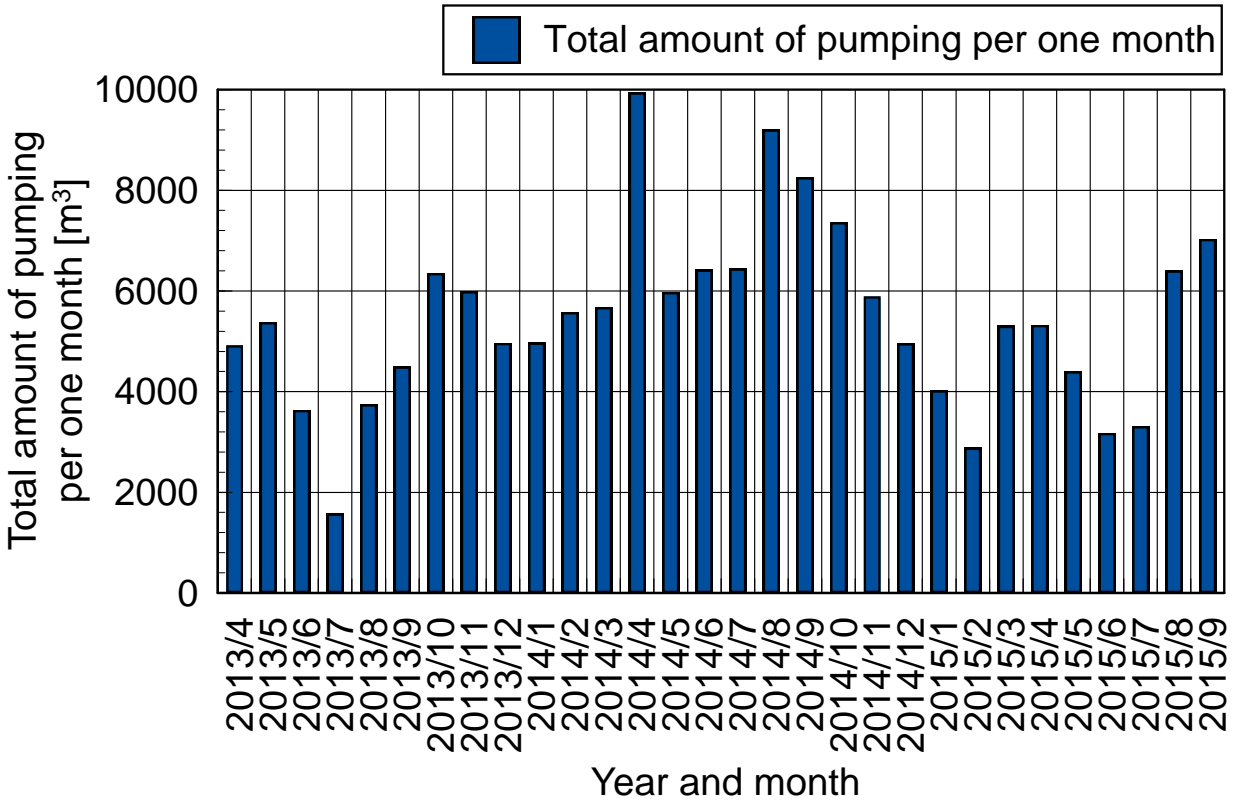
Figure 2-8. Total amount of pumping per one month except the M and N areas.

Table 2-3 Cumulative pumping rates for each area except the M and N areas.

Area	Cumulative pumping volume from Apr. 2013 to Sep. 2015 [m³]	Pumping rate per year [m³/year]
A	4,268	2,134
B	944	472
D	10,131	5,066
F	4,027	2,014
G	49	25
H	7,345	3,673
E, K	1,939	970
O	6,727	3,364

Based on the above calculation, the pumping rates at each pumping well were set as follows. From August 2007 to March 2013, when the remediation measures by pumping started in the entire area, four pumping wells, D-4, D-5, M-2, and M-3, were given constant pumping rates of 5.9 m³/day, 2.3 m³/day, 6.4

m^3/day, and 41.3 m^3/day, respectively. In addition, during 6 months, from July to December 2009, four sites corresponding to the range of remediation measure in the N area (x=160 m, y=50 m), (x=265 m, y=50 m), (x=160 m, y=110 m) and (x=265 m, y=100 m) were given a pumping rate at a rate of 40 m^3/day for each. The pumping rate after April 2013 was calculated as that per a single well by dividing the pumping rate per year in each area by the number of active wells and the period of operation after excluding wells and months with missing 1,4-dioxane concentration levels data. Moreover, after the operation of the large-diameter collection wells, the pumping rate only for these wells was considered throughout the year for numerical analysis. In addition, in area A, a large-scale water collecting well A-5 (x=35 m, y=355 m) has been operated since August 2015; its pumping rate was assumed to be 30.0 m^3/day, based on a preliminary analysis of the hydraulic head distribution during pumping so that a hydraulic gradient is generated in the direction of A-5 from the surrounding area. From the above, the variation of pumping rates at each well is shown in Figure 2-9, and these pumping rates Q_{wp} [m^3/day] are multiplied by the molar density of water ρ_w [kmol/m^3] at the pumping well location and divided by ($\Delta x \Delta y \Delta z$) to obtain the outflow rate q_{wp} [kmol/m^3/sec], which is introduced into Eqs. 2-2 and 2-4.

$$q_{wp} = \frac{Q_{wp}\rho_w}{60 \times 60 \times 24 \times \Delta x \Delta y \Delta z}$$

(2-15)

Conversely, in B-6 (x=185m, y=420m), located downstream of the B area, a decrease in 1,4-dioxane concentration has been observed due to pumping remediation for VOCs removal from October 2011 to July 2012.

In addition, a collection pond was constructed in April 2015 and measures were taken to facilitate the discharge of surrounding groundwater into the collection pond through horizontal borings. However, the preliminary simulation shows that it was difficult to reproduce the groundwater flow directions caused by the pumping because the groundwater level on the east side of the B Area changed significantly. Therefore, the decrease in the concentration of 1,4-dioxane due to these measures was reproduced by introducing the following attenuation rate $R_{A,1}$ [kmol/m^3/sec] to Eq. (2-4).

$$R_{A,1} = k_{A,1}x_{w,1}\phi\rho_w S_w$$

(2-16)

where $k_{A,1}$ is the attenuation rate constant [1/sec]. The range of $R_{A,1}$ introduction for numerical analysis, $k_{A,1}$ value and the period are 1) downstream of B area (x=155~250 m, y=370~430 m, 3.86×10^{-5} 1/sec (October 2011 to July 2012)), 2) collection pond (x=115~155m, y=365~425m, 7.72×10^{-6} 1/sec (from April 2015), 3) downstream of collection pond (x=155~185m, y=365~425m, 7.72×10^{-5} 1/sec (October 2014 to June 2015), 1.93×10^{-5} 1/sec (From June 2015)
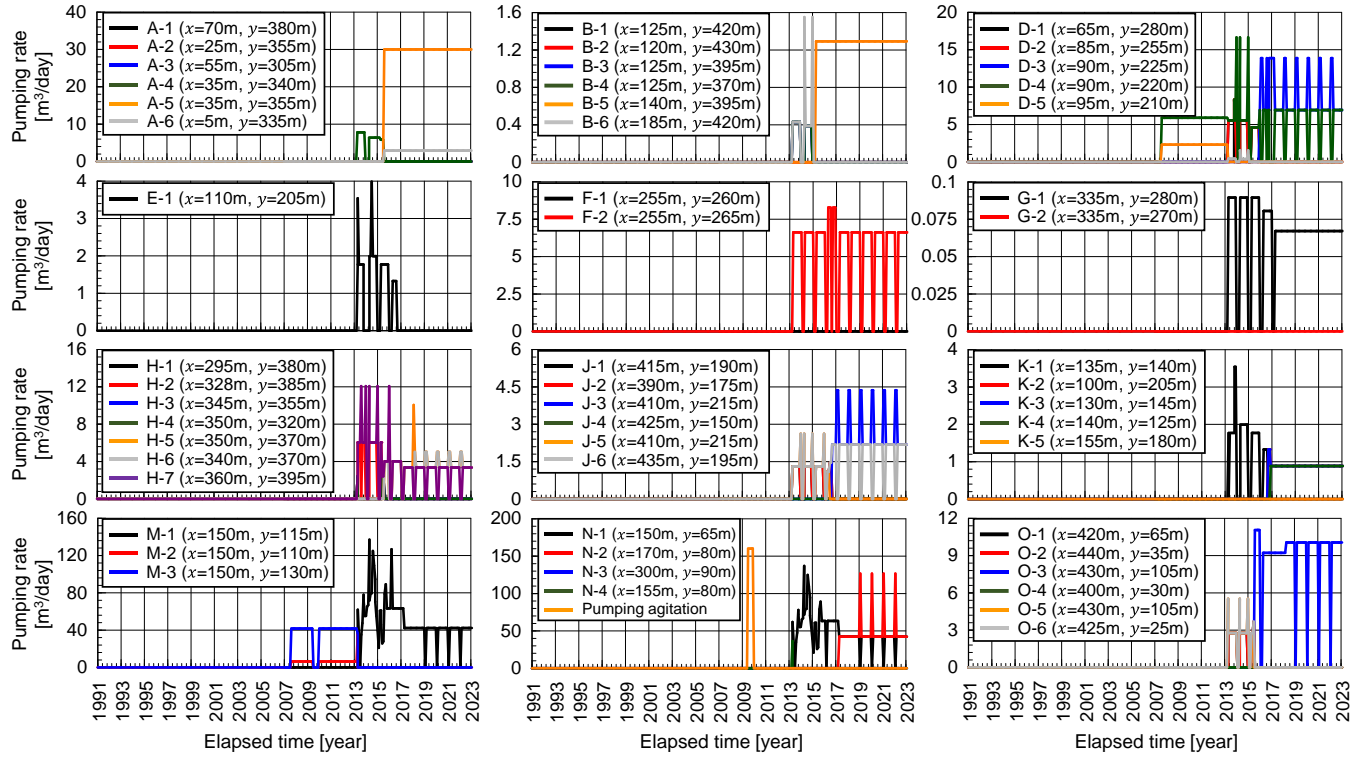
Figure 2-9. Calculated remediation pumping rate in each pumping wells used for a series of numerical analysis based on the total historical cumulative pumping water data in remediation activity

2.4 Spatio-temporal interpretation of contamination spreading behavior across the site

The simulation period was set to 32 years, from January 1991, when the said company started composting industrial waste at the site, to December 2022. Based on the reproduced contamination situation, the effects of the impermeable wall on the control of contamination spreading and the remediation effect of pumping water were studied. The details of the calculation conditions are described below.

Prior to history matching, a preliminary analysis of the temporal and spatial spreading behavior of the contamination with the changes in the distribution of the groundwater level caused by the installation of the impermeable wall and pumping operation was performed. According to the actual remediation results in November 2012 (Figure 2-3), several 20×20 m contamination sources were placed in areas D, E, G, J, N, and O, as shown with red boxes in Figure 3. As the excavation at the western boundary of Area A and at the boundaries of Areas A and B has been removed since 2014, contamination sources were also placed in the corresponding locations. The amount of 1,4-dioxane inflow $Q_{nwi,1}$ at each contamination source was set to 10 kg. The numerical treatment of the inflow of 1,4-dioxane follows Eq. 14.

The groundwater flow behaviors of the site can be divided into four main stages, corresponding to changes in the boundary conditions induced by remediation measures: 1) installation of the impermeable wall (March 2007) and the start of pumping (September 2007), 2) operation of pumping aeration treatment in area N (July 2009), 3) start of pumping in the entire area as remediation measure for 1,4-dioxane contamination (April 2013), and 4) extension of the impermeable wall (July 2014). Based on a comparison of the groundwater level distribution and the spreading behavior of the contamination plumes shown in Figure 2-10, the site-wide spreading behavior as a function of changes in the groundwater level distribution can be interpreted as follows.
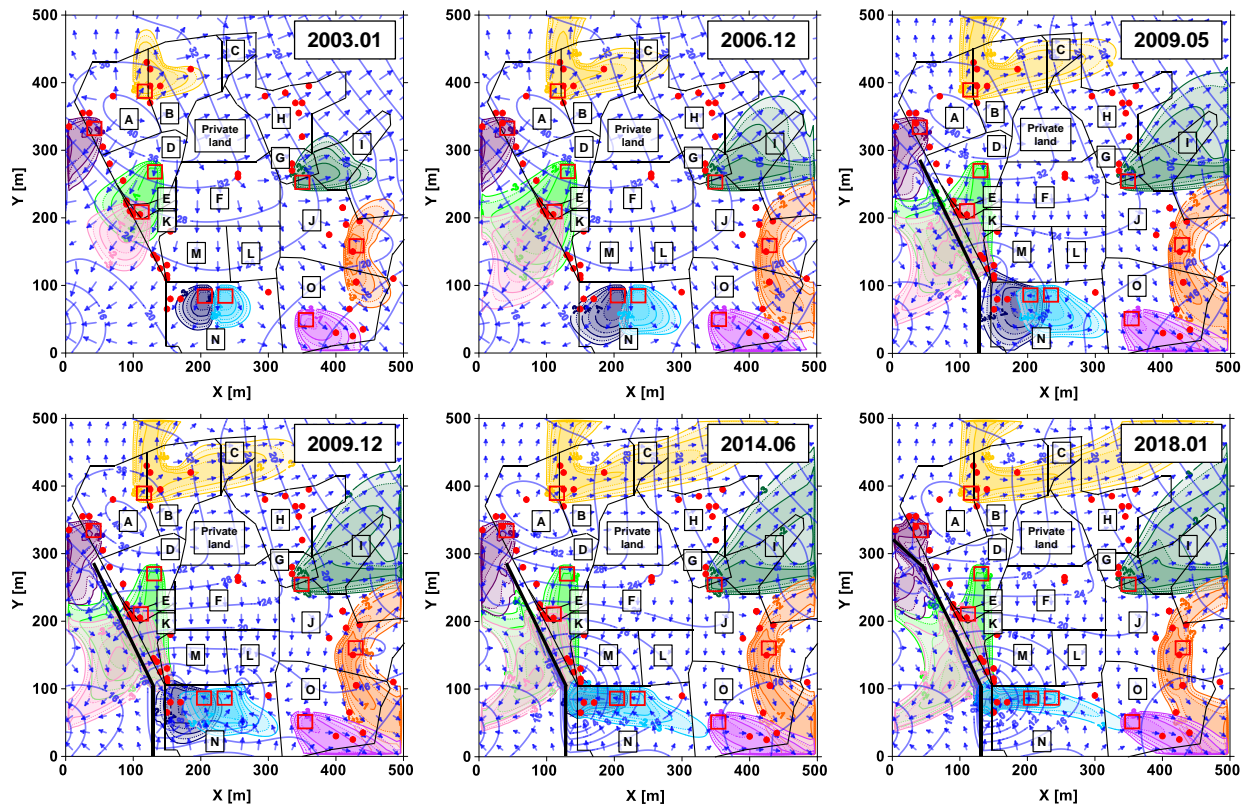
Figure 2-10. The potential distribution of contamination sources (shown as red boxes) in the site from 1999-2022. The distributions of contaminants from different contamination sources are shown in different colors.

(1) The spread of the contamination plumes through December 2006 is due to the initial distribution of the groundwater level. Groundwater flows primarily in two directions, to the southwest and to the northeast, bounded by a watershed that crosses the site from northwest to southeast. Accordingly, plumes spread to the southwest in Areas A, D, and E; to the northeast in Area G; and to the southeast in Area O. Furthermore, because Area E is downstream of Area D, the plume originating from Area D overlaps with that of Area E. In Areas B, J, and N, however, the plume spreads in two different directions, depending on the local distribution of flow direction within the areas: to the north and east in Area B, to the northeast and southeast in Area J, and to the southwest and southeast in Area N.

(2) The May 2009 distribution shows that with the construction of the impermeable wall and the start of pumping near the wall, the groundwater flow direction along the impermeable wall in areas D, E, and M changed from southwest to south. The contamination plumes originating from Areas D, E, M, and N overlap near the boundary between Areas M and N. In contrast, the effect of the impermeable wall and pumping on the flow direction in Areas B, G, J, and O is relatively small. Thus, the spreading direction of the

26

contamination plumes has not changed significantly. In Area A, the plume continues to spread to the southeast because the impermeable wall had not been extended.

(3) In December 2009, when pumping and aeration treatment was conducted in the N area, Figure 2-10 shows that a hydraulic gradient toward the inside of the site was generated from the southern boundary of the N area, and the spreading direction of the plume is shifting toward the north. In addition, the influx of groundwater from the outside expectedly would have had a dilution effect on the 1,4-dioxane concentration in the site. However, no significant change was observed in the distribution of flow direction and spread of contamination across the site compared with (2).

(4) In June 2014, after water pumping in the entire area had started, the hydraulic gradient near the boundary between the M and N areas increased with the increase in pumping near the impermeable wall, and the extent of the plumes tended to increase in that direction.

(5) In January 2018, after the extension of the impermeable wall, the distribution shows that the flow direction in Area A changed and the plume has partially spread along the impermeable wall toward the southeast. In addition, in Area O, which is downstream of Area N, the plume originating from Area N partially overlaps with the plume in Area O.

Although 1,4-dioxane concentrations in Areas F and H were above the standard in May 2010, each well is outside the area where the contamination plume is spreading, as shown in Figure 2-4. Based on the flow distribution as of December 2009, it is difficult to explain why F-2 (x=255 m and y=265 m) exceeded the standard as the range for remediation in area F is x=190-220 m and y=230-250 m as shown in Figure 2. In area F, groundwater flows in from the northwest and discharges mainly in the south direction, with some discharging to the northeast. Given that the possibility of contamination spreading from private land located north of area F is extremely low, the exceedance of the standard in F-2 can be interpreted to be due to surface contamination in its vicinity, and the contamination plume originating from area F is expected to overlap in the downstream of area G. In addition, area H, which is located downstream of both area B and private land, exceeded the standard. Thus, the possibility of contamination spreading from private land is extremely low. Furthermore, depending on the location of the contamination source in area B, there is a possibility that the contamination plume could reach area H. However, H-1 (x=295 m, y=380 m), the most upstream well on the streamline from area B, has maintained below-standard concentrations throughout 2013-2021, unlike other wells in the same area. Therefore, as in Area F, the exceedance of the standard may be due to surface soil contamination in this area although no implementation of remediation measures was reported in November 2012.

It is usually necessary to consider the spreading of the contamination plume across areas in the matching of 1,4-dioxane concentration changes. However, based on the observed site-wide plume spreading behavior, conducting matching based on an area-specific interpretation of contamination is possible because there is a low possibility of inflow from another area for areas A, F, H, and J. In other areas, however, a gradual matching process is required, taking into account the concentration changes due to the influx of 1,4-dioxane from upstream, for instance, from area A to D and from area D to E. In particular, for areas M and N, the spread of the contamination plume from several directions in the surrounding area must be taken into account.

2.5   Conclusion

In this chapter, the groundwater flow field model was calculated with consideration of remediation measures, and initial and boundary conditions were set up. The obtained results underscore the importance of incorporating the effects of remediation measures on groundwater flow field calculation for pollution modeling. It is essential to apply such dynamic groundwater flow field for pollution reproduction and prediction. In addition, the manner in which these remediation strategies influence the movement of pollutants should be elucidated.

Chapter 3 Modeling of groundwater pollution and remediation processes

3.1 Introduction

According to the successful establishment of the groundwater flow field model based on the effects of rainfall and remediation measures in Chapter 2, in this chapter, we utilize the groundwater flow field model to reproduce multiple pollution sources in an illegal waste dumping site under non-stationary conditions, and to predict the concentration levels of 1,4-dioxane and remediation measures in the site. In addition, we show the potential transport behavior of 1,4-dioxane pollutant in each area. The simulation results enables us decide the sequence of identified pollution sources in an illegal waste dumping site.

The sequencing of areas for the reproduction process considers from areas least influenced by other source areas to areas highly influenced by other source areas. For instance, A-area has been uninfluenced by other source areas, as shown in Figure 3-1; this area should be the first area selected for reproduction of previous monitoring data. Areas B and D have only been influenced by A-area; E, K, M, N have been the sequence of pathways for the influence; H has been influenced by B and G areas; J-area might be influenced by G-area; O-area has been influenced by J-area; C, I, and L are supposed to have no pollution sources.
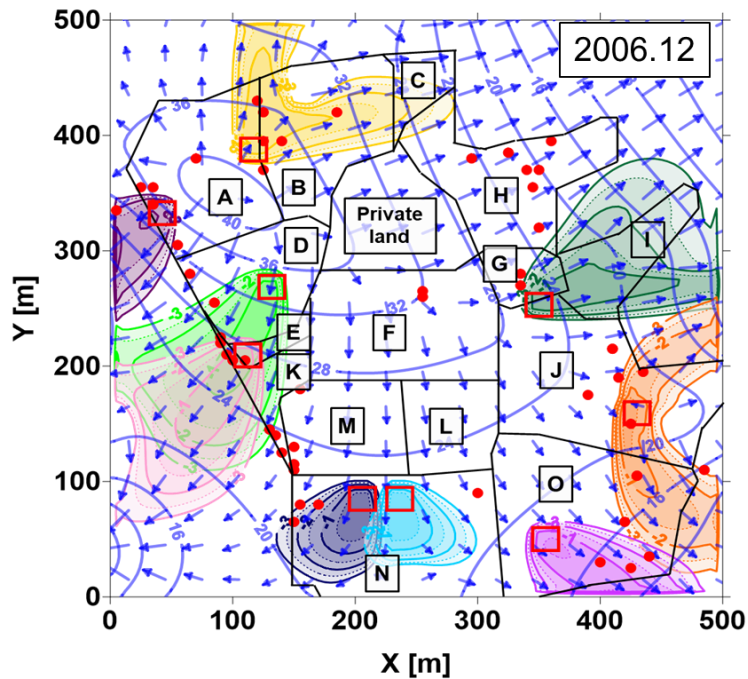

Figure 3-1 the influenced of pollution source from other area

3.2 Methodology

Figure 3-2 presents a flow chart illustrating the process of identifying multiple and non-stationary pollution sources in each area of the site. The flow chart begins with the evaluation of the potential groundwater flow field using monitoring data. By analyzing the monitoring wells, the locations with the highest concentrations of 1,4-dioxane are identified, suggesting that the pollution source might be in close proximity to these wells. Based on this information, in the study, we conducted several trials to reproduce the concentration of 1,4-dioxane. Factors such as source location, level of pollution, and duration of the source input were taken into account during the trials. The reproduction results were then verified by comparing them with the observed concentrations in influenced wells. This process was repeated for all the wells in each area of the site until all wells were assessed.
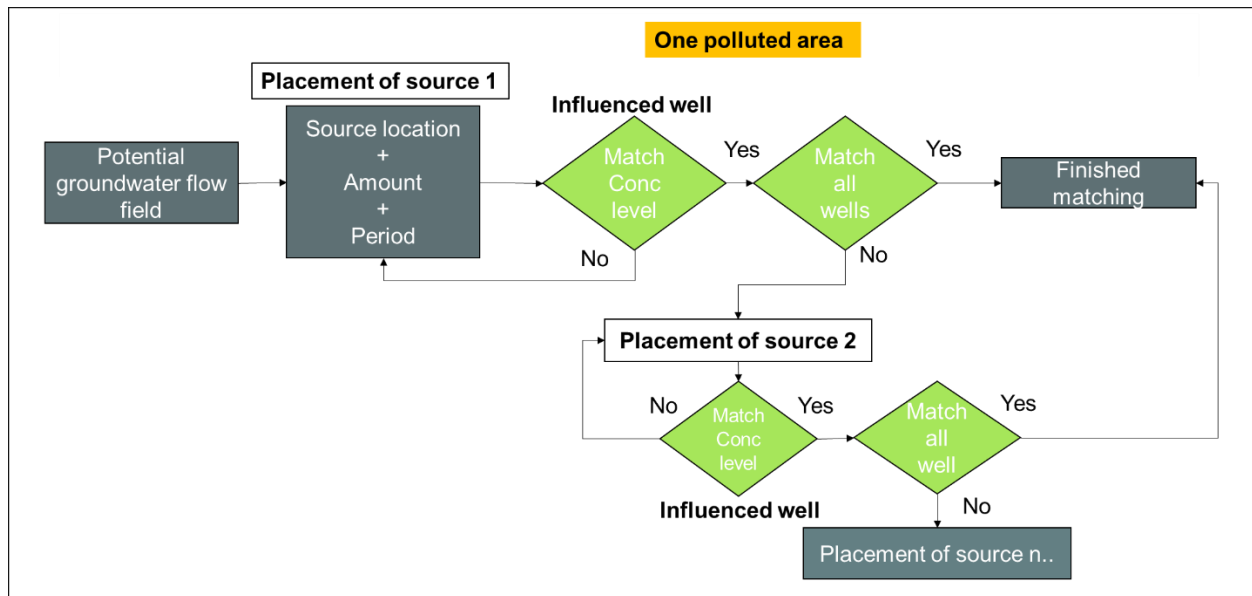

Figure 3-2 the flow chart of source placement process of reproduction part

3.2.1 History matching on spatial-temporal 1,4-Dioxane concentration changes for area A

We use Area A here as an example to show the progression of changes in 1,4-dioxane concentration in this study because for Area A the possibility of influx of 1,4-dioxane from other areas is very low and the effects of spreading contamination from other areas can be virtually ignored. To establish the boundary conditions for the inflow of 1,4-dioxane into a site's aquifer, the correlation between the change in the groundwater flow direction distribution and the effects of remedial action was first interpreted based on the monitoring results of 1,4-dioxane concentration for each pumping well in Area A, and the calculated groundwater level distribution is shown in Figure 3-3.
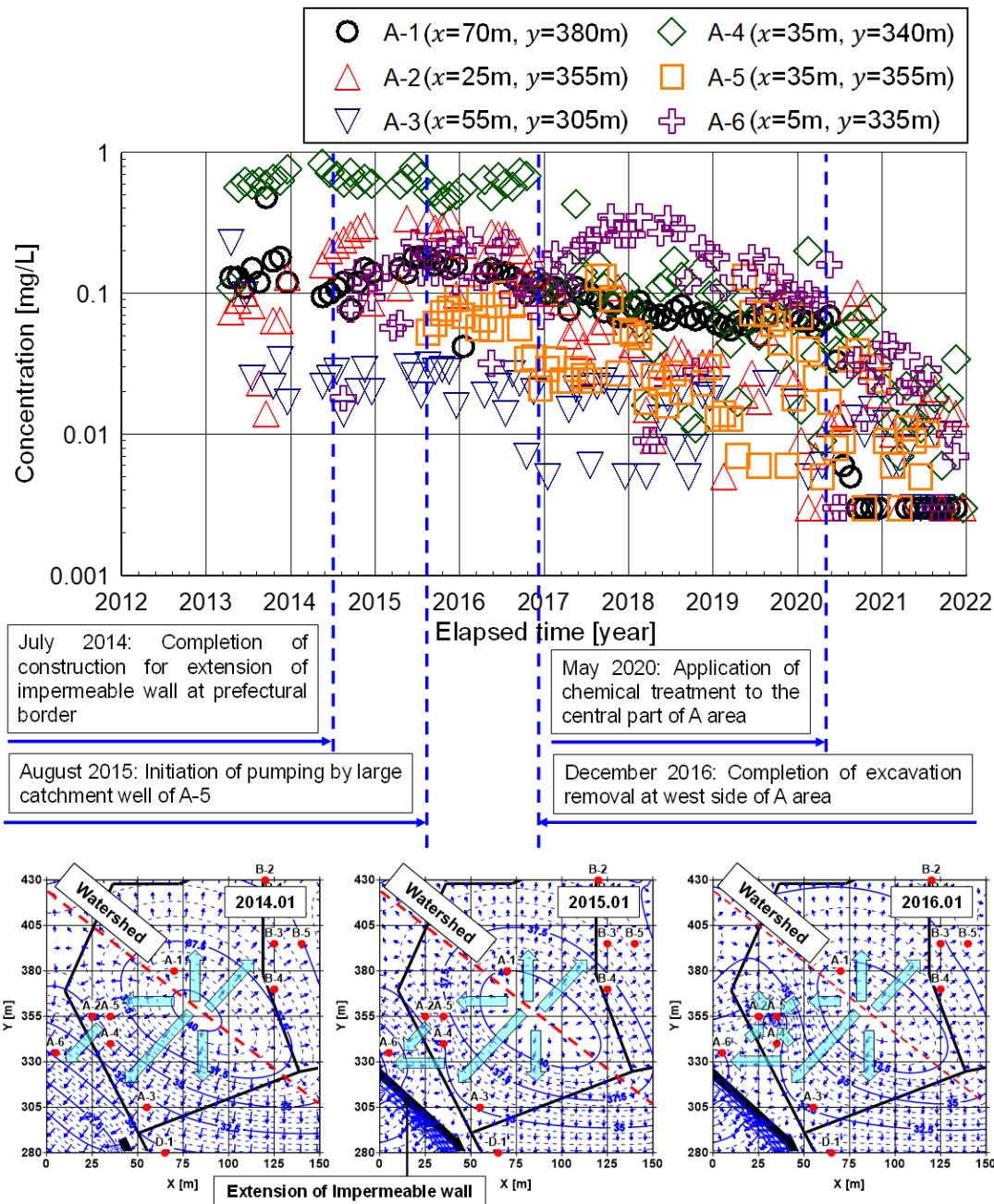
Figure 3-3. 1,4-dioxane concentration monitoring results for each pumping well in area A and the calculated groundwater level distribution.

In A-4 (x=35m, y=340m), the concentration had been more than ten times higher than the environmental standard (0.05 mg/L) for more than three years since the start of monitoring in April 2013. Nevertheless, after the excavation and removal of contaminated soil near the western boundary in December 2016, a significant decrease in the concentration was confirmed. Therefore, the inflow of 1,4-dioxane into the aquifer after this date is interpreted as a converging trend. Corresponding to the actual result of remedial

action, the area around the western boundary, including A-4, can be considered a source of contamination (source of inflow to the aquifer), which is referred to below as CSA-1. In Area A, an extension of the impermeable wall was constructed in July 2014 to prevent contamination on the side of Aomori Prefecture. The groundwater level distribution shows that before the extension of the impermeable, wall in January 2014, groundwater flowed mainly in the southwest direction around A-4, whereas it turned to the A-6 side (x=5m, y=335m) in the west direction after the extension (January 2015). The concentration at A-6 was 0.018 mg/L in August 2014 but has since increased to above the standard, which can be interpreted to be because of the change in the flow direction caused by the extension of the impermeable wall, and the contamination plume that spread in the direction of A-6 originated from CSA-1.

By contrast, the increase in concentration at A-2 (x=25m, y=355m) after April 2013 is unlikely to have originated from CSA-1, considering its locational relationship with A-4 and the difference in their contamination levels, in addition to the groundwater flow direction in January 2014, suggesting the existence of another contamination source near A-2. This contamination source is referred to as CSA-2. In CSA-2, the inflow into the aquifer can be considered to have started around April 2013, corresponding to the trend of increase in concentration at A-2. In addition, remediation measures by pumping began in August 2015 at A-5 (x=35m, y=355m), which is located immediately adjacent to A-2. The distribution of groundwater levels since pumping began shows the formation of a hydraulic gradient from the surrounding area toward A-5 (January 2016). The decrease in concentration in A-2 since November 2015 is interpreted mainly to be as a result of remediation measure by pumping. After that, the decrease became remarkable since January 2017, suggesting that the inflow from CSA-2 has been a converging trend since then.

In A-1 (x=70 m, y=380 m), which is the only well located across the watershed in area A, the concentration had already exceeded the standard in April 2013 and, although it showed a slight downward trend after 2016, the concentration level remained above the standard. In May 2020, a chemical treatment method was applied in the central area of area A, and a significant decrease in concentration was confirmed after this period. According to the actual results of these remediation measures, the area near the center of area A could be regarded as the third contamination source, referred to as CSA-3. Based on the concentration change in A-1, it is interpreted that the inflow from CSA-3 into the aquifer ceased after May 2020. The distribution of groundwater levels shows that the water level is highest near the center of this area, and the streamlines radiate in the directions of A-2 to A-5 in addition to the direction of A-1 on the north side. A-2 is located on the streamline westward from the center. However, the concentration at A-2 was 0.29 mg/L in October 2014, while that at A-1 was 0.12 mg/L. A-2, located downstream of A-1 according to the locational relationship with the central area, showed a higher concentration. Therefore, the presence of CSA-3 is expected to have little effect on the increase in the concentration of A-2. In addition, CSA-3 is expected to

be located slightly on the side of A-1 across the watershed where the spreading of the contamination plume toward A-2 and A-5 will have little effect. In addition, A-3 (x=55m, y=305m), with a concentration of approximately 0.01 mg/L, which is below the environmental standard, continued to be detected until 2022, possibly due to the spreading of the contamination plume, which originated from CSA-3, to the south.

Based on the above discussion, for area A, history matching of 1,4-dioxane concentrations will be performed by a placing of three contamination sources: CSA-1 (near the western boundary), CSA-2 (just near A-2), and CSA-3 (near the central area). In the matching process, in addition to the locational relationship of the pumping well to each contamination source, the amount of 1,4-dioxane inflow, $Q_{nwi,1}$ [kg], area of the contamination source A_{cs} [m²], inflow start time ST [years before], and inflow end time ET [years after] described in Eq. 3 are treated as parameters. For the inflow end time ET, the values could be set based on concentration changes and actual results of remediation measures, namely, December 2016 for CSA-1 and CSA-2, and May 2020 for CSA-3. The inflow start time ST of CSA-2 was set to April 2013, at which time the concentration in A-2 increased. For CSA-1 and CSA-3, the ST should be set to an earlier time because the concentrations of A-1 and A-4, which are in the vicinity of CSA-1 and CSA-3, had already increased in April 2013. However, it was difficult to determine ST only from the changes in concentrations. However, a survey conducted in 2009 for the entire site, when 4-dioxane was included as a new environmental criterion, did not detect contamination in Area A. Therefore, the spreading of contamination into the aquifer originating from CSA-1 and CSA-3 could be regarded to have occurred after 2009, and ST was assumed to be January 2013 for CSA-1 and January 2012 for CSA-3, respectively. Multiple repeated preliminary analyses were conducted to determine the detailed condition setting of the contamination source area A_{cs} and its locational relationship with the pumping wells; however, because of space limitation, these analyses will not be described here. The calculation conditions for this matching process are shown in Table A1. The matching process consists of three steps: Step 1: CSA-1, Step 2: CSA-2, and Step 3: CSA-3, in which the amount of 1,4-dioxane, $Q_{nwi,1}$, at each contamination source is appropriately changed in that order. The details of the history matching process are described below.

3.2.2 Step 1: Placement of contamination source CSA-1 near the western boundary of Area A

In the first step, contamination source CSA-1 is placed near the western boundary of area A. Then the monitoring results are compared with the calculated results by using the concentration changes at A-4 and A-6 as indicators. CSA-1 was placed in the range of x=25 to 40 m and y=325 to 340 m, including A-4, with an area A_{cs} of 225 m², so as to locate A-6 on the west side of CSA-1, because the flow direction to the southwest near A-4 had turned to the west toward A-6 after the impermeable wall was installed. The period of inflow of 1,4-dioxane into the aquifer in CSA-1 was set to four years, from January 2013 to December 2016, when a significant decrease in concentration was observed in A-4 due to excavation removal. The

analysis was conducted by changing the amount of 1,4-dioxane inflow, $Q_{nwi,1}$, in four cases: Case-01: 5.00 kg, Case-02: 10.0 kg, Case-03: 20.0 kg, and Case-04: 40.0 kg.

As representative calculated results, Figure 3-4a shows the 1,4-dioxane concentration and groundwater level distribution changes over time for Case-02, where $Q_{nwi,1}$ is 10.0 kg. The location of CSA-1 is shown by the red box in the figure. The July 2013 and January 2014 distributions show that prior to the extension of the impermeable wall, the contamination plume originating from CSA-1 spread in the same direction as groundwater flow in the region, including CSA-1 and its downstream side. After the extension of the impermeable wall, the direction of the plume spreading turned to the west, as shown for January 2015, which corresponds with the westward shift of the flow direction near CSA-1, and an increase in the concentration near A-6 is observed. In addition, the distributions in January 2016 and 2017 show that the plume spread toward A-2 and A-5 north of CSA-1 after pumping at A-5, as a hydraulic gradient formed toward A-5. Between CSA-1 and A-6, the likelihood of the plume spreading to the west tends to be stronger, and the concentration near A-6 remains at a high level. Because the CSA-1 site also includes A-4, the concentration near A-4 will remain high as long as inflow from CSA-1 into the aquifer continues. However, by January 2018, inflow to the aquifer had ceased and as a result, a significant decrease in concentration near A-4 was recognized. A general downward trend was observed at A-5 due to the dilution effect from groundwater flow in addition to pumping remediation.

Figure 3-4b compares the calculated concentration changes over time at each pump well determined for cases-01 through 04 with the monitoring results. Corresponding to the changes in concentration distribution shown in Figure 4a, the concentration in A-4 remained beyond the environmental standard for four years after January 2013 and then decreased significantly with the end of the inflow in December 2016, while the concentration in A-6 increased after 2013 and decreased after 2018. These calculations adequately reflect the trend of concentration change shown in the monitoring results. Furthermore, in Case-02, where $Q_{nwi,1}$ is set to 10.0 kg, the concentration in A-4 and A-6 are the closest to the monitoring results. Based on the results of Case-02, to validate the above interpretation that the increase in concentration at A-6 was due to the spreading of the contamination plume originating from CSA-1, we conducted a series of analyses by varying the placement of CSA-1, the inflow period, and adsorption coefficients.

As shown in Figure 3-5a, the source placement was varied from x=25 to 40 m and y=325 to 340 m in Case-02, to x=20 to 35 m and y=340 to 355 m on the north side along the district boundary in Case-05, to x=30 to 45 m and y=310 to 325 m on the south side along the area boundary in Case-06, and finally to x=35 to 50 m and y=325 to 340 m further inside the area boundary in Case-07. The analysis was conducted

with $Q_{nwi,1}$ and the inflow period set equal to those in Case-02, and the results were compared with the monitoring results using A-4 and A-6 as indicators, shown in Figure 3-5b.

In Case 05, the contamination plume reached the site of A-6 earlier due to the southwestern groundwater flow before the extension of the impermeable wall, and the trend of the concentration increase after 2013 is significant; with the change of the dispersion direction of the plume due to the change of the flow direction after the extension, the concentration decrease occurred as early as the second half of 2015, resulting in a significant difference from the monitoring results. In case 06, the concentration increase in A-4 cannot be reproduced because A-4 is not included within the range of CSA-1. In addition, the spreading direction of the contamination plume is different, and the concentration in A-6 remains more than an order of magnitude lower than the monitoring results. In Case-07, the distance between CSA-1 and A-6 is greater than in Case-02, and the timing of the concentration increase is delayed due to the delay in the arrival of the contamination plume at the position of A-6. Based on the above results from Case-05 to Case-07, the placement of CSA-1 in Case-02 is considered appropriate. It supports the interpretation that the increase in concentration at A-6 is due to the spread of the contamination plume originating from CSA-1.
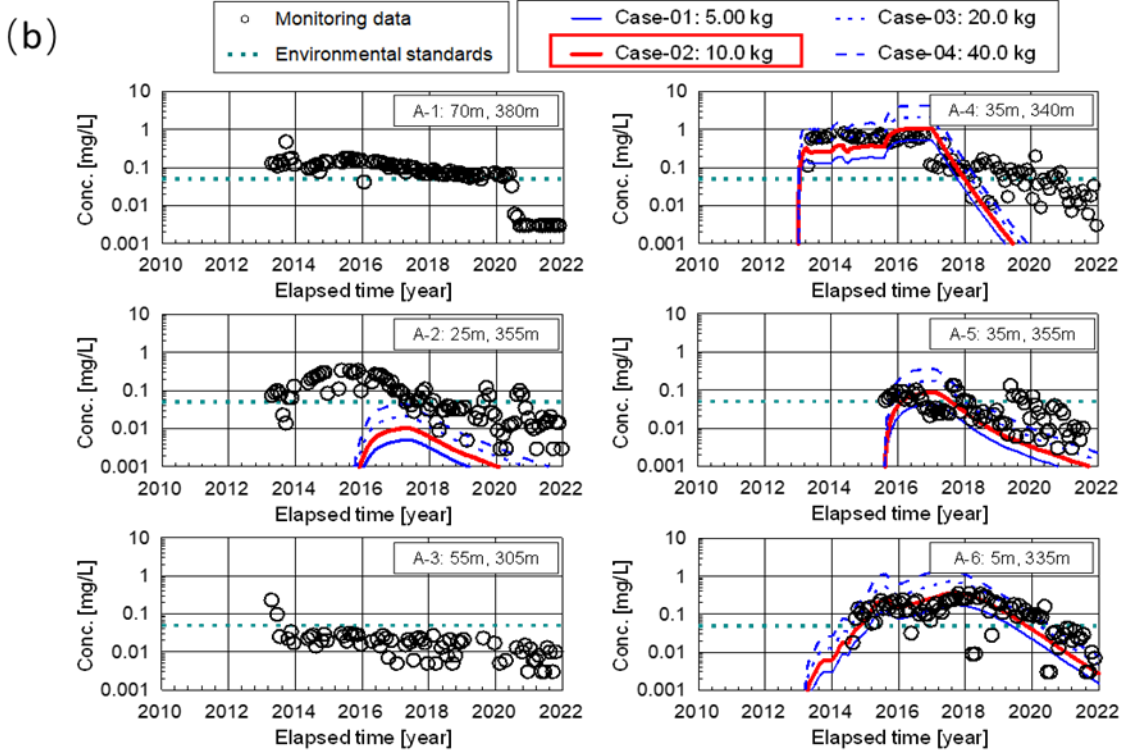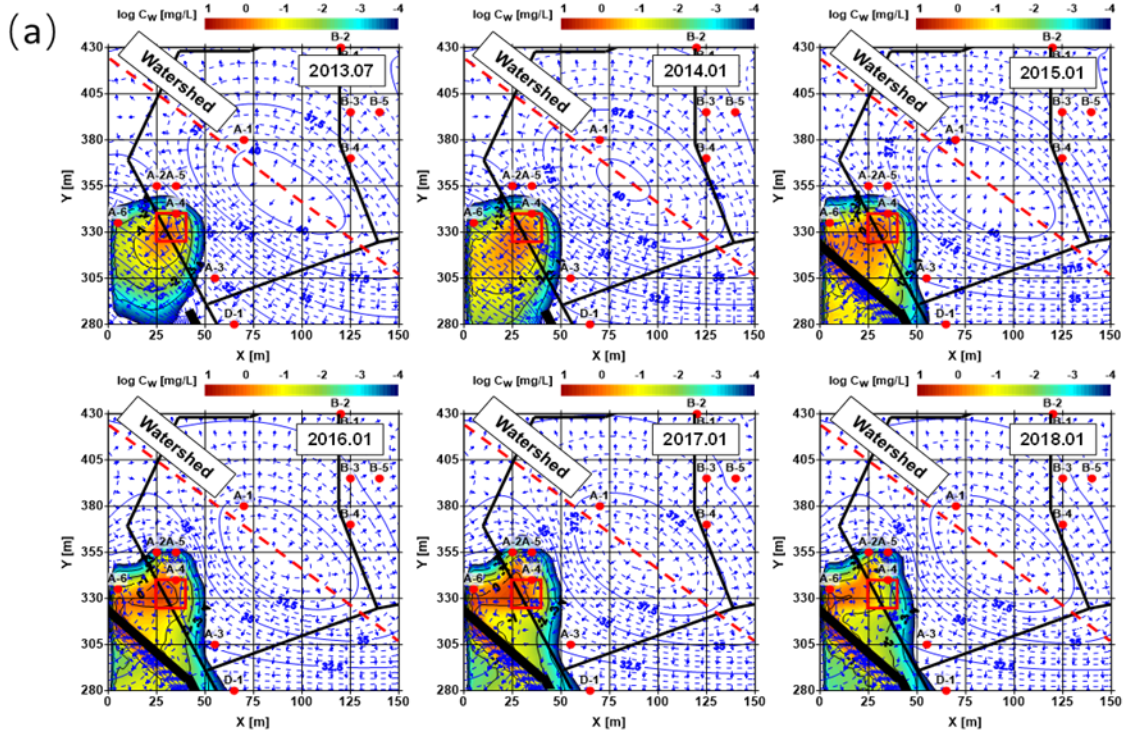
Figure 3-4 (a) 1,4-dioxane concentration and groundwater level distribution changes over time for Case-02; (b) comparison of the calculated concentration changes over time at each pumping well with the monitoring results (Cases-01, 02, 03 and 04).
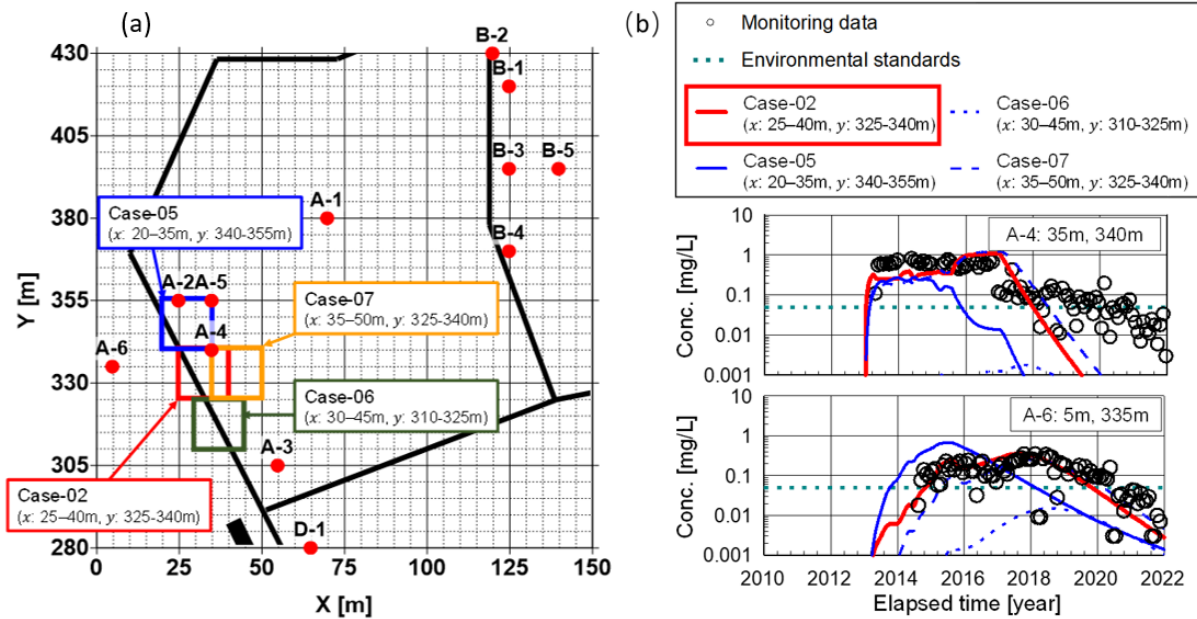
Figure 3-5 (a) The placement of contamination sources in A-area and (b) the verification of the placement of contamination source by comparing the calculation result with monitoring results (Cases-02, 05, 06 and 07).

To verify the inflow period, Cases 08 to 10 were tested with CSA-1 and $Q_{nwi,1}$ equal to those in Case-02. In Case-08, Case-09, and Case-10, the period of inflow was set from January 2011 to December 2016 (6 years), from January 2015 to December 2018 (4 years), from January 2013 to December 2014 (2 years), respectively. Case-08 assumes an early spreading of contamination, Case-09 assumes a later spreading, and Case-10 assumes an early excavation removal compared to Case-02 (January 2013 to December 2016). The obtained results in the different cases of the period of inflow are shown in Figure 3-6 and are compared with the monitoring data using A-4 and A-6 as indicators.
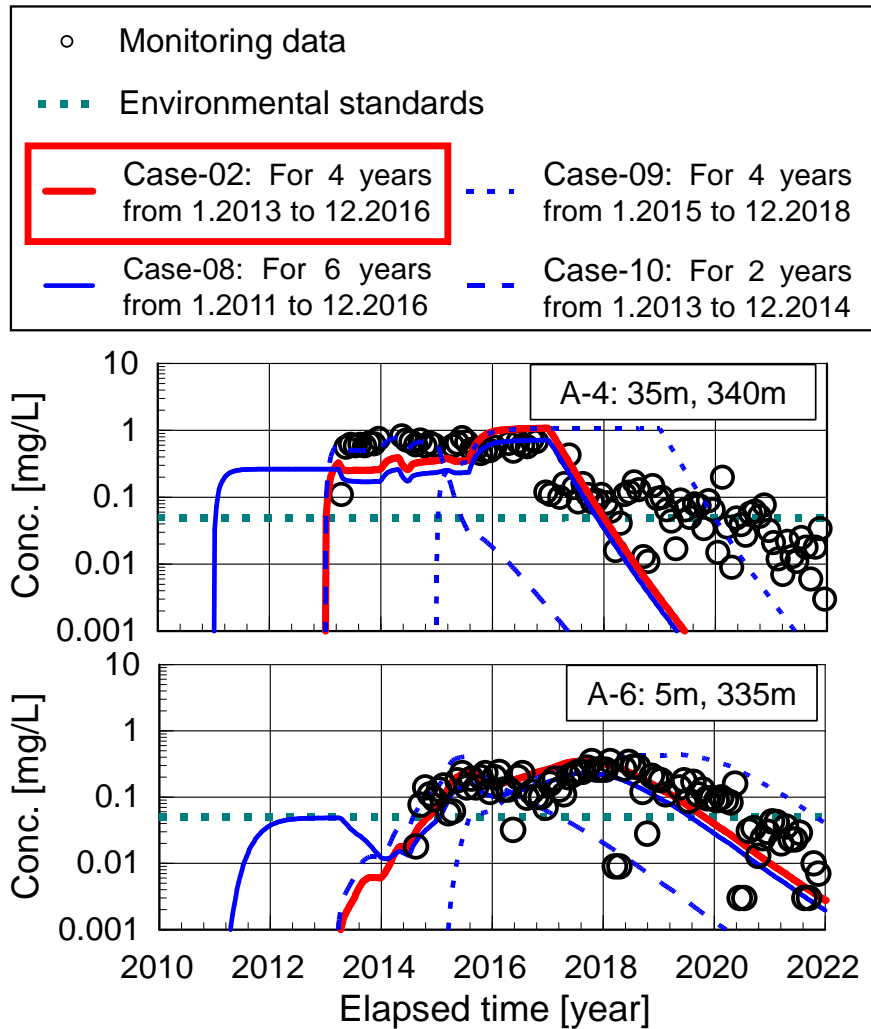
Figure 3-6 Comparison of calculated and monitored results for verification of the discharge period from contamination source in A-area (Cases-02, 08, 09 and 10).

In Case-08, the concentration of A-6 had already exceeded the standard in early 2012, which is different from the monitoring results. In Case-09, the concentration changes to be exceeded beyond the standard in the two years by 2015 could not be well reproduced in either well. In addition, because the inflow of 1,4-dioxane to the aquifer continued after December 2016, there was a delay in the decrease in concentration, resulting in a significant difference from the monitoring results. In Case 10, since the inflow to the aquifer stopped after January 2016 due to excavation and removal, it is impossible to reproduce the concentration changes that are above the standard since 2016. Based on the above results for Cases 08 through 10, under the assumption that the placement of CSA-1 is appropriate, the condition of four years of inflow from

January 2013 through December 2016 can be considered appropriate, indicating that the spread of contamination into the aquifer originating from CSA-1 occurred relatively recently.

Furthermore, as described in Section 2.2 (2), in this study, considering the relatively low adsorptive of 1,4-dioxane in the sandy soil, the adsorption coefficient $K_{d,1}$ for a series of numerical analyses was set to 1.00×10^4 m^3/kg instead of 7.88×10^4 m^3/kg that was obtained experimentally. A validation of this $K_{d,1}$ value was also conducted using the same 1,4-dioxane inflow condition of Case-02, and the $K_{d,1}$ values were changed in four steps, Case-11: 7.88×10^4 m^3/kg (corresponding to the experimental value), Case-12: 5.00×10^4 m^3/kg, Case-13: 5.00×10^3 m^3/kg and Case-14: 0.00×10^0 m^3/kg (without consideration of adsorption) with respect to 1.00×10^4 m^3/kg for Case-02, respectively. The results obtained and the comparison with the monitoring results are shown in Figure 3-7. In cases 11 and 12, 1,4-dioxane had a higher absorption capacity than in case 02 and the amount of 1,4-dioxane retained on the surface of soil particles as an adsorbent increased, resulting in delayed advection and dispersion in the aquifer. As a result, the concentration at A-4 after the excavation and removal in January 2017 is declining slowly, and the timing of the concentration increase at A-6 has also delayed. In contrast, at Cases 13 and 14, the amount of 1,4-dioxane absorbed is lower and the mobility of 1,4-dioxane due to advection and dispersion in the aquifer increases, resulting in a significant decrease in concentration in both wells compared to the monitoring results. The above results suggest that the adsorptive of 1,4-dioxane to the soil is low but has a certain level of adsorptive and that the use of a $K_{d,1}$ value of approximately 1.00×10^4 m^3/kg best reproduced the plume spreading behavior caused by advection and dispersion.

Based on the above validity verification of the placement of CSA-1, the inflow period, and the adsorption treatment, a comparison of the calculated and monitored concentration changes at A-1, A-2, A-3, and A-5 was again made in Figure 3-4. Because A-1 and A-3 are independent of changes in groundwater flow direction and are outside the range of the spreading contamination plume originating from CSA-1, it is difficult to reproduce the concentration changes in these wells. In contrast to A-1 and A-3, A-2 and A-5 are not located in the main direction of spreading of the contamination plume, therefore the increase in concentration in these wells can be interpreted to be due to pumping at A-5. In particular, at A-2, the difference between the calculated results and the monitoring results in terms of the concentration level and the timing of the concentration increase is so large that the effect of CSA-1 on the concentration increase at A-2 is very small. This result provides a basis for considering CSA-2 as a separate source of contamination from CSA-1 and to reproduce the concentration change in A-2. In addition, based on the results of the study in Step 1, the conditions in Case-02 that best reproduce the concentration changes in A-4 and A-6 are used in subsequent Steps 2 and 3 for the conditions related to CSA-1.
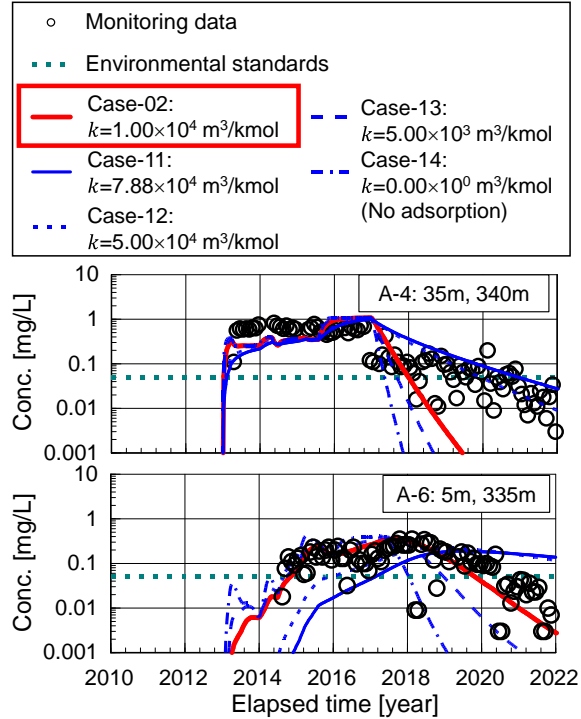
Figure 3-7 Comparison of calculated and monitored results for verification of adsorption coefficient 1,4-dioxine in A-area (Cases-02, 11-14).

3.2.2 Step 2: Placement of contamination source CSA-2 in the vicinity of A-2

In Step 2, CSA-2 is newly placed in addition to CSA-1 in Step 1, using the changes in concentration of A-2 and A-5 as indicators to reproduce the monitoring results. A-2 and A-5 are only 10 m apart in the x direction, and both wells were located almost on the same streamline to the west direction, with A-5 upstream with respect to A-2 before the start of pumping at A-5. Concentration levels were generally higher in A-2, which was located downstream. Therefore, we performed a series of preliminary analyses to determine the placement of CSA-2, under the conditions that CSA-2 should have little effect on the concentration increase of A-5 and should be located just near A-2. As a result, the contamination source area A_{cs} is set as 100 m² (10×10 m) and is placed in the range of x=20 to 30 m and y=360 to 370 m to the north of the vicinity of A-4. The period of inflow of 1,4-dioxane from CSA-2 into the aquifer was defined as 3.75 years, from April 2013, when the concentration in A-2 started to increase, to December 2016, when a significant decrease in concentration was observed, according to the monitoring results. The analysis was conducted by changing the amount of 1,4-dioxane inflow $Q_{nwi,1}$ during this period in four steps: Case-15: 1.00 kg, Case-16: 2.00 kg, Case-17: 5.00 kg, and Case-18: 10.0 kg.

40

As an example of calculated result, the changes in 1,4-dioxane concentration and groundwater level distributions with time obtained for Case-16 when $Q_{nwi,1}$ was set to 2.00 kg, is shown in Figure 3-8a. The distributions in July 2013, January 2014, and January 2015 show that before the start of pumping at A-5 in August 2015, there was no significant change in the flow direction near A-2 and A-5 before and after the extension of the impermeable wall, and the contamination plume spread mainly toward the southwest side. According to the positional relationship with CSA-2, A-5 is outside the main spreading direction of the plume, and the increase in concentration at A-5 is probably mainly due to dispersion. From the January 2016 distribution, after the start of pumping at A-5, a hydraulic gradient has developed from A-2 toward A-5, and the further spreading of the plume has been controlled by the pumping. Since January 2017, because the inflow from CSA-2 into the aquifer has stopped, concentrations near A-2 and A-5 will decrease over time as pumping continues at A-5. A-1 and A-3 are outside the area where the contamination plume from CSA-2 is spreading, regardless of the change in groundwater flow direction.
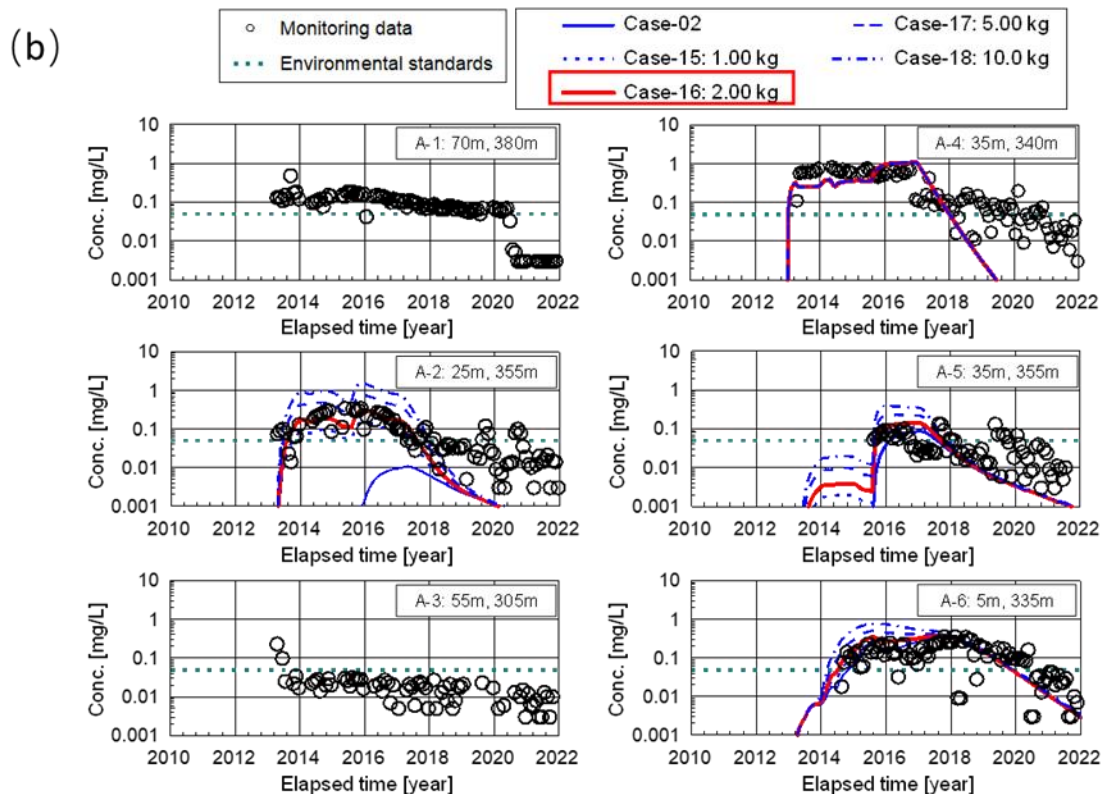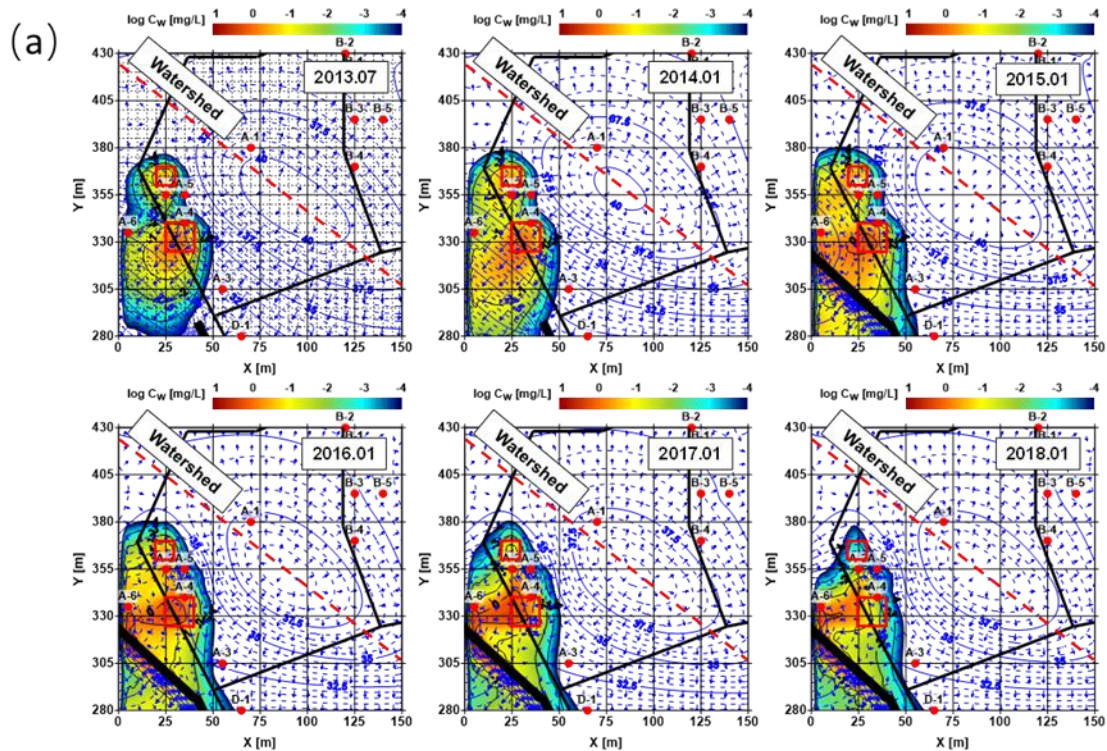
Figure 3-8 Verification of the second source. (a) 1,4-dioxane concentration and groundwater level distribution changes over time for Case-16; (b) comparison of the calculated concentration changes over time at each pumping well with the monitoring results (Cases-01, 15-18).

Figure 3-8(b) compares the monitoring results with the concentration changes over time in each pumping well obtained in Cases 15 through 18. The results from Case-02 are also shown in this figure. Prior to pumping in April 2015, concentrations in A-2 had gradually been increasing since April 2013 and were beyond the environmental standard, while concentrations in A-5 remained below the standard, although a slight increase was observed. The change in concentration in A-5 during this phase is consistent with the interpretation of the concentration distribution shown in Figure 3-8(a), which is due to the lateral spread of the contamination plume. A significant increase in the concentration in A-5 was observed with the start of pumping, and the concentration in A-4 also increased once, due to a spatial relationship with CSA-2.

After that, with the end of 1,4-dioxane inflow from CSA-2 to the aquifer in December 2016, the concentrations in both wells showed a decrease. This trend of concentration changes is regardless of $Q_{nwi,1}$, and indicate that the monitoring results have been well reproduced. Especially for Case-16, with $Q_{nwi,1}$ set to 2.00 kg, the calculated results show that concentration levels in A-2 and A-5 approximate the monitoring results. It also confirms that the spreading of the contamination plume originating from CSA-2 has little effect on the concentration change in A-6, which is located downstream. Based on the above results in Step 2, in addition to the conditions obtained in Case-02 for CSA-1, the conditions obtained in Case-16, which best reflect the concentration changes in A-2 and A-5, are adopted in Step 3 for the set of conditions for CSA-2.

3.2.3 Step 3: Placement of contamination source CSA-3 near the center of Area A

In step 3, we perform the analyses with the newly placed CSA-3 in addition to CSA-1 in step 1 and CSA-2, using the concentration changes in A-1 and A-3 as indicators as well. From monitoring results, after the chemical treatment in the central part of Area A corresponding to CSA-3 was conducted in May 2020, a significant decrease in the concentration in A-1, which is close to CSA-3, was observed. According to the monitoring results and groundwater level distribution shown in Figure 3-3, based on the interpretation that the presence of CSA-3 has little effect on the concentration change at A-2 and A-5, and the increase in concentration at A-3 is caused by the southward advection and dispersion originating from CSA-3, through multiple repeated preliminary analyses, the CSA-3 area A_{cs} was set to 400 m^2 (20×20 m) and placed in the range of x= 65 to 85 m and y= 355 to 375 m across the watershed just near A-1. The period of 1,4-dioxane inflow from CSA-3 to the aquifer was assumed to be 8.4 years from January 2012 to May 2020, when a significant decrease in concentration at A-1 was confirmed by the application of the chemical method. The analyses were conducted by changing the amount of 1,4-dioxane inflow $Q_{nwi,1}$ in four steps: Case-19: 3.00 kg, Case-20: 6.00 kg, Case-21: 12.0 kg, and Case-22: 24.0 kg.

As a representative result, Figure 3-9(a) shows the changes in 1,4-dioxane concentration and groundwater level distribution over time obtained for Case-20 when $Q_{nwi,1}$ is set to 6.00 kg. Before and after the extension of the impermeable wall in July 2014 and the startup of pumping at A-5 in April 2015, the distribution of radial groundwater flowing directly from the center of Area A did not change significantly. Accordingly, the area where 1,4-dioxane concentrations increased spread over time. Both A-1 and A-3 were contained within this area in January 2013. Especially because the concentration on the north side of CSA-3 is higher, it indicates that the contamination plume originating from CSA-3 spreads mainly toward A-1 on the north side.
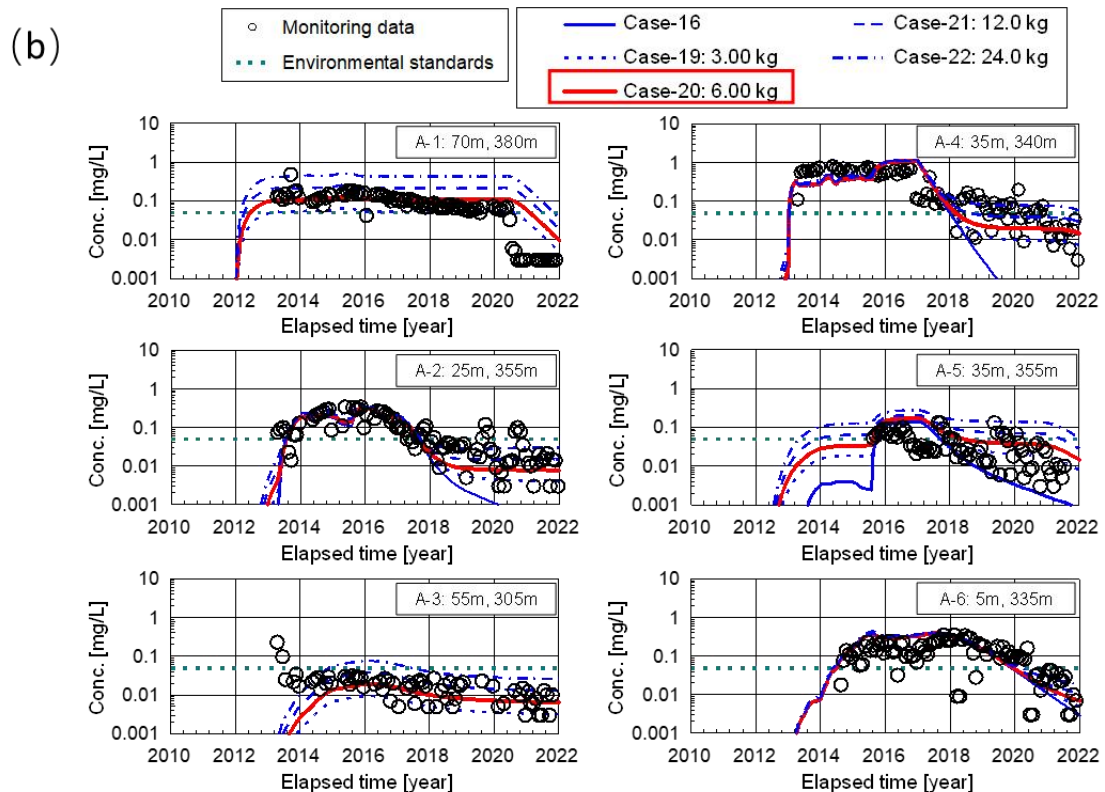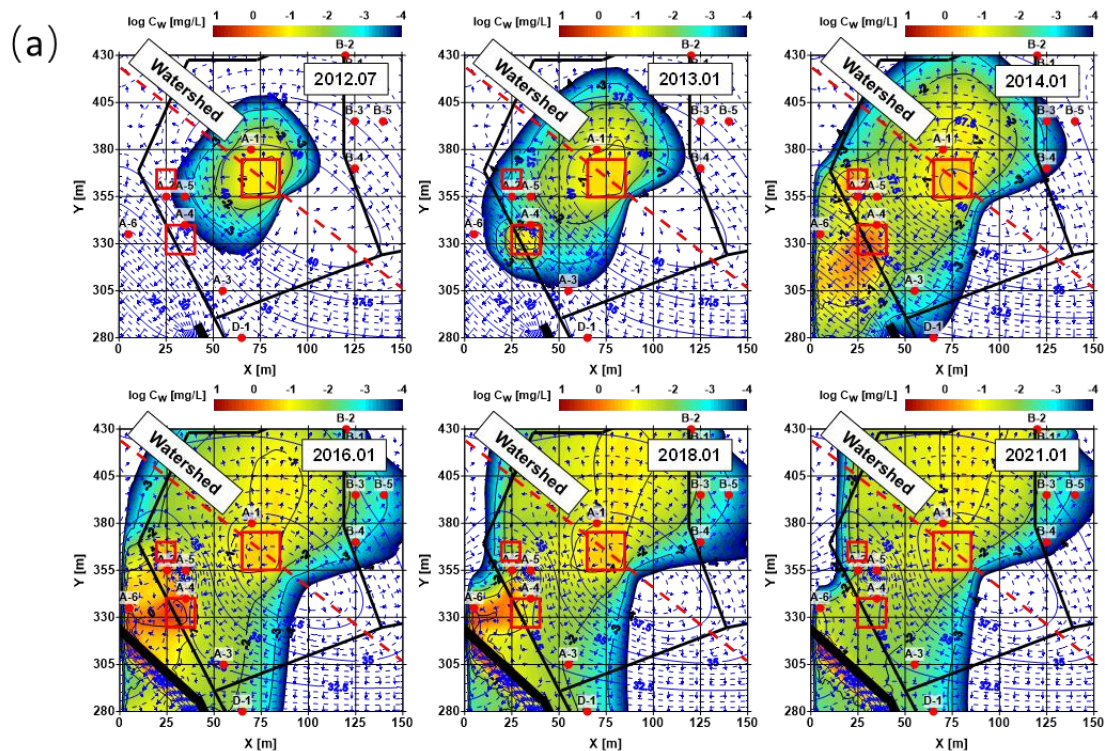
Figure 3-9 Verification of the third source. (a) 1,4-dioxane concentration and groundwater level distribution changes over time for Case-16; (b) comparison of the calculated concentration changes over time at each pumping well with the monitoring results (Cases-01, 15-18).

45

Figure 3-9(b) compares the monitoring results with the concentration changes over time in each of the pump wells obtained in Cases 19 through 22. This figure shows that the concentration in A-1 was beyond environmental standards for eight years, beginning in January 2012, and then decreased significantly with the end of inflow to the aquifer in May 2020. In addition, an increase in concentration was observed in A-3 due to advection and dispersion of 1,4-dioxane over a large area in Area A (see Figure 3-9 (a)). Compared to Case 16, the increase in A-5 occurred earlier in Cases 19 through 22, and the decrease in concentration in each well after the cessation of 1,4-dioxane inflow from each contamination source was relatively slower. However, the concentrations change at a lower level than the standard. Thus, the effect of advection/dispersion from CSA-3 on the concentration changes in A-2, A-4, A-5, and A-6 can be considered relatively small. These behaviors are common regardless of the values set for $Q_{nwi,1}$, and the trend of concentration change obtained from monitoring results are well reproduced. In particular, the results of Case-20, with $Q_{nwi,1}$ set to a value of 6.00 kg, showed the best matching with monitoring results for concentration levels in A-1 and A-3.

From the results of Steps 1 to 3, the final matching of spatial-temporal changes in 1,4-dioxane concentrations in the aquifer for area A was made based on the calculation conditions of Case-20 slightly by adjusting the amount of 1,4-dioxane inflow, $Q_{nwi,1}$, and the inflow period for better reproducing. In the series of analyses, the boundary condition for the termination of inflow into the aquifer was given based on the actual results of remediation measures. However, because the decrease in concentration in the monitoring results is slower compared to the results of Case-20, it is reasonable to think that the inflow into the aquifer may continue, although only slightly. Therefore, the boundary condition should be defined newly for subsequent inflows as well. In addition, the distribution of $Q_{nwi,1}$ within each contamination source, and its time variation was also partially considered to better reproduce the concentration changes at each pumping well. Moreover, to reproduce the rapid decrease in concentration just after April 2013 at A-3, CSA-4 was placed as an additional contamination source at x=55-65 m and y=305-315 m upstream of A-3. The conditions for the inflow of 1,4-dioxane into the aquifer at each contamination source are shown in Table 3-2.

Table 3-2 The conditions for the inflow of 1,4-dioxane into the aquifer at each contamination source

Source	Period	$Q_{nwi,1}$ (kg)
CSA-1	2013.1~2014.12	1.00 (x=25~40 m, y=325~335 m) 4.00 (x=25~40 m, y=335~340 m)
	2015.1~2016.12	2.50

	2017.1~2020.12	0.66
CSA-2	2013.7~2016.6	1.50
	2016.7~2022.12	0.30
CSA-3	2012.1~2015.12	4.00
	2016.1~2020.4	2.00
CSA-4	2012.11	0.25

Furthermore, we interpreted that the remediation measure to the aquifer, in addition to the surface soil by application of chemical treatment, had also been achieved based on the rapid decrease in concentration after May 2020 in A-1 and introduced the attenuation rate by Eq. 17 within the range of CSA-3 for better reproduction of the concentration change in A-1. The final matching results for area A are shown in Figure 3-10.
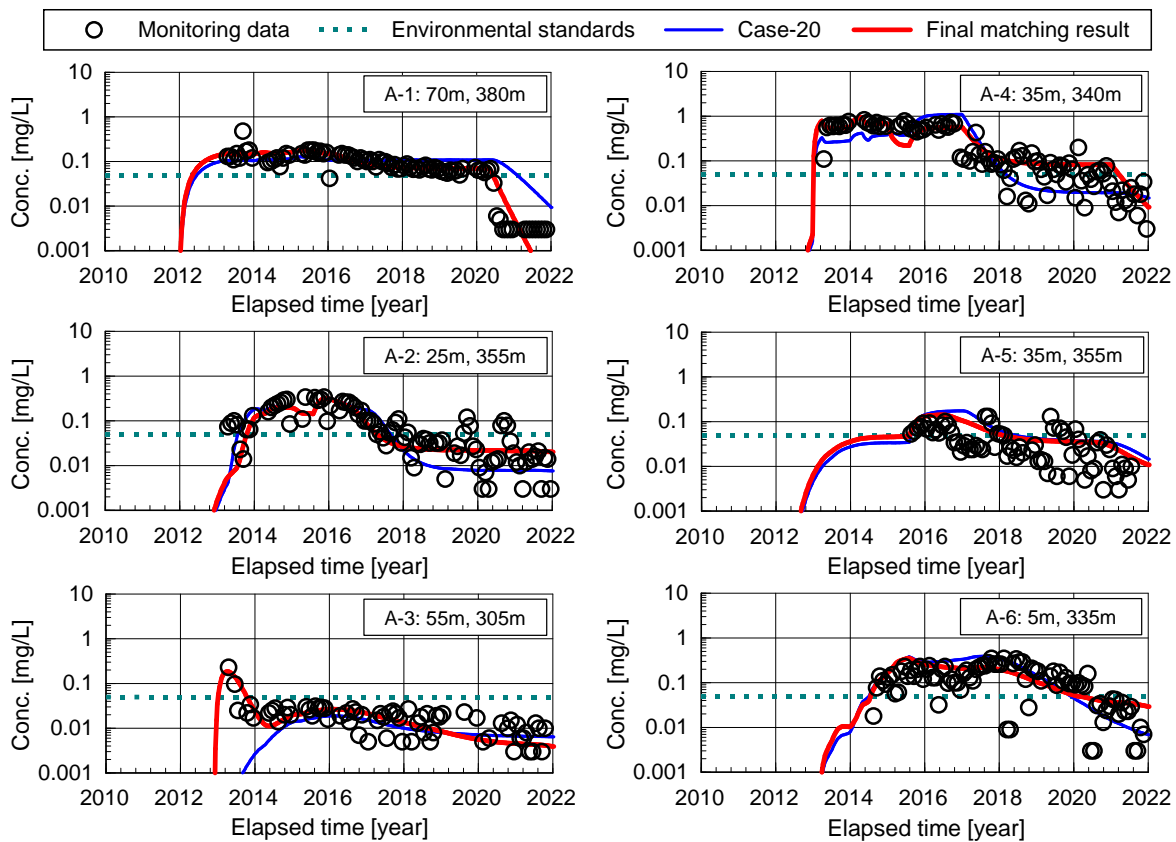

Figure 3-10 The final matching results for area A. Comparison of the calculated concentration changes over time at each pumping well for Case 20 with the monitoring results.

3.3 Validity of the simulation results and evaluation of the effectiveness of the impermeable wall and pumping

From the history matching process described in the previous sections and taking into account the major remediation activities conducted since 2014 at the boundaries of Areas A and B, the history matching for the changes in 1,4-dioxane concentrations throughout the area was also conducted by defining the surface contamination sources in other areas. The changes in 1,4-dioxane concentration, the distribution of groundwater levels, and the example results of the history matching for each pumping well are all shown in Figure 3-11. Furthermore, this study successfully conducted history matching of data in 14 areas, incorporating 50 monitoring data points. The study achieved this by considering 28 sources under non-stationary conditions. The detailed information on the source conditions and results of historical matching with the distribution of 1,4-dioxane can be found in the Appendix.

The contamination plume spread behavior in each area follows the interpretation of Figure 3-3. Even for the location where multiple contamination plumes occur, such as M-2 (x=150m, y=110m) and N-1 (x=150m, y=65m), the changes in the concentrations can be well-reproduced.
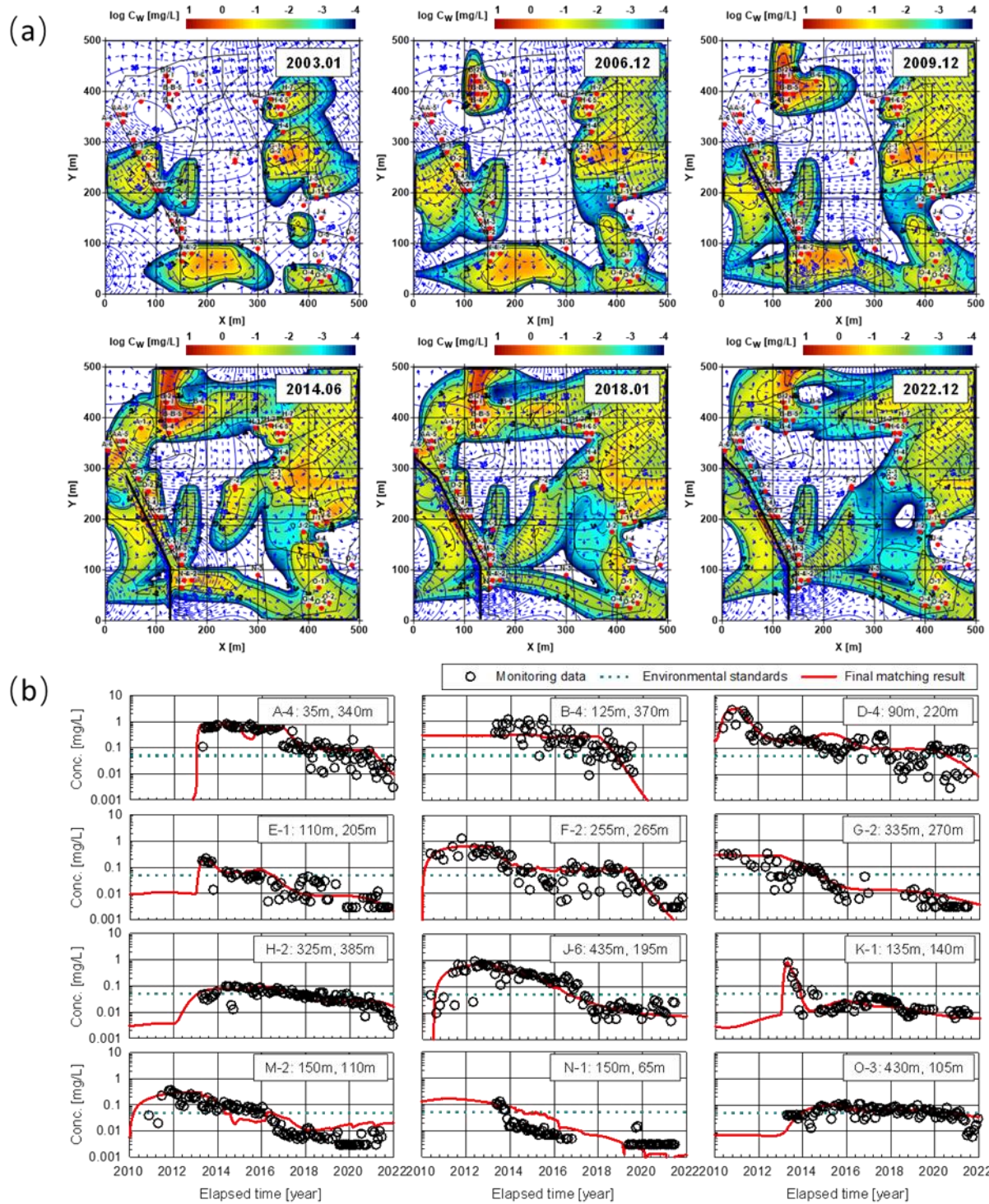
Figure 3-11 Comprehensive reproduction results of Iwate site and simulation of contaminated situation from 2010 to 2022.

49

The measured and calculated amount of total 1,4-dioxane recovery for the period from April 2013 to March 2014, when total 1,4-dioxane recovery by pumping was recorded, were compared in Figure 3-12. The measured total recovery in February 2014 was 7.37 kg, while the calculated total recovery was 8.64 kg, which generally reflected the trend of increased recovery of 1,4-dioxane by pumping. The calculated results of the distribution of 1,4-dioxane concentrations at the site, at least in April 2013 when pumping began throughout the area, reflect the actual contamination situation both temporally and spatially. Thus, the reliability of the historical matching was confirmed, and the calculated results were considered fully applicable for quantitative assessment of remedial actions as well as for prediction of future contamination levels.
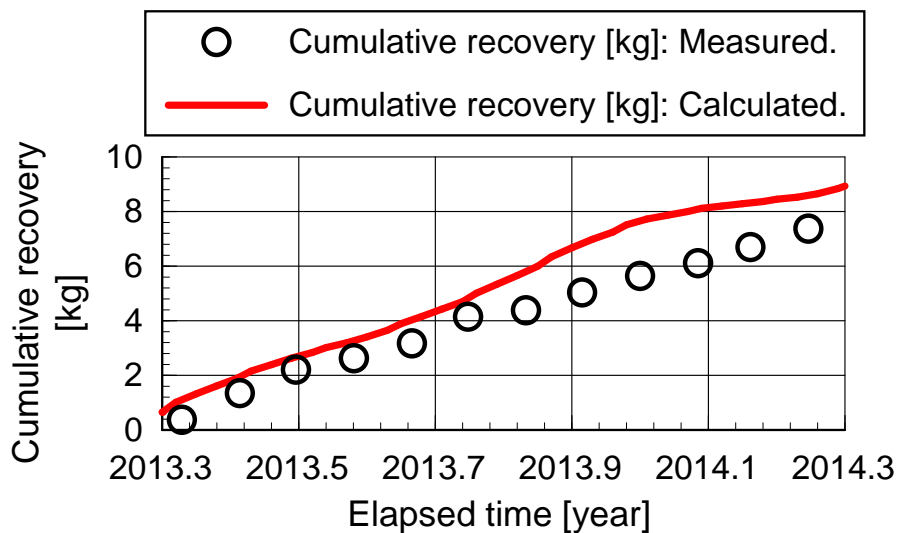

Figure 3-12. The measured and calculated amount of cumulative recovery of 1,4-dioxane for the period from April 2013 to March 2014.

Figure 3-13 shows the areas that exceed the environmental standard and pose a health risk at the end of 2022 in the case of remediation measures. For the health risk determination, the groundwater was assumed to be consumed as drinking water, and the daily exposure [mg/kg/day] was calculated by dividing the cumulative exposure $EC_{w,1}$ [mg] by the exposure time, 32 years ($ETime$=11680 days), and the body weight $BWeight$ [kg]. In Japan, there is no standard value for chronic toxicity, and 0.05 mg/L corresponding to the environmental standard is taken as a temporary reference value. Therefore, the daily exposure amount per 1 kg of body weight is divided by the oral reference dose ($ORfD_1$ [mg/kg/day]) according to U.S. EPA, which is defined as the risk level, and when the risk level exceeds 1, it is judged as risky according to the following formula.

$$\text{Risk level} = \left.\frac{EC_{w,1}}{BWeight \times ETime}\right/ORfD_1 \qquad (3\text{-}1)$$

Here, the $ORfD_1$ value of 1,4-dioxane is 1.60×10^{-2} mg/kg/day, and the $BWeight$ and daily water intake are set to 50 kg and 2 L/day, respectively, according to the Ministry of Health, Labor and Welfare and Environment Agency (Japan). As the figure shows, almost the entire area within the site has been remediated below the environmental standard by the end of 2022. In addition, it has been reported by Iwate Prefecture that the areas on the north side of Areas A and B and the off-site areas on the east side of Areas I and J have also exceeded the standard. Although not included in this analysis, Iwate Prefecture has taken additional measures. In addition, the areas identified to be risky were limited to Area B and its north side; even in areas exceeding the environmental standard, the health risk was judged to be generally low, confirming the fact that the remediation measures taken by Iwate Prefecture were sufficient.
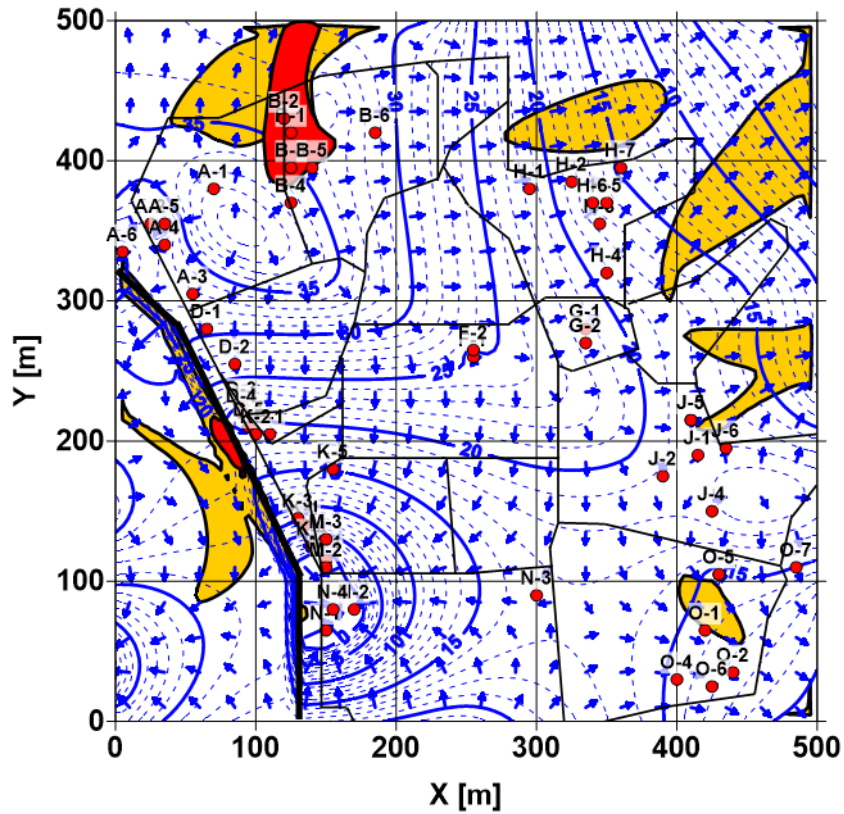

Figure 3-13 The areas that exceed the standard and pose health risk at the end of 2022 in the case with remediation measures.

51

3.4. Conclusion

The feasibility and effectiveness of the modeling process was confirmed. It can be used to identify the most likely multiple contamination sources, and the historically monitored spatial-temporal 1,4-dioxane concentration changes in the aquifer of the site were precisely reproduced through historical matching. Previous remediation measures did successfully eliminate groundwater pollution.; however, in some area, the remediation efficiency is possible to be further improved by applying the developed model.

Chapter 4 Evaluation and improvement on the groundwater remediation measures

4.1 Introduction

According to the findings from Chapter 3, the simulation results indicate the potential distribution of 1,4-dioxane groundwater pollutant and demonstrate the impact of previous remediation measures on the transport behavior of 1,4-dioxane in the illegal waste dumping site. Despite the significant efforts made through previous remediation measures and management practices to prevent the flow of pollutants beyond the prefecture border, all the measures taken without adequate understanding of pollutant transportation and the impact and effectiveness of each remediation measure on pollutant transport and removal have not been evaluated.

The simulation results of the current situation (as of 2023), as depicted in Figure 3-13, indicate that high concentrations of 1,4-dioxane continue to persist in certain areas of the dumping site, surpassing environmental standards and presenting a substantial threat to human health. Furthermore, owing to the uncertainty in pollutant transport within the site, some pumping operations have low efficiency. All these factors underscore the potential for enhancing the remediation measures implemented based on the model developed in this study.

To develop an effective pumping plan for pollutant removal from groundwater, several considerations should be addressed. Understanding pollutant distribution and groundwater flow is crucial for optimal well placement (Freeze and Cherry, 1979), which can be reproduced and predicted using the modeling that was developed in Chapters 2 and 3. By incorporating these proposals, the pumping plan can be enhanced to maximize the capture of contaminated groundwater and improve the overall effectiveness of the pump and treat system.

This chapter aims to evaluate the previous remediation measures and to improve the remediation plan using the developed numerical modeling and the simulation results of distribution of 1,4-dioxane pollutant.

4.2 Methodology

4.2.1 Evaluation of previous remediation measures

Two remediation measures are evaluated in this chapter: the installment of impermeable walls (in 2014 and 2017) and pumping operations (from 2011 to 2022). To assess the effectiveness of these remediation measures, the study considers three distinct situations:

1) Situation without any remediation measures. This scenario represents the conditions where no specific remediation actions were taken.

2) Situation with only the installment of an impermeable wall. This evaluates the impact of solely implementing an impermeable wall as a remediation measure.

3) Situation with both the pumping operation and the installment of an impermeable wall. This scenario considers the combined effects of the pumping operation and the installation of the impermeable wall.

The evaluation criteria include 1,4-dioxane removal (by pumping), residue of 1,4-dioxane inside the site and out flow of 1,4-dioxane at boundaries.
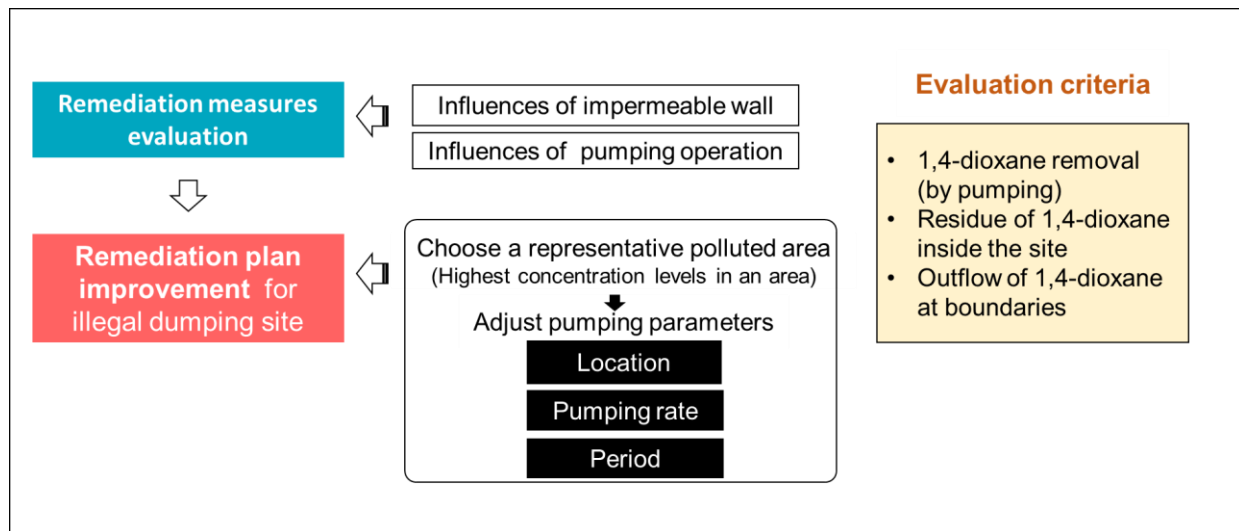

Figure 4-1 Flow chart of remediation improvement

4.2.2 Improvement of pumping operation

Based on the area exceed standard and risk map from Figure 3-13, it was identified that there is room for improvement in the previous remediation measures, particularly in the pumping operation. In this study, the aim is to enhance the pumping plan using numerical modeling. The focus on testing various pumping

parameters, including the location of pumping wells, the pumping rate, and the duration of the pumping operation. By utilizing numerical simulations, the pumping plan can be improved and optimized to more effectively remove contaminants from the illegal waste dumping site. The simulation results from this study can also serve as valuable guidance for similar sites facing contamination issues or as a reference for developing pumping plans prior to implementing remediation measures.
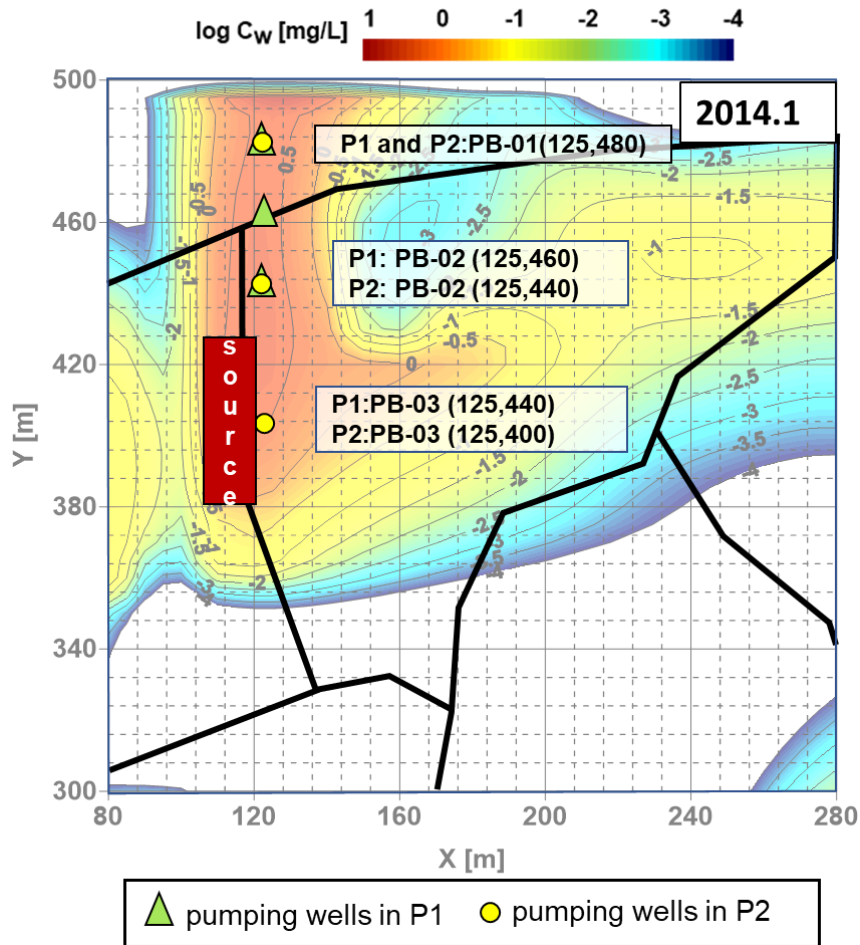

Figure 4-2 Simulation results of 1,4-dioxane situation in representative B-area (2014.01) with the location of pumping plan

To improve the remediation process, this study focuses on the "B-area" as a representative area to assess the efficiency and effectiveness of the pumping plan. Figure 4-2 provides a visual representation of this area, while Table 4-1 presents the specific pumping plan parameters that are examined, including pumping location, pumping rate, and pumping period. Parameters P-01 and P-02 of the pumping plan evaluate the effects of different pumping locations by assuming distances between pumping wells of 20 m and 40 m, respectively. P-2-1, P-2-2, and P-2-3 explore the impact of different pumping rates of 20, 30, and 50 m^3/d,

respectively. P2-3-1 further investigates the effect of different pumping rates in different pumping wells. Lastly, P3 examines the cessation of pumping operations in PB-01 and PB-02 in 2016 and 2017, respectively.

By analyzing the results obtained from these various pumping plan scenarios, this study aims to identify the most effective combination of pumping parameters to optimize the remediation process and reduce the concentration of contaminants in the targeted B-area.

Table 4-1 Improved pumping plan in B-area

Plan	Pumping rate (m^3/d)			Distance between pumping	Period
	Well PA-01	Well PA-02	Well PA-03		
P1	10	10	10	20 m	2013-2023
P2	10	10	10	40 m	
P2-1	20	20	20		
P2-2	30	30	30	40 m	2013-2023
P2-3	50	50	50		
P2-3-1	20	30	50	40 m	2013-2023
P3	20	30	50	40 m	2013-2016
	0	30	50		2016-2017
	0	0	50		2017-2023

4.3 Evaluation of previous remediation measures

4.3.1 Impacts of impermeable wall installation

Figure 4-3 illustrates the distribution of 1,4-dioxane pollutants in two scenarios: without any remediation measures and with only the installment of an impermeable wall. The purpose of installing the impermeable wall is to prevent the transport of 1,4-dioxane pollutants to other prefectures. The simulation results indicate that the impermeable wall effectively prevents the horizontal transport of 1,4-dioxane pollutants beyond the wall towards the south side direction.

However, the simulation results also reveal an unexpected effect of the impermeable wall. It increases the hydraulic gradient of the site, as depicted in Figure 4-3. This increase in hydraulic gradient leads to the acceleration of groundwater flow and consequently enhances the transport of 1,4-dioxane pollutants. As a result, the concentration of 1,4-dioxane residues in the area with only the installment of the impermeable wall is higher compared to the scenario without any remediation measures, as shown in Figure 4-4. This finding highlights the importance of considering the unintended consequences of remediation measures and the need for a comprehensive evaluation of their effectiveness in addressing contamination issues.
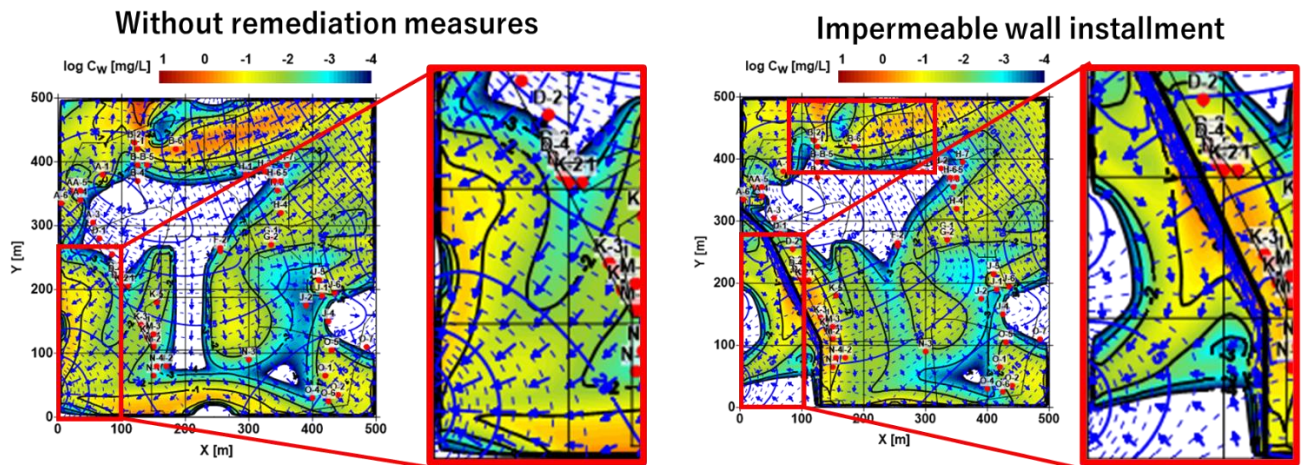

Figure 4-3 effects of impermeable installment

4.3.2 Impacts of previous pumping operation

Figure 4-4a depicts the effectiveness of the previous remediation measures in eliminating approximately 80 kg of 1,4-dioxane pollutants from a total input of 160 kg of 1,4-dioxane in the illegal waste dumping site. This result highlights the efficiency of the previous remediation measures, as they have successfully reduced more than half of the total amount of 1,4-dioxane present in the site. However, the simulation results of the 1,4-dioxane distribution in 2023 (Figure 4-3) indicate that certain areas of the site exhibit inefficient pumping operations. This inefficiency may be attributed to inappropriate pumping locations and inadequate pumping rates. These findings emphasize the need for improvements in the pumping plan, including optimizing the selection of pumping locations and adjusting pumping rates, to enhance the overall efficiency and effectiveness of the remediation measures.
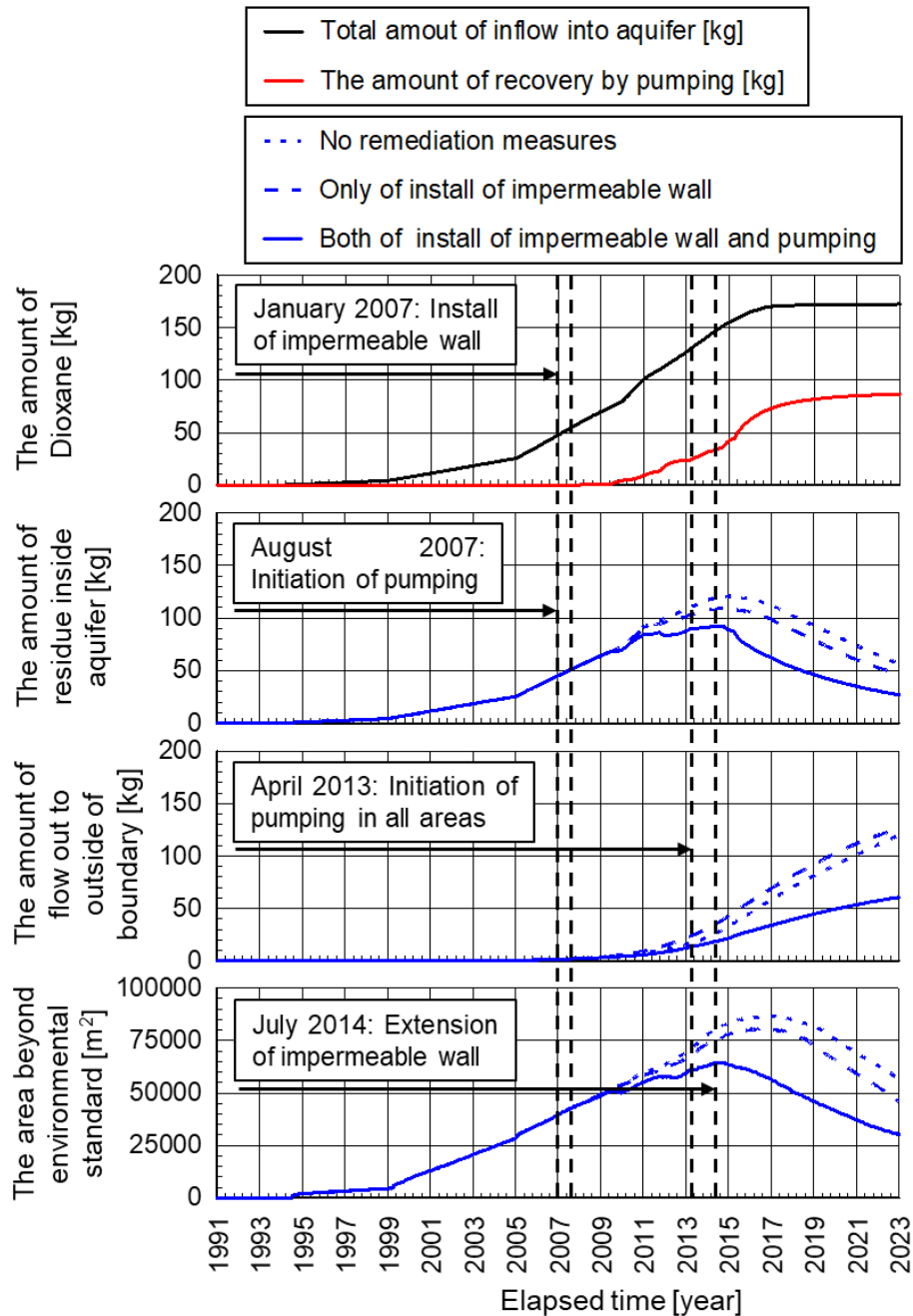
Figure 4-4 comparison of the outflow of 1,4-Dioxane amount at each boundary over the time

4.4 Improvement on pumping operations

4.4.1 Pumping well placement

To evaluate the effects of pumping well placement/distance, two plans were designed and assessed. Plan 1 (P1) with a 20 m distance between each pumping well and P2 with a relatively longer distance, with

a 40 m distance between pumping wells, all the pumping wells were located inside the area with 1,4-dioxane contamination.

Figure 4-5 illustrates the total removal accumulation of 1,4-dioxane for these two different pumping plans, namely P1 and P2. The results indicate that for P2, with the greater distance between pumping wells, exhibits higher total removal of 1,4-dioxane compared to P1. In particular, P2 demonstrates a total removal quantity of 56.56 kg of 1,4-dioxane, whereas P1 exhibits a slightly lower total removal quantity of 53.62 kg of 1,4-dioxane. This demonstrates that P2 exhibits a higher rate of 1,4-dioxane removal in comparison to P1.

Furthermore, the simulation results depicted in Figure 4-6 indicate that pumping plan P1 can effectively reduce the concentration of 1,4-dioxane in a limited area, particularly during the initial stages of the pumping operation, in contrast to pumping plan P2. Following the initial pumping phase, the migration of the 1,4-dioxane plume from its source to the pumping well requires a certain amount of time. This temporal delay is the primary factor contributing to the slower removal rate of 1,4-dioxane in P1 compared to P2, as observed since 2014.

From these findings, it can be concluded that the pumping plan with a relatively far distance between pumping wells, which in the case of area B in this study is 40 m (P2), is more effective in removing 1,4-dioxane. Therefore, P2 will be used for further examination of pumping rate operations in the subsequent steps of the study.
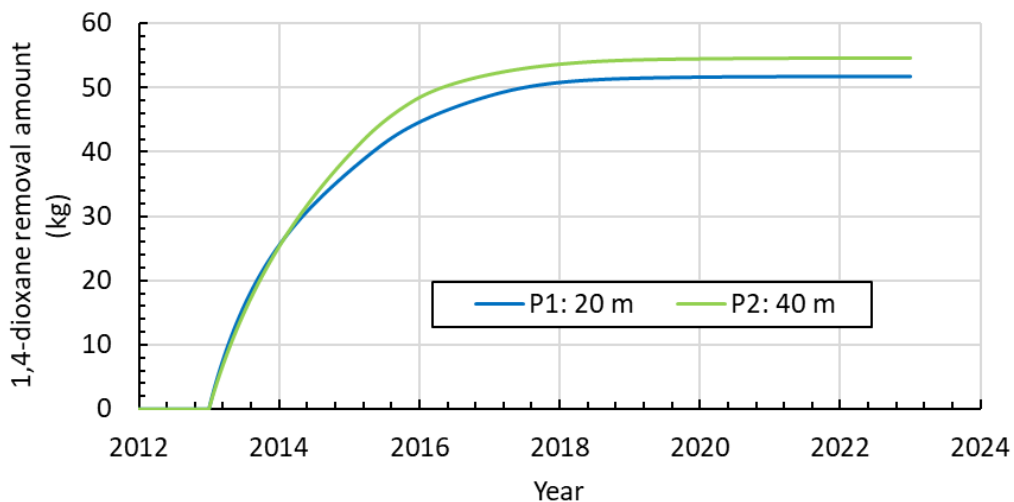

Figure 4-5 Accumulation results of 1,4-dioxane removal in different distance of wells
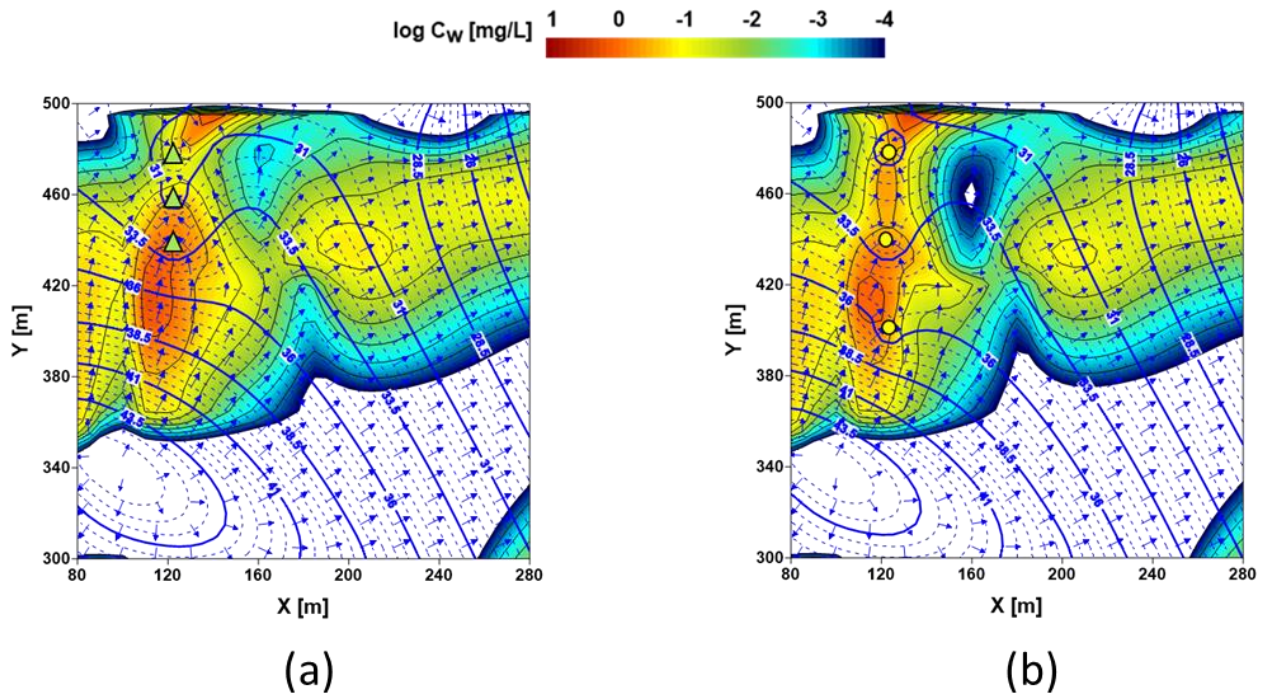
Figure 4-6 the simulation results of pumping plan operation in B-area a) Pumping plan P1 (20 m distance between pumping wells) b) Pumping plan P2 (40 m distance between pumping wells

4.4.2 Pumping rate adjusting

Different pumping rates were also tested to find the optimum one for 1,4-dioxane removal, using the pumping locations in P2 plan. Three pumping rate options were tested: P2-1 at 20 m^3/d, P2-2 at 30 m^3/d, and P2-3 at 50 m^3/d.

Table 4-2 presents the calculated results. Generally, higher pumping rates lead to a greater amount of 1,4-dioxane removal (kg), as expected. Nevertheless, the investigation also unveiled a contrasting pattern in terms of removal efficiency for pumping per unit of groundwater. Notably, despite the augmented quantity of 1,4-dioxane eradicated through higher pumping rates, there was a reduction in the removal efficiency from 0.51 to 0.13 kg/1000 m^3. This observation implies that while escalating the pumping rate may augment the total amount of removal, it may not necessarily yield a commensurate enhancement in removal efficiency.

Table 4-2 Difference high pumping rate operation on the pumping plan

Plan name	Pumping rate (m^3/d) 10 years operation (2013-2023)				
	PB-01 (m^3/d)	PB-02 (m^3/d)	PB-03 (m^3/d)	1,4-dioxane removal amount (kg)	Removal efficiency (kg/1000 m^3)
P2	10	10	10	56.56	0.51
P2-1	20	20	20	63.92	0.29
P2-2	30	30	30	66.53	0.20
P2-3	50	50	50	68.96	0.13

The results depicted in Figure 4-7 highlight the importance of carefully considering the pumping rate for each well for 1,4-dioxane removal. The pumping well near the pollution source (PB-03) consistently showed an expected increase in the removal amount with higher pumping rates. Interestingly, the pumping well far from the source (PB-01) displayed a different trend, a high pumping rate of 50 m^3/d resulted in a lower removal amount of 1,4-dioxane compared to the lower pumping rates.

These findings suggest that a lower pumping rate operation in the well far from the source may be more appropriate for effectively eliminating 1,4-dioxane pollutant. As a next step, the pumping rate in each pumping well was separately determined to further increase its efficiency in 1,4-dioxane removal while maintaining a high effective removal amount.
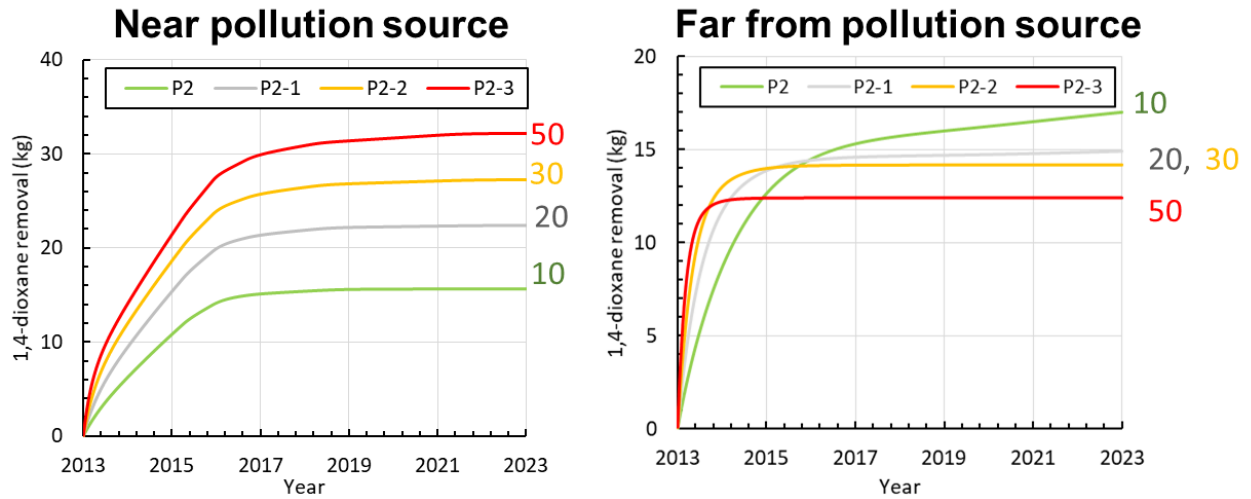
Figure 4-7 Accumulation of 1,4-dioxane removal amount in well far from pollution source PB-01 and well near pollution source

The pumping rates were set with a low rate for the well far from the pollution source and gradually increasing towards the well near the source, as outlined in Table 4-3. Specifically, P-2-1 involved a pumping rate of 20 m^3/d in PB-01, 30 m^3/d in PB-02 and 50 m^3/d in PB-03.

The accumulation of 1,4-dioxane removal amount results in Figure 4-8 indicates that there is only a slight difference between P2-3 and P2-3-1. However, the removal efficiency of P2-3-1 was 1.5 times greater than that of P2-3. This suggests that a high pumping rate for all pumping wells may not always correspond to higher removal efficiency, and thus not necessarily result in optimal pumping operation for groundwater pollutants removal. This can be considered for other contaminated sites remediation as well.

Table 4-3 Comparison between high pumping rate with the different pumping rate

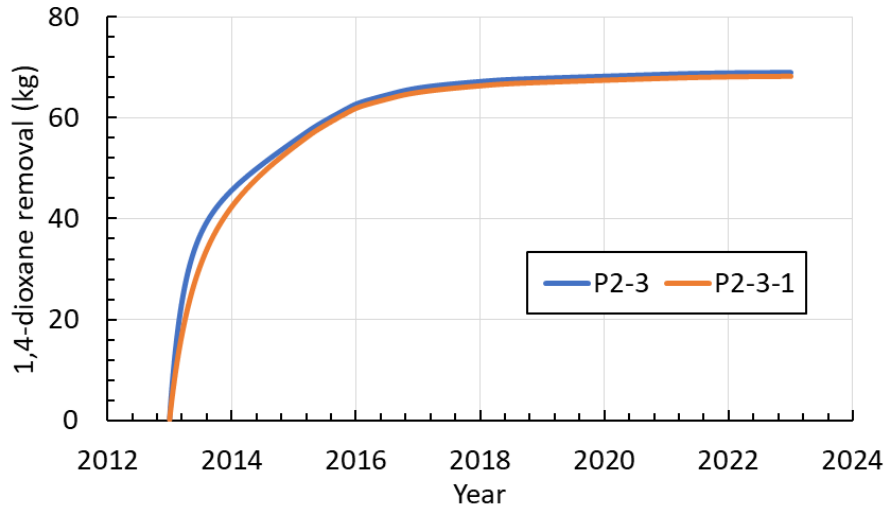| Plan name	Pumping rate (m^3/d) 10 years operation (2013-2023)				
	PB-01 (m^3/d)	PB-02 (m^3/d)	PB-03 (m^3/d)	1,4-dioxane removal amount (kg)	Removal efficiency (kg/1000 m^3)
P2-3	50	50	50	69.2	0.126
P2-3-1	20	30	50	68.2	0.187

Figure 4-8 Ability of pollutant extraction between P2-3 plan and P2-3-1 plan

Further analysis was conducted to understand the removal amount of 1,4-dioxane in each pumping well as a function of time. The results are shown in Figure 4-9 and indicate that in well PB-01, which is far from the source location, the total removal amount remains stable from 2015 to 2018. Similarly, well PB-02 showed a similar trend for total removal amount, which almost stopped from 2016 to 2018. And Figure 4-10 illustrate the concentration of 1,4-dioxane near three pumping wells, the results show the concentration of 1,4-dioxane in PB-01 and PB-02 rapidly decreased and met the environmental standard in 2015 and 2016, respectively.

This suggests that pumping from these two wells, starting from 2016 and 2017 respectively, may be ineffective and could be shut shown to obtain a higher removal efficiency. In contrast, well PB-03 continued to accumulate efficient removal amounts of 1,4-dioxane from 2013 to 2018.
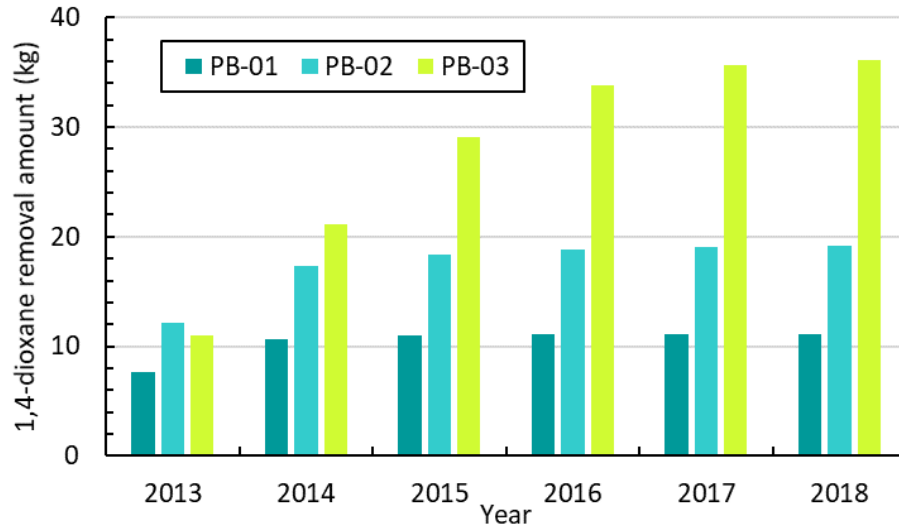
Figure 4-9 Accumulate 1,4-dioxane removal from each pumping well (PB-01, PB-2, and PB-03) when applying P2-3-1 plan
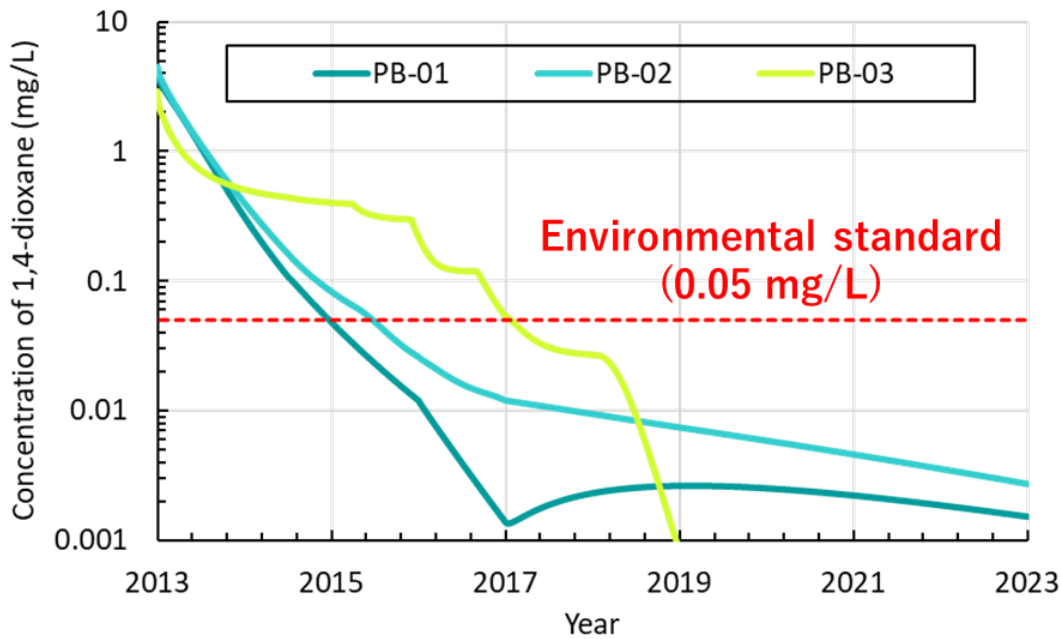

Figure 4-10 Concentration of 1,4-dioxane around pumping wells (PB-01, PB-02, and PB-03) when applying P2-3-1 plan

4.4.3 Pumping period adjusting

Based on the calculated accumulated 1,4-dioxane removal amounts, shutting down ineffective pumping wells was suggested to obtain a higher 1,4-dioxane removal efficiency; i.e., shutdown well PB-01 from 2016

and well PB-02 from 2017, as indicated in the P3 plan outlined in Table 4-4. A comparison between pumping plans P2-3-1 and P-3 is also shown in Table 4-4. The total accumulation of 1,4-dioxane removal amount is only slightly decreased from 68.23 to 67.81 when shuting shown two pumping wells, while the removal efficiency of the latter is significantly higher, being 1.5 times greater. Therefore, P-3 plan ends up with a higher 1,4-dioxane removal amount and not just a high removal efficiency.

Table 4-4 Period of pumping operation consideration

| Plan | Pumping rate (m³/d) 10 year operation (2013-2023) | | | | | |
	PB-01 (m^3/d)	PB-02 (m^3/d)	PB-03 (m^3/d)	Time operate	1,4-dioxane removal (kg)	Removal efficiency ($kg/1000m^3$)
P2-3-1	20	30	50	2013-2023	68.23	0.187
P3	20	30	50	2013-2016	67.81	0.270
	0	30	50	2016-2017		
	0	0	50	2017-2023		

Furthermore, the accumulate pollutant removal amount from each pumping well shown in Figure 4-11 reveals 1,4-dioxane removal amount from 3 pumping wells did not show difference from 2013-2018, even stop opearating of well PB-01 and well PB-02.
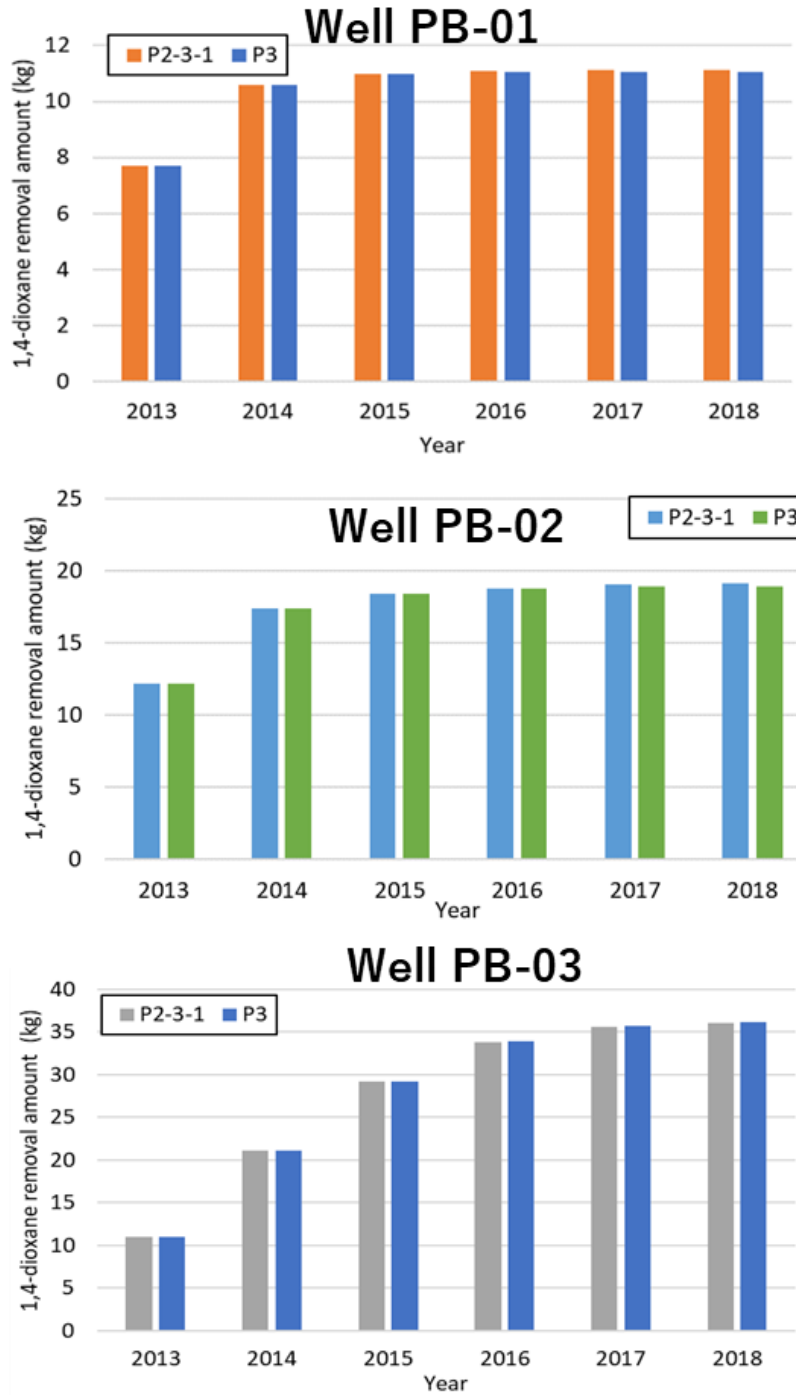
Figure 4-11 Cumulative of 1,4-dioxane removal amount in P3 pumping plan in each pumping wells

Nevertheless, the pumping plan results was operated in the multiple pollution sources conditions in whole area which might not be comparred the efficiency of pumping plan to the previous B-area pumping operation. Because of the influenced pollution source from A-area might effect to our pumping plan. Thus,

this study attempts to evaluate the P3 pumping plan in the only B-area source condition and be compared with previous pumping operation in B-area. This comparison will show our successful pumping plan which considers efficient 1,4-dioxane removal amounts and effective removal. Fortunately, the influence of pollution sourcec from A-area was less influence to pumping plan in B-area. However, the influence of pollution source from other area should be considered and suggest the remediation process to cope this scenario of contamination in an illegal waste dumping site.

The total removal, flow out, and residue amounts of 1,4-dioxane in B-area was calcuated and summarized in Figure 4-12. More than 75% of the total 1,4-dioxane amount could be removed in approximately 5 years of pumping operation when applying plan P3. In addition, the P3 results indicate a significant decrease in the residue of 1,4-dioxane inside B-area in comparison with the previous (historical) plan, with more than 16 kg 1,4-dioxane reduced in 4 years. Moreover, the residue of 1,4-dioxane under the previous remediation measures gradually decreased over a period of 10 years (2013-2023), which could be attributed to the flow out of the boundary.
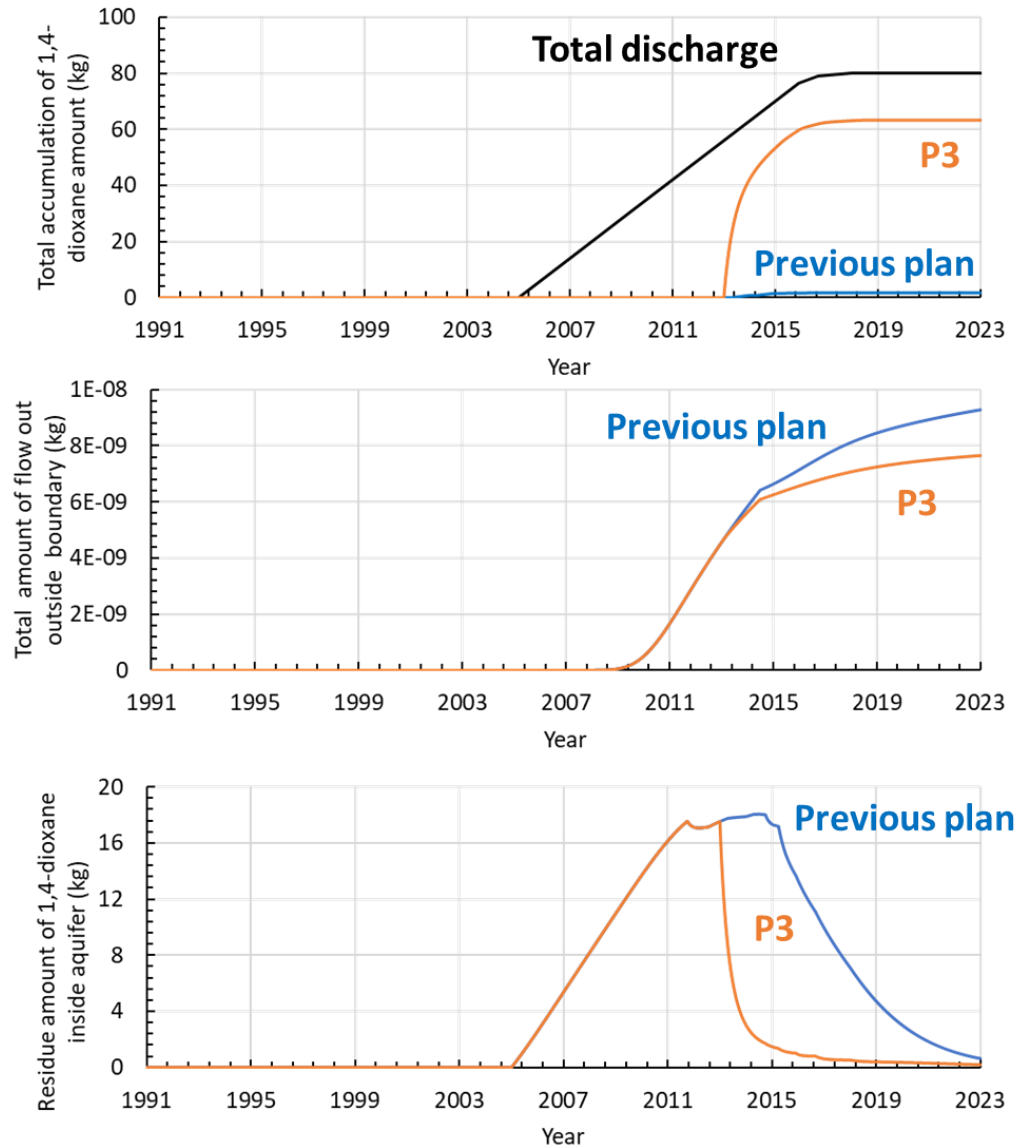
Fig. 4-12 Simulation results regarding the total removal amount, flow out amout and residue amount of 1,4-dioxane in P3 plan and previous plan in B-area

A numerical simulation on 1,4-dioxane distribution in 2023, with P3 applied from 2013, was conducted and results are shown in Figure 4-13. It should be noted that this kind of simulation is solely for numerical modeling to comprehend 1,4-dioxane transport behavior during pumping; it is acceptable that remediation measureare stopped when concentrations are below environmental standard or pose a health risk to the human body in reality. Figure 4-13a and Figure 4-13b show the distribution of 1,4-dioxane pollutant in B-area by applying the previous remediation and pumping plan P3, repectively (contuning pumping until the concentartion reached zero seem unrealistic). The results show P3 plan can remove the high concentration

68

of 1,4-dioxane in B-area compared with the previous remediation. Figure 4-13c and Figure 4-13d compared the area exceeds standard between previous remediation and P3 pumping plan. The results shows no areas exceeds the environmental standard in the aquifer when P3 is applied, whereas with the previous remediation, a significant number of areas still exceed the standard. Moreover, the area with residue 1,4-dioxane also significantly reduced when P3 is applied. However, some areas still exist with low concentrations, especially near the northern boundary with a trend of transport in the Eastern direction, as shown in Figure 4-13b. This can be addressed by: 1) extending the pumping operation of Plan P3 in both well PB-01 and PB-02, 2) continuing the pumping operation of well PB-01 with a low pumping rate from the year 2016, and 3) removing the remaining 1,4-dioxane through pumping operations in other areas.
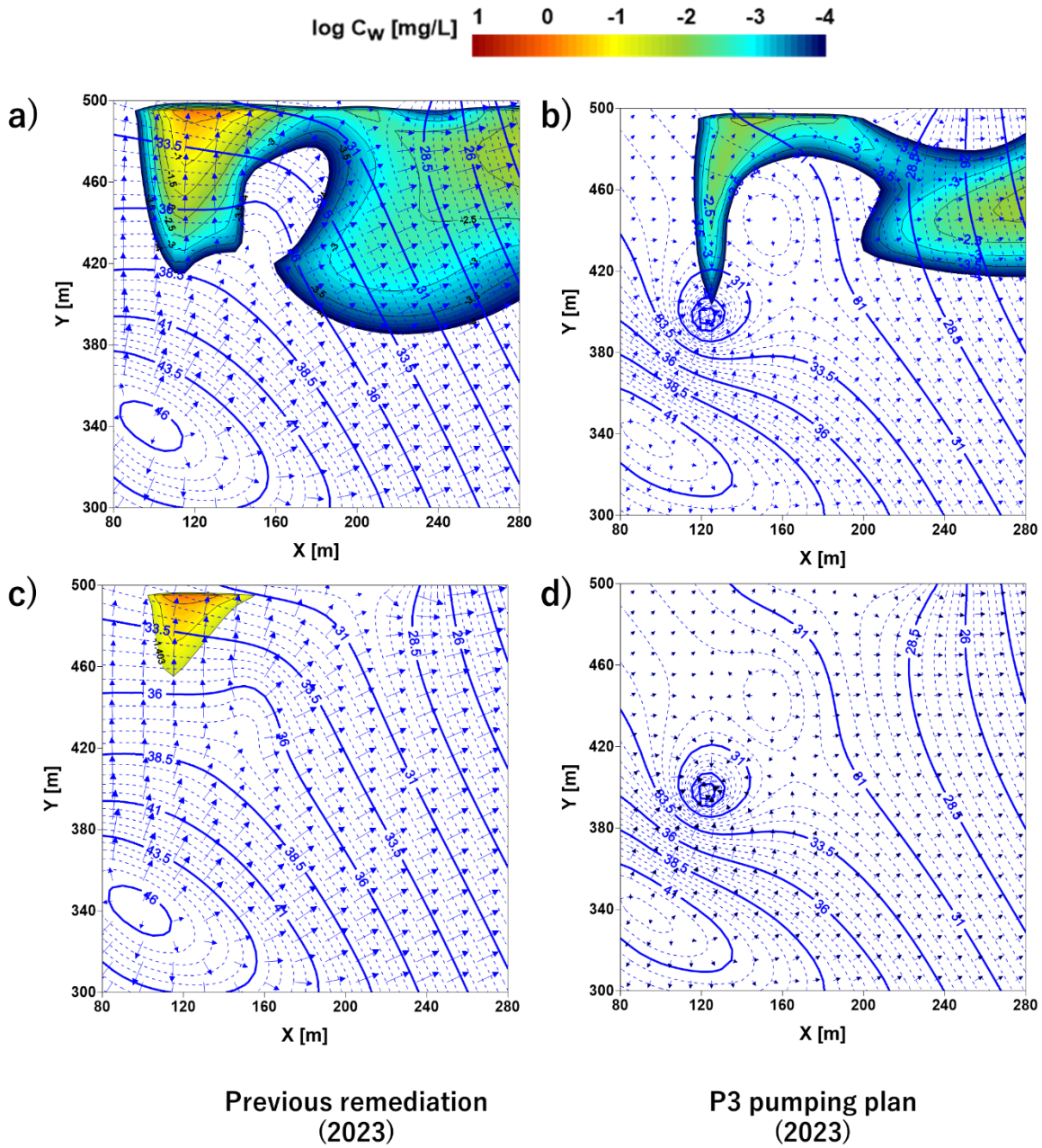
Figure 4-13 a) Distribution of residue 1,4-dioxane in previous remediation, b) Distribution of residue of 1,4-dioxane in P3 pumping plan, c) the area exceeds standard between previous remediation and, d) the area exceeds standard in P3 pumping plan

4.5   Conclusion of this chapter

Through numerical modeling, the impacts of remediation measures were clarified, and pumping processes were improved to increase the efficiency of pollutant removal. The evaluation of previous

remediation measures indicates that the installation of impermeable walls may inadvertently increase the transport of 1,4-dioxane and result in a runoff from the site due to the increased water head. Therefore, appropriate pumping measures are necessary when considering the construction of impermeable walls. The pumping process was improved by adjusting location, rate and period using the modeling developed in this study, with general suggestions given as follows: 1) placement of pumping wells at relatively long distances, 2) higher pumping rates near pollutant sources, but lower rates further away from sources, 3) timely shutdown (use a very low pumping rate) of wells further away from pollutant sources (when their pollutant removal efficiency drops below a threshold); all these combined can be effective in increasing pollutants removal efficiency.

Chapter 5 Conclusion

5.1 Conclusion of this study

In this study, an effective numerical model for predicting contamination was developed based on a review of groundwater flow direction distributions caused by remedial actions; that is, the construction of impermeable walls and pumping operations. The simulation first identified the most likely multiple sources of contamination, including the location, inflow volume, and period of each contamination source in the illicit waste site, as well as the adsorption coefficients. Based on these, the historically monitored spatial temporal 1,4-dioxane concentration changes in the aquifer of the site from the past to the present (1991–2022) were precisely reproduced through historical matching. Using this model, remediation measures were quantitatively evaluated and improved.

Chapter 2 of this study successfully established a numerical modeling approach that considered the effects of remediation measures (pumping operation and impermeable wall installment) on groundwater flow field calculations. The modeling also incorporated the calculation of pumping rates in each well, based on historical total water extraction volumes in each area. The simulation results provided insights into the potential flow of 1,4-dioxane pollutant in groundwater, demonstrating how the groundwater flow direction changed under the influence of remediation measures during the historical remediation period. This modeling approach proved valuable in reproducing the concentration levels and trends of 1,4-dioxane in monitoring wells, allowing for the prediction of the actual distribution of pollutant in the illegal waste dumping site.

Chapter 3 of this study addressed the complexity and challenges associated with multiple pollution sources in an illegal waste dumping site. It considered multiple and nonstationary source conditions using the successful numerical modeling framework established in Chapter 2. The simulation results, which accurately reproduce 1,4-dioxane concentration levels, indicated that the previous remediation measures implemented by Iwate municipality were effective in eliminating approximately half of the total 1,4-dioxane discharges. However, there was still room for improvement because certain areas did not undergo adequate pumping operations, and the pumping locations may not have been suitable for addressing the 1,4-dioxane pollution in the complex hydrogeological conditions of the site.

Chapter 4 of this study focused on evaluating and improving the remediation measures, particularly the pumping operation. The evaluation results demonstrated that the impermeable wall was successful in preventing groundwater pollutants from crossing the border into Aomori prefecture. However, the simulation results revealed an unexpected outcome, showing that the installation of the impermeable wall

alone increased the hydraulic gradient and accelerated the transport of groundwater pollutants compared to a no remediation scenario. Consequently, it is preferable to implement a pumping plan in conjunction with the impermeable wall to effectively eliminate groundwater pollutants. Furthermore, the evaluation of pumping operations indicated that there was room for improvement in the previous pumping operation, namely in terms of setting optimal pumping rates and ensuring adequate distancing (or locations) between pumping wells.

Therefore, this chapter aimed to improve the pumping operation and provide suggestions for other sites. The results of the improvement efforts highlighted the impact of the distance between pumping locations and the source location on the required pumping rates to achieve both the desired removal amounts and removal efficiency of pollutants.

5.2 Suggestion for illegal waste dumping site remediation

Considering the lack of detailed monitoring data and groundwater flow information at the real illegal waste dumping site, acquiring such data can be costly. Therefore, conducting a preliminary analysis becomes crucial in order to minimize expenses and make informed decisions regarding the necessary remediation actions. The specifics of this analysis are presented in Figure 5-1. The flow chart begins with preliminary data analysis, utilizing elevation data obtained from a GIS database to calculate groundwater levels roughly. These groundwater levels are then used to estimate potential groundwater flow patterns. Simultaneously, waste excavation is conducted to remove all waste from the dumping site.

Once the potential groundwater flow patterns are determined, they are used to identify sampling locations downstream of the site, where pollution and concentration levels can be assessed. If the concentration levels of pollution exceed the environmental standards and pose a significant risk to human health, the potential groundwater flow patterns are used to establish monitoring wells along the main groundwater flow, from downstream to upstream. These monitoring wells are crucial for implementing remediation measures.

Conversely, while the numerical analysis was performed under the condition the remediation measures were continued until the concentration reached endlessly zero because the case study in chapter 4 focused on the transport phenomena of 1,4-dioxane in the aquifer. If the pollution levels are below the environmental standards in a particular area, no remediation action is required for that specific section of the dumping site. in such cases, only waste excavation from the surface soil is necessary.
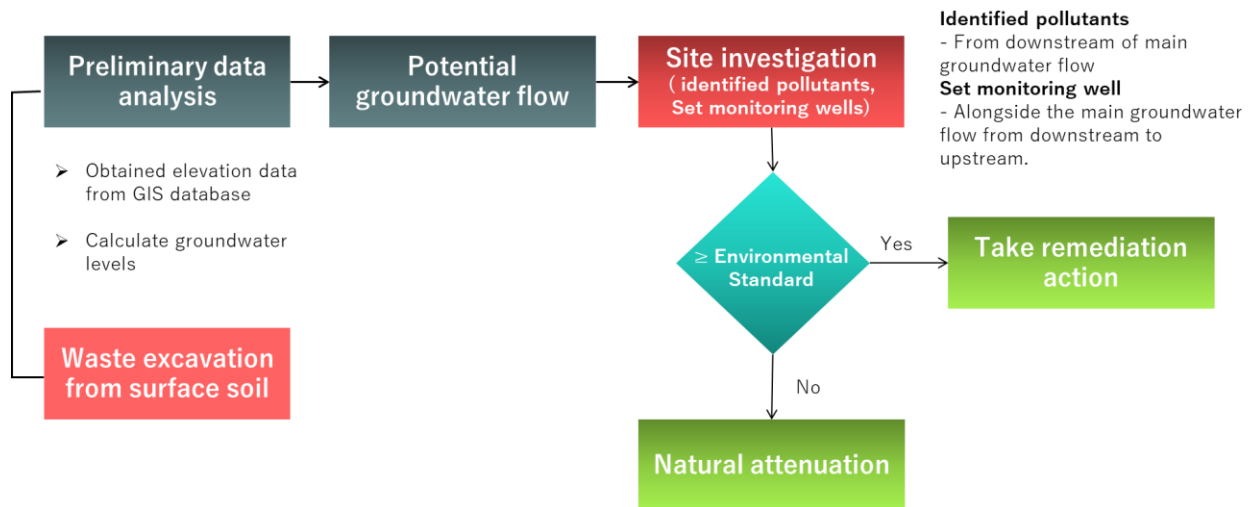
Figure 5-1 Decision making of remediation action by preliminary data analysis

If remediation action is required for the dumping site, the decision-making process for remediation action, as depicted in Figure 5-2. The initial step involves acquiring monitoring data from the designated monitoring well locations, which are planned to be positioned alongside the flow of groundwater from downstream to upstream. Subsequently, the groundwater flow field calculation needs to be utilized, taking into account the impacts of the remediation action, as well as the pollutant characteristics obtained through laboratory experiments and the monitoring data. These factors enable the reproduction of pollutant concentrations in each monitoring well, facilitating the prediction of potential pollutant transport.

The information regarding potential pollutant transport is then utilized to develop a remediation plan, considering various remediation techniques such as pump and treat, bioremediation, permeable reactive barriers, and more. Additionally, the efficiency and cost-effectiveness of the remediation plan are assessed by comparing it to the environmental standards and the acceptable costs. Through this comparison, a suitable remediation action for the dumping site is determined.

Once the remediation plan using the model is confirmed, the implementation of the remedy begins, and the results of the remediation efforts are continuously monitored in the subsequent steps. This ensures that the chosen remediation action remains effective, and any necessary adjustments can be made based on the monitoring data.
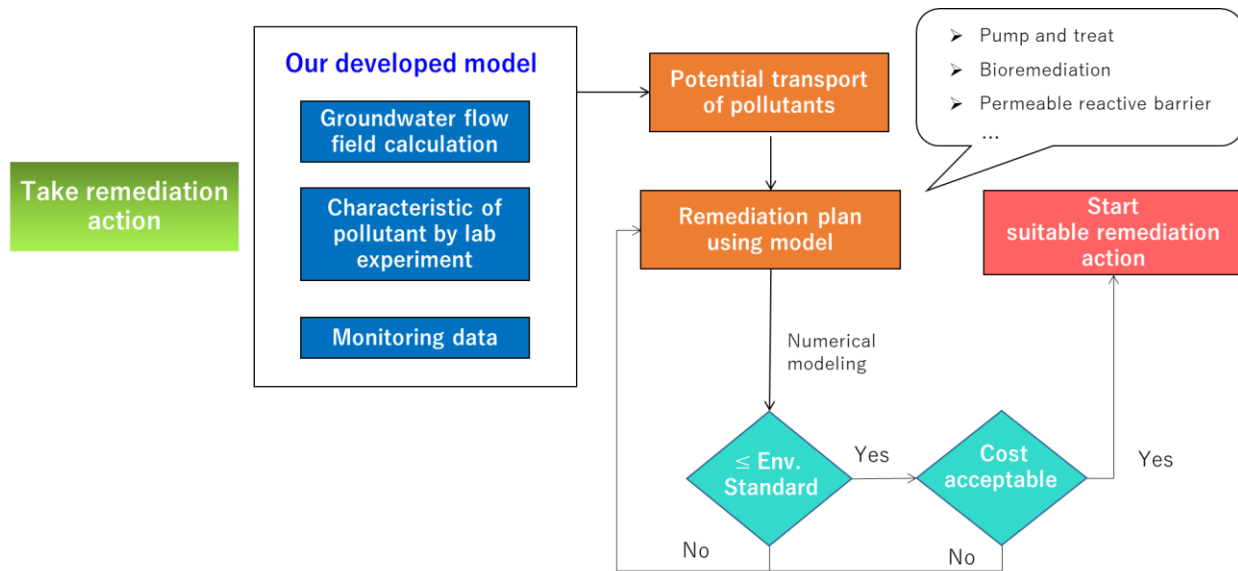
Figure 5-2 Flow chart of remediation plan using numerical modeling

5.3 Limitation of our model and Future research

In the current research, the reproduction of groundwater flow field still remains uncertain parameters of heterogeneous layer and unknown effects of unsaturated zone. Although, our research was successful established the developed numerical model to reproduce the groundwater flow field with time by considering the effects of remediation. But the homogeneous condition was selected into developed model because of the multiple and non-stationary pollution source conditions.

The next step in future research would be to consider the actual characteristics of pollution sources during waste deposit and effects of remediation (before monitoring data), and the actual characteristic of pollution sources should be reproduced and the amounts of pollutants approximately estimated. Consequently, estimated pollution sources could turn out to be important parameters in examining the characteristics of leakage pollutants in unsaturated and heterogeneous soil conditions. These two parameters might reveal unexpected effects that enable the understanding of the transport behavior of pollutants in unsaturated soils to aquifers. In addition, the relation between seasonal rainfall and water infiltration in different geological structures would be considered in future research to examine the influence of climate change in the transport behavior of pollutants in the subsurface environment. Moreover, it is imperative to identify suitable monitoring locations and minimize the number of monitoring wells and monitoring periods to enhance cost-efficiency during the remediation of the dumping site. This study will serve as a valuable research topic for future studies in the field of illegal waste dumping site remediation.

However, In the developing countries situation did not have the sufficient preliminary data (e.g., detailed elevation data, region geological conditions, groundwater levels data, etc.) and the non-remediation budget on the soil and groundwater pollutions. Thus, the new approach on remediation implementation using numerical modeling might help to reduce the site survey, investigation, and remediation of the illegal waste dumping site in the developing countries.

Reference

A., B., Hartmann, C., & Lesturgez, G. (2005). Physical properties of tropical sandy soils: A large range of behaviours. In Physical properties of tropical sandy soils: A large range of behaviours.

Akpan Usoh, G., Edwin Ahaneku, I., Taiwo Horsfall, I., Uwadiegwu Alaneme, G., & Hogan Itam, D. (2022). Numerical modeling and simulation of leachate transport in MSW contaminated soil: Impact on seasonal changes. Cleaner Materials, 4, 100089. https://doi.org/10.1016/j.clema.2022.100089

Allen, A. (2001). Containment landfills: The myth of sustainability. Engineering Geology, 60(1), 3–19. https://doi.org/10.1016/S0013-7952(00)00084-3

Atlabachew, A., Shu, L., Wu, P., Zhang, Y., & Xu, Y. (2018). Numerical modeling of solute transport in a sand tank physical model under varying hydraulic gradient and hydrological stresses. Hydrogeology Journal, 26(6), 2089–2113. https://doi.org/10.1007/s10040-018-1758-6

Banejad, H., Mohebzadeh, H., Ghobadi, M. H., & Heydari, M. (2014). Numerical simulation of groundwater flow and contamination transport in Nahavand plain aquifer, west of Iran. Journal of the Geological Society of India, 83(1), 83–92. https://doi.org/10.1007/s12594-014-0010-9

Bangani, L., Kabiti, H. M., Amoo, O., Nakin, M. D. V., & Magayiyana, Z. (2023). Impacts of illegal solid waste dumping on the water quality of the Mthatha River. Water Practice & Technology, 18(5), 1011–1021. https://doi.org/10.2166/wpt.2023.053

da Paz, D. H. F., Lafayette, K. P. V., Holanda, M. J. de O., Sobral, M. do C. M., & Costa, L. A. R. de C. (2020). Assessment of environmental impact risks arising from the illegal dumping of construction waste in Brazil. Environment, Development and Sustainability, 22(3), 2289–2304. https://doi.org/10.1007/s10668-018-0289-6

Di Fiore, V., Cavuoto, G., Punzo, M., Tarallo, D., Casazza, M., Guarriello, S. M., & Lega, M. (2017). Integrated hierarchical geo-environmental survey strategy applied to the detection and investigation of an illegal landfill: A case study in the Campania Region (Southern Italy). Forensic Science International, 279, 96–105. https://doi.org/10.1016/j.forsciint.2017.08.016

Đidelija, M., Kulo, N., Mulahusić, A., Tuno, N., & Topoljak, J. (2022). Segmentation scale parameter influence on the accuracy of detecting illegal landfills on satellite imagery. A case study for Novo Sarajevo. Ecological Informatics, 70, 101755. https://doi.org/10.1016/j.ecoinf.2022.101755

Ferronato, N., & Torretta, V. (2019). Waste Mismanagement in Developing Countries: A Review of Global Issues. International Journal of Environmental Research and Public Health, 16(6), 1060. https://doi.org/10.3390/ijerph16061060

Ferronato, N., Torretta, V., Ragazzi, M., Rada, E. (2017). Waste mismanagement in developing countries: A case study of environmental contamination. UPB Scientific Bulletin, Series D: Mechanical Engineering. 79. 185-196. Freeze, R.A., & Cherry, J.A. (1979). Groundwater. Prentice Hall.

Hem, R., Furuichi, T., Ishii, K., & Weng, Y.-C. (2013). A New Approach for Prediction of 1,4-Dioxane Distribution in Groundwater at an Illegal Dumping Site in Japan. Journal of Japan Society of Civil Engineers, Ser. G (Environmental Research), 69(6), II_247-II_258. https://doi.org/10.2208/jscejer.69.II_247

Houben, G., Schotting, R., & Van Houten, G. (2016). Real-time control of pump and treat systems: case study. In Proceedings of the 13th International Conference on Environmental Science and Technology.

Huang, G., Hou, Q., Han, D., Liu, R., & Song, J. (2023). Large scale occurrence of aluminium-rich shallow groundwater in the Pearl River Delta after the rapid urbanization: Co-effects of anthropogenic and geogenic factors. Journal of Contaminant Hydrology, 254, 104130. https://doi.org/10.1016/j.jconhyd.2022.104130

Huang, G., Song, J., Han, D., Liu, R., Liu, C., & Hou, Q. (2023). Assessing natural background levels of geogenic contaminants in groundwater of an urbanized delta through removal of groundwaters impacted by anthropogenic inputs: New insights into driving factors. Science of The Total Environment, 857, 159527. https://doi.org/10.1016/j.scitotenv.2022.159527

Huang, J., & Hartemink, A. E. (2020). Soil and environmental issues in sandy soils. Earth-Science Reviews, 208, 103295. https://doi.org/10.1016/j.earscirev.2020.103295

Iguro, C., Furuichi, T., Ishii, K., & Kim, S. (2012). Prediction of 1,4-Dioxane Dispersion Based on Change in Groundwater Flow After Remedial Measures by Three-Dimensional Numerical Simulation— Toward a Permanent Measure for Aomori-Iwate Illegal Dumping Site -. Journal of Japan Society of Civil Engineers, Ser. G (Environmental Research), 68(6), II_265-II_272. https://doi.org/10.2208/jscejer.68.II_265

Inoue, D., Tsunoda, T., Sawada, K., Yamamoto, N., Saito, Y., Sei, K., & Ike, M. (2016). 1,4-Dioxane degradation potential of members of the genera Pseudonocardia and Rhodococcus. Biodegradation, 27(4–6), 277–286. https://doi.org/10.1007/s10532-016-9772-7

Jakiel M., Bernatek-Jakiel, A., Gajda, A., Filiks, M., Marta, P. (2019). Spatial and temporal distribution of illegal dumping sites in the nature protected area: the Ojców National Park, Poland. Journal of Environmental Planning and Management. 62. 286-305. 10.1080/09640568.2017.1412941.

Karimi, N., Ng, K. T. W., & Richter, A. (2022). Development and application of an analytical framework for mapping probable illegal dumping sites using nighttime light imagery and various remote sensing indices. Waste Management, 143, 195–205. https://doi.org/10.1016/j.wasman.2022.02.031

Kondo, M., Sakamoto, Y., Kawabe, Y., Nakamura, K., Watanabe, N., & Komai, T. (2022). Development of a Model for Predicting the Volatilization Flux from Unsaturated Soil Contaminated by Volatile Chemical Substances. Environmental Modeling & Assessment, 27(2), 251–273. https://doi.org/10.1007/s10666-021-09796-0

Langevin, C.D., Thorne, D.T., Dausman, A.M., Sukop, M.C., & Guo, W. (2008). SEAWAT Version 4: A Computer Program for Simulation of Multi-Species Solute and Heat Transport. U.S. Geological Survey Techniques and Methods 6-D1.

Lerner, D.N., & Trudell, M.R. (1990). Contaminant plume containment using permeable barriers. In Groundwater Contamination and Analysis at Hazardous Waste Sites (pp. 274-294). Marcel Dekker.

Nakamura, K.; Ito, H.; Kawabe Y.; Komai T. Study on Partitioning and Distribution in soil-water phases for 1,4-Dioxane in Geo-Environment. JSCE Transactions G (Environment), 2018, Volume 74, Issue 2, p. 59-66, open access date 2018/05/20, online ISSN 2185-6648, https://doi.org/10.2208/jscejer.74.59,

Navarro, J., Grémillet, D., Afán, I., Ramirez, F., Bouten, W., & Forero, M. (2016). Feathered Detectives: Real-Time GPS Tracking of Scavenging Gulls Pinpoints Illegal Waste Dumping. PLoS ONE, 11, e0159974. https://doi.org/10.1371/journal.pone.0159974

Niyobuhungiro, R. V., & Schenck, C. J. (2021). The dynamics of indiscriminate/ illegal dumping of waste in Fisantekraal, Cape Town, South Africa. Journal of Environmental Management, 293, 112954. https://doi.org/10.1016/j.jenvman.2021.112954

O'Connor, D., Müller-Grabherr, D., & Hou, D. (2019). Strengthening social-environmental management at contaminated sites to bolster Green and Sustainable Remediation via a survey. Chemosphere, 225, 295–303. https://doi.org/10.1016/j.chemosphere.2019.03.035

Otto, M., & Nagaraja, S. (2007). Treatment technologies for 1,4-Dioxane: Fundamentals and field applications. Remediation Journal, 17(3), 81–88. https://doi.org/10.1002/rem.20135

Otwong, A., Jongmeewasin, S., & Phenrat, T. (2021). Legal obstacles for the circular economy in Thailand: Illegal dumping of recyclable hazardous industrial waste. Journal of Cleaner Production, 302, 126969. https://doi.org/10.1016/j.jclepro.2021.126969

Pongritsakda, T., Nakamura, K., Wang, J., Watanabe, N., & Komai, T. (2021). Prediction and Remediation of Groundwater Pollution in a Dynamic and Complex Hydrologic Environment of an Illegal Waste Dumping Site. Applied Sciences, 11(19), 19. https://doi.org/10.3390/app11199229

Pongritsakda, T., Sakamoto, Y., Wang, J., Kawabe, Y., Sirivithayapakorn, S., Komai, T., Watanabe, N., Prediction of 1,4- Dioxane migration in groundwater and evaluation of remediation measures in an illegal dumping site using a 2D-numerical model. Sustainability, 15, 3930.

Pugazhendi, A., Rajesh Banu, J., Dhavamani, J., & Yeom, I. T. (2015). Biodegradation of 1,4-dioxane by Rhodanobacter AYS5 and the role of additional substrates. Annals of Microbiology, 65(4), Article 4. https://doi.org/10.1007/s13213-015-1060-y

Ritter, K. S., Paul Sibley, Ken Hall, Patricia Keen, Gevan Mattu, Beth Linton, Len. (2002). Sources, Pathways, and Relative Risks of Contaminants in Surface Water and Groundwater: A Perspective Prepared for the Walkerton Inquiry. Journal of Toxicology and Environmental Health, Part A, 65(1), 1–142. https://doi.org/10.1080/152873902753338572

Saadatpour M., Goeini M., Afshar A., Shahmirnoori A., (2023) A preliminary approach based on numerical simulation modelling and evaluation of permeable reactive barrier for aquifer remediation susceptible to selenium contaminant, Journal of Environmental Management, Volume 331, 117242, ISSN 0301-4797, https://doi.org/10.1016/j.jenvman.2023.117242.

Sales, C., Grostern, A., Parales, J., Parales, R., & Alvarez-Cohen, L. (2013). Oxidation of the Cyclic Ethers 1,4-Dioxane and Tetrahydrofuran by a Monooxygenase in Two Pseudonocardia Species. Applied and Environmental Microbiology, 79. https://doi.org/10.1128/AEM.02418-13

Seror, N., & Portnov, B. A. (2020). Estimating the effectiveness of different environmental law enforcement policies on illegal C&D waste dumping in Israel. Waste Management, 102, 241–248. https://doi.org/10.1016/j.wasman.2019.10.043

Shao S., Yang X., Jia C., (2022) Combining multi-source data to evaluate the leakage pollution and remediation effects of landfill, Journal of Hydrology, Volume 610, 127889, ISSN 0022-1694, https://doi.org/10.1016/j.jhydrol.2022.127889.

Shen, H., Huang, Y., Su, Y., (2023) Experimental investigation of light non-aqueous phase liquid mobilization in filled fractured network media. Environ Sci Pollut Res 30, 32628–32640. https://doi.org/10.1007/s11356-022-24511-6

Smith, L. M., & Collins, B. (2021). Sustainable remediation column–Experts' perspectives on the past and future of the practice. Remediation Journal, 31(4), 123–125. https://doi.org/10.1002/rem.21700

Takai S., Shimada T., Takeda S., Koike K., (2022) Evaluating the effectiveness of a geostatistical approach with groundwater flow modeling for three-dimensional estimation of a contaminant plume, Journal of Contaminant Hydrology, Volume 251, 104097, ISSN 0169-7722, https://doi.org/10.1016/j.jconhyd.2022.104097.

U.S. EPA. Engineering Issue Paper: In-Situ Chemical Oxidation. 2006. Available online: https://clu-in.org/download/contaminantfocus/pcb/ISCO-600R06072.pdf. (accessed 10 June 2023).

U.S. EPA. Remedial Technology Fact Sheet-Activated Carbon-Based Technology for In-Situ Remediation. 2018. Available online: https://semspub.epa.gov/work/HQ/100001159.pdf. (accessed 10 June 2023)

U.S. EPA. Technical Fact Sheet-1,4-Dioxane. 2017. https://www.epa.gov/sites/default/files/2014-03/documents/ffrro_factsheet_contaminant_14-dioxane_january2014_final.pdfVelis, C. A., & Cook, E. (2021). Mismanagement of Plastic Waste through Open Burning with Emphasis on the Global South: A Systematic Review of Risks to Occupational and Public Health. Environmental Science & Technology, 55(11), 7186–7207. https://doi.org/10.1021/acs.est.0c08536. (accessed 10 June 2023)

Vitali, M., Castellani, F., Fragassi, G., Mascitelli, A., Martellucci, C., Diletti, G., Scamosci, E., Astolfi, M. L., Fabiani, L., Mastrantonio, R., Protano, C., Spica, V. R., & Manzoli, L. (2021). Environmental status of an Italian site highly polluted by illegal dumping of industrial wastes: The situation 15 years after the judicial intervention. Science of The Total Environment, 762, 144100. https://doi.org/10.1016/j.scitotenv.2020.144100

Vrijheid, M. (2000). Health effects of residence near hazardous waste landfill sites: A review of epidemiologic literature. Environmental Health Perspectives, 108(suppl 1), 101–112. https://doi.org/10.1289/ehp.00108s1101

Xing, Z., Qu, R., Zhao, Y., Fu, Q., Ji, Y., & Lu, W. (2019). Identifying the release history of a groundwater contaminant source based on an ensemble surrogate model. Journal of Hydrology, 572, 501–516. https://doi.org/10.1016/j.jhydrol.2019.03.020
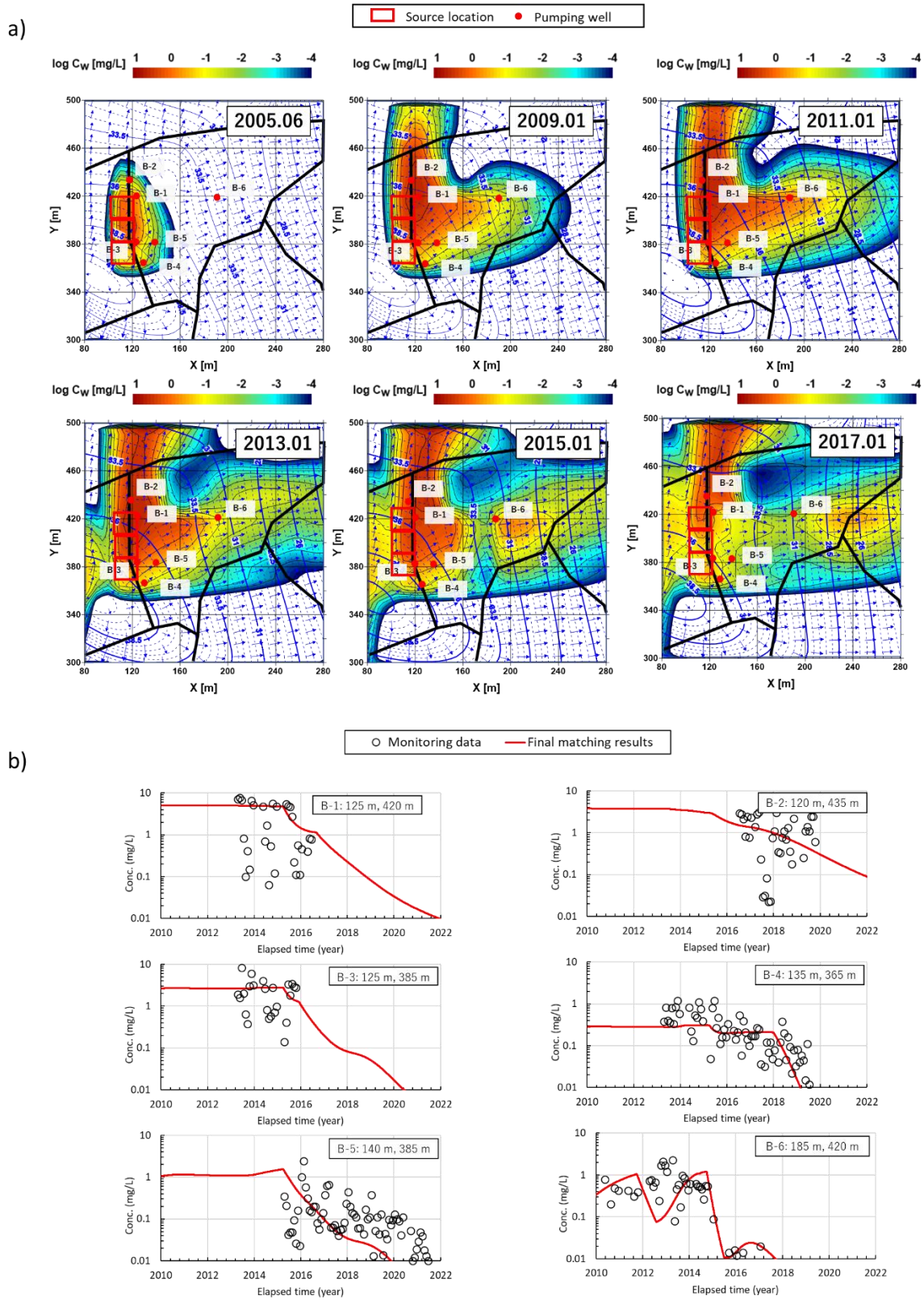
Xu, T., Gómez-Hernández, J. J., Chen, Z., & Lu, C. (2021). A comparison between ES-MDA and restart EnKF for the purpose of the simultaneous identification of a contaminant source and hydraulic conductivity. Journal of Hydrology, 595, 125681. https://doi.org/10.1016/j.jhydrol.2020.125681

Appendix

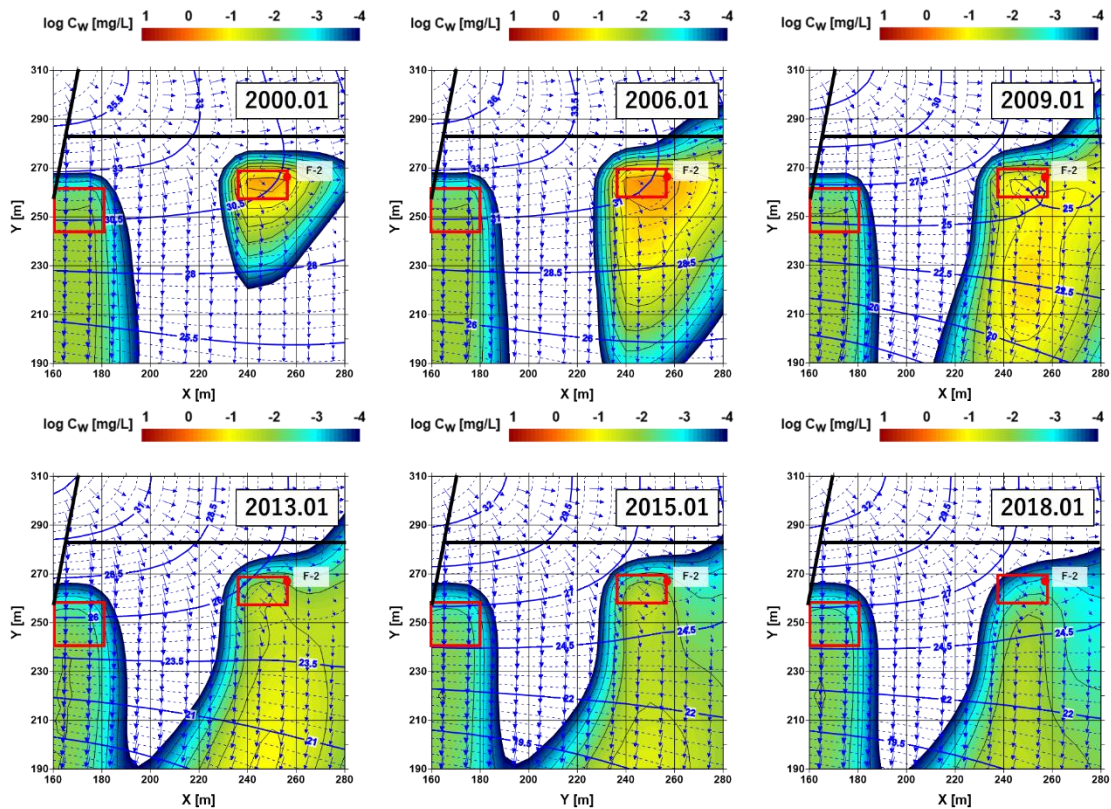**Table A1. List of inflow conditions for dioxane following the matching process.**

Area	Name of contamination source	Range in x-direction [m]	Range in y-direction [m]	Area of contamination source [m²]	The amount of 1,4-dioxane inflow [kg]	Inflow start time	Inflow end time	Inflow period [years]	Inflow rate [kg/month/m²]
A	CSA-1	25-40	325-340	225	4.00 (335-340 m in y-direction)	Jan. 2013	Dec. 2014	2.00	2.22×10^{-3}
					2.00 (325-335 m in y-direction)				5.56×10^{-4}
					2.50	Jan. 2015	Dec. 2016	2.00	4.63×10^{-4}
					0.66	Jan. 2017	Dec. 2020	4.00	6.11×10^{-5}
	CSA-2	20-30	360-370	100	1.50	Jul. 2013	Jun. 2016	3.00	4.17×10^{-4}
					0.30	Jul. 2016	Dec. 2022	6.50	3.85×10^{-5}
	CSA-3	65-85	355-375	400	4.00	Jan. 2012	Dec. 2015	4.00	2.08×10^{-4}
					2.00	Jan. 2016	Apr. 2020	4.33	9.62×10^{-5}
	CSA-4	55-65	305-315	100	0.25	Nov. 2012	Dec. 2012	0.05	4.17×10^{-3}
B	CSB-1	105-125	360-380	400	10.0	Jan. 2005	Dec. 2017	13.0	1.60×10^{-4}
	CSB-2	105-125	380-400	400	40.0	Jan. 2005	Nov. 2015	10.9	7.63×10^{-4}
	CSB-3	105-125	400-420	400	30.0	Jan. 2005	Aug. 2016	11.7	5.36×10^{-4}
D	CSD-1	75-85	225-235	100	10.0	Jan. 2010	Dec. 2010	1.00	8.33×10^{-3}
	CSD-2	75-85	255-265	100	2.50	Mar. 2013	Feb. 2014	1.00	2.08×10^{-3}
	CSD-3	85-105	245-265	400	5.00	Jan. 1999	Dec. 2012	14.0	7.44×10^{-5}
					2.00	Jan. 2013	Dec. 2018	6.00	6.94×10^{-5}
	CSD-4	85-105	265-285	400	5.00	Jan. 1999	Dec. 2012	14.0	7.44×10^{-5}
					2.00	Jan. 2013	Dec. 2018	6.00	6.94×10^{-5}
E	CSE-1	100-110	205-215	100	0.20	Jan. 2013	Mar. 2013	0.20	8.33×10^{-4}
F	CSF-1	235-255	260-270	200	2.00	Jan. 2010	Dec. 2012	3.00	2.78×10^{-4}
					1.30	Jan. 2013	Jun. 2018	6.50	8.33×10^{-5}

	CSF-2	150-180	245-265	600	1.00	Jan. 1999	Dec. 2022	24.0	5.79×10^{-6}
G	CSG-1	315-365	230-255	1250	5.00	Jan. 1999	Dec. 2012	14.0	2.38×10^{-5}
	CSG-2	315-365	255-280	1250	15.0	Jan. 1999	Dec. 2012	14.0	7.14×10^{-5}
H	CSH-1	295-315	365-385	400	0.70	Jan. 2012	Dec. 2015	4.00	3.65×10^{-5}
					0.20	Jan. 2016	Dec. 2020	5.00	8.33×10^{-6}
	CSH-2	315-335	345-365	400	4.30	Jan. 1999	Dec. 2013	15.0	5.97×10^{-5}
	CSJ-1	415-435	135-155	400	0.50 (140-150 m in y-direction)	Jan. 2012	Feb. 2012	0.10	2.08×10^{-3}
					0.10	Mar. 2012	Dec. 2015	3.90	2.08×10^{-4}
	CSJ-2	420-440	185-205	400	2.80	Jul. 2010	Dec. 2012	2.50	2.33×10^{-4}
					1.00	Jan. 2013	Dec. 2014	2.00	8.33×10^{-5}
					0.10	Jan. 2015	Dec. 2022	8.00	1.04×10^{-5}
J	CSJ-3	385-415	135-155	600	1.00	Jan. 2014	Dec. 2014	1.00	1.39×10^{-4}
	CSJ-4	365-385	135-155	400	1.50	Jan. 2001	Dec. 2012	12.0	2.60×10^{-5}
	CSJ-5	375-395	165-185	400	0.05 (385-395 m in x-direction) (165-175 m in y-direction)	Jul. 2013	Aug. 2013	0.10	4.17×10^{-4}
					0.01	Aug. 2013	Dec. 2015	2.40	8.68×10^{-7}
	CSJ-6	395-415	195-205	400	1.50	Jan. 1999	Dec. 2020	22.0	1.42×10^{-5}
K	CSK-1	125-135	140-150	100	0.70	Jan. 2013	Mar. 2013	0.20	2.92×10^{-3}
N	CSN-1	180-230	65-95	1500	10.0	Jan. 1994	May. 2009	15.4	3.60×10^{-5}
	CSN-2	230-250	65-95	600	3.00	Jan. 1994	May. 2009	15.4	2.70×10^{-5}
O	CSO-1	355-415	25-55	1800	1.50	Jan. 1999	Dec. 2010	12.0	5.79×10^{-6}

Figure A1 a) simulation of 1,4-dioxaone contaminants in B-area b) the final matching results with historical monitoring data in B-area

Figure A2 a) simulation of 1,4-dioxaone contaminants in D-area b) the final matching results with historical monitoring data in D-area
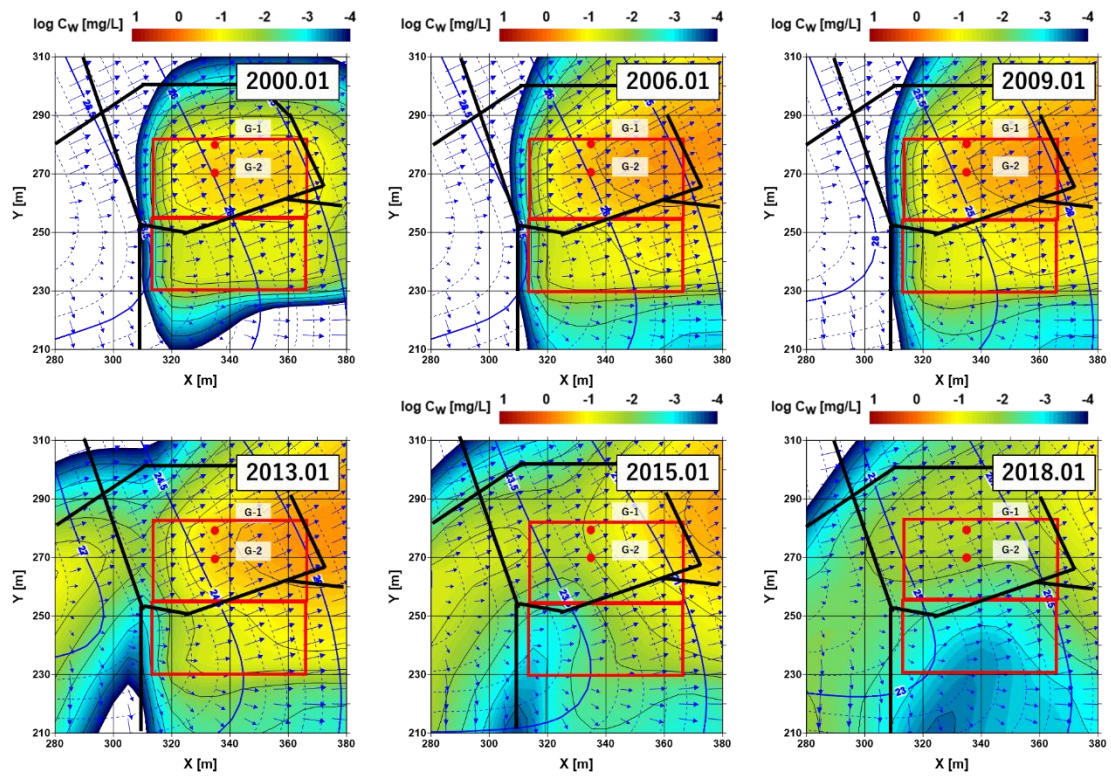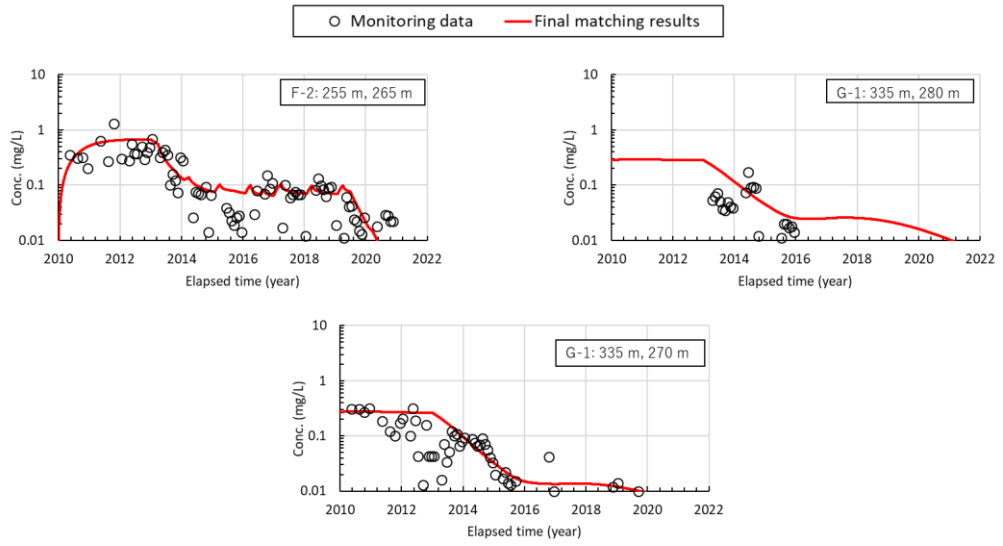
c)

Figure A3 a) simulation of 1,4-dioxaone contaminants in F-area b) simulation results of 1,4-dioxane contaminant in G-area c) the final matching results with historical monitoring data in D-area
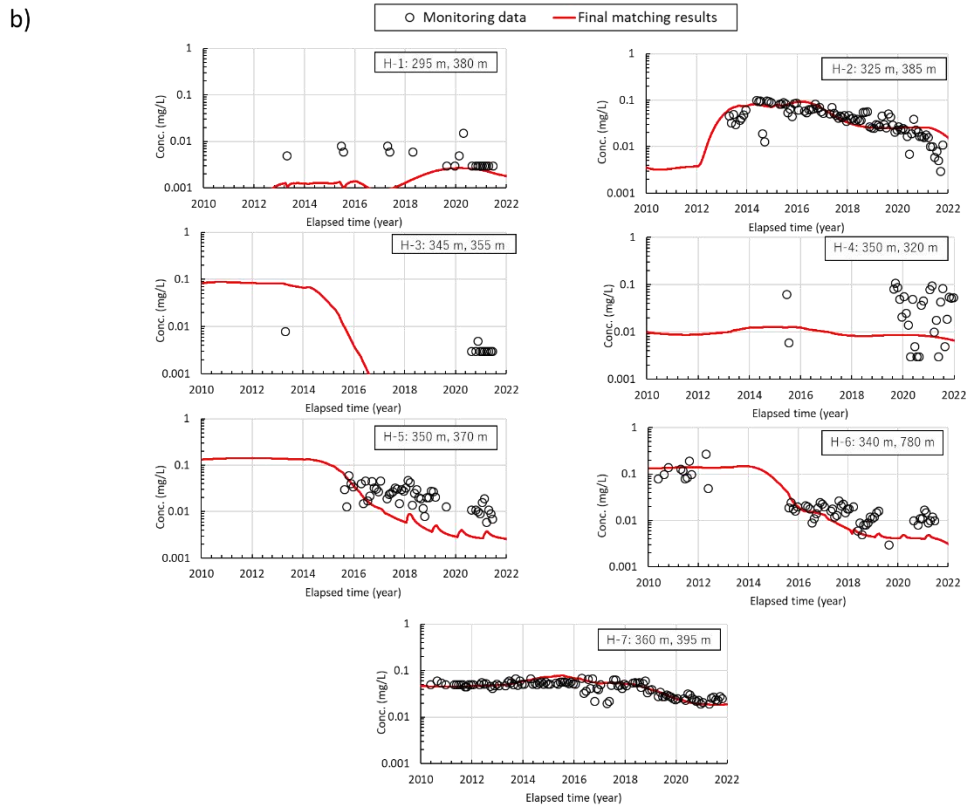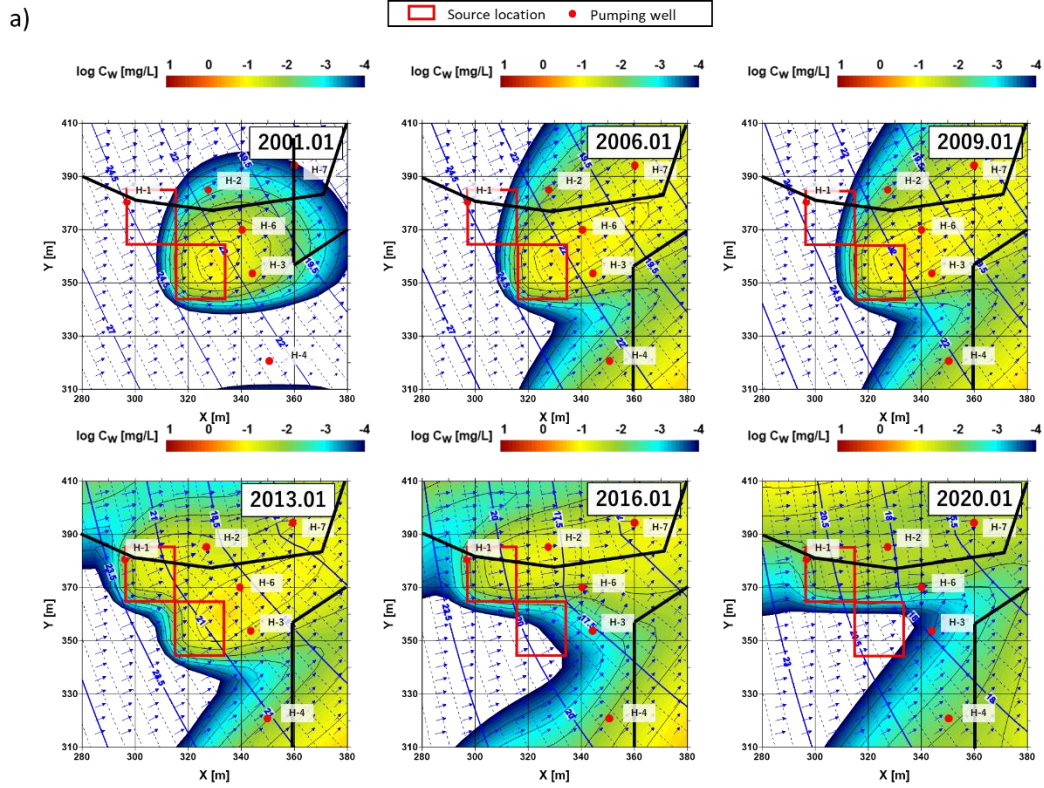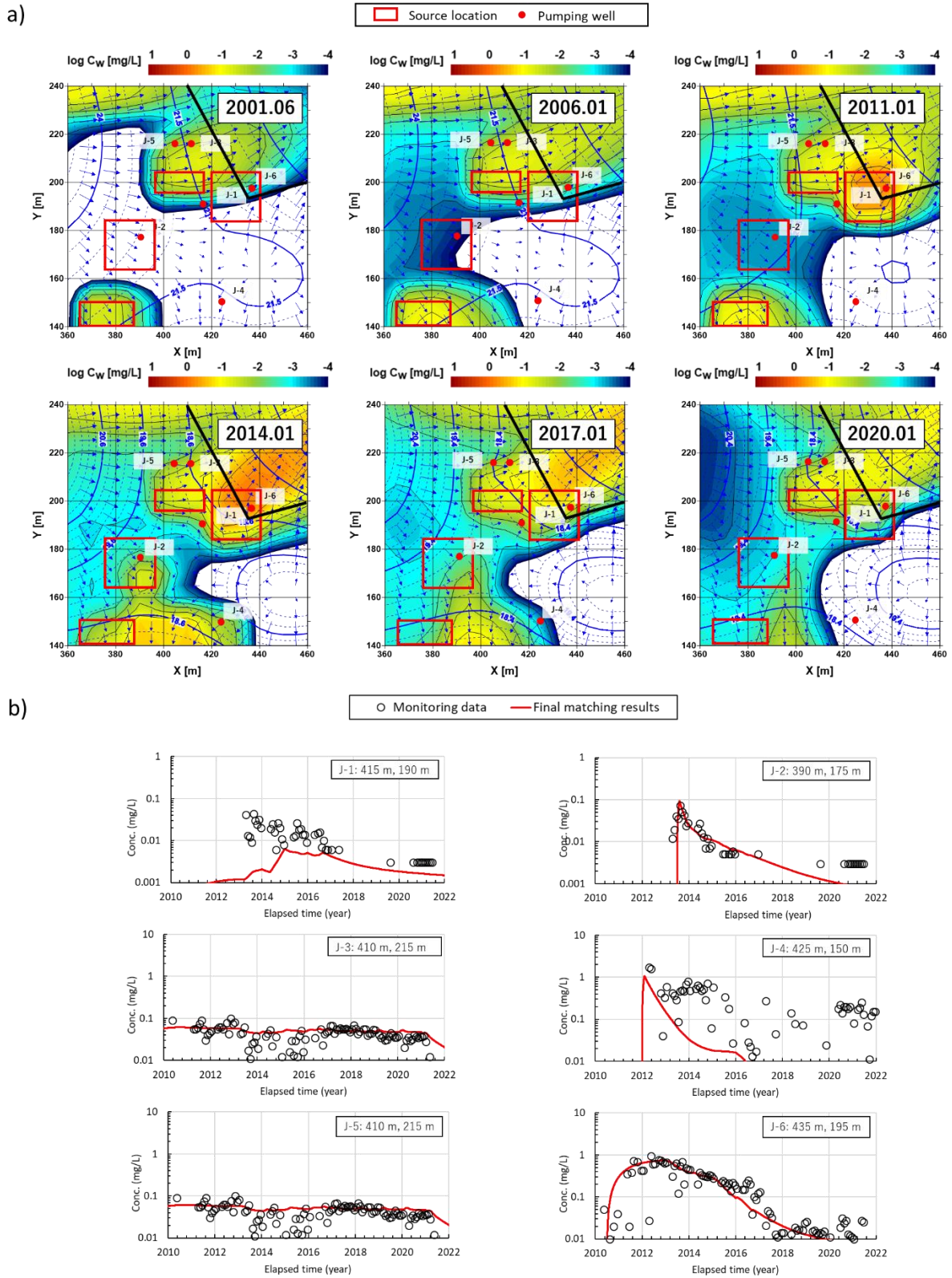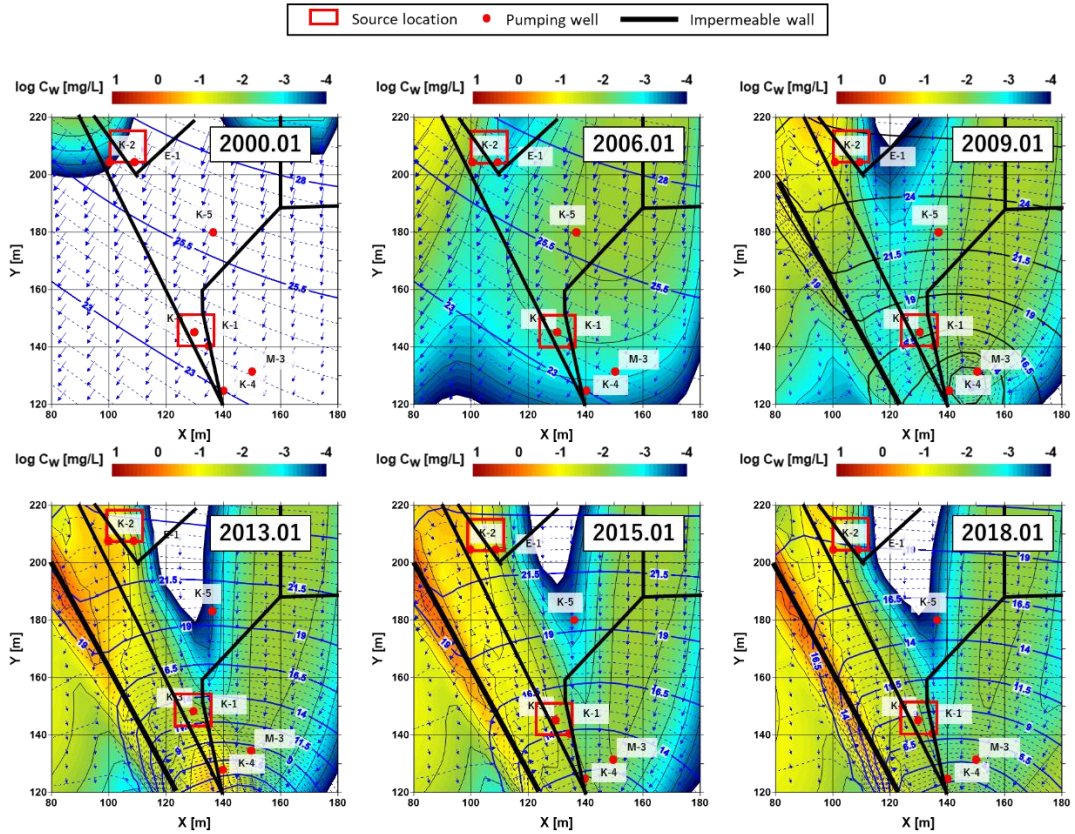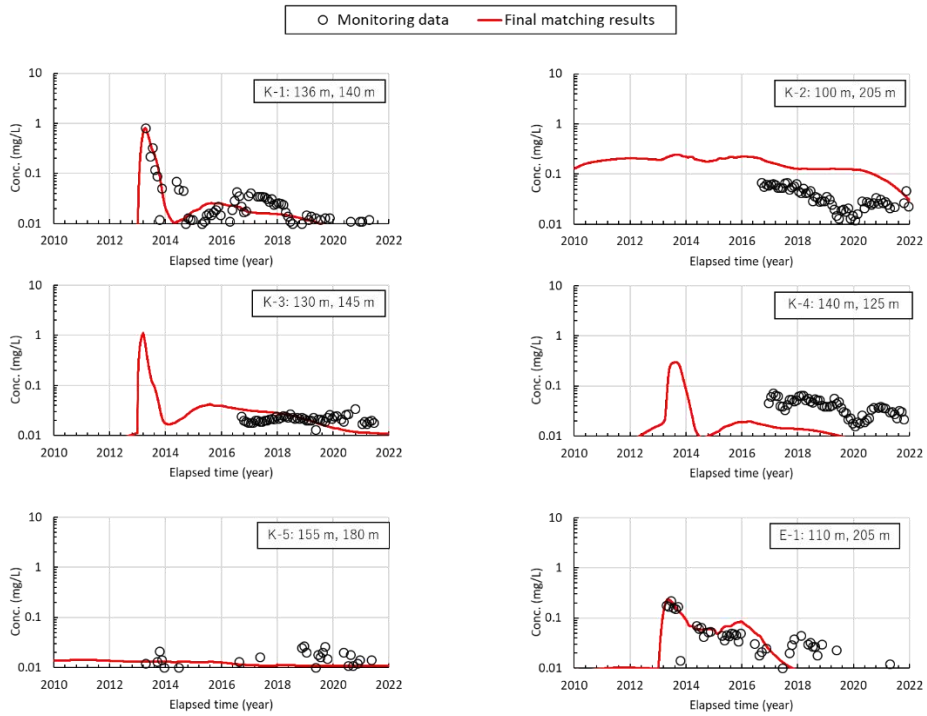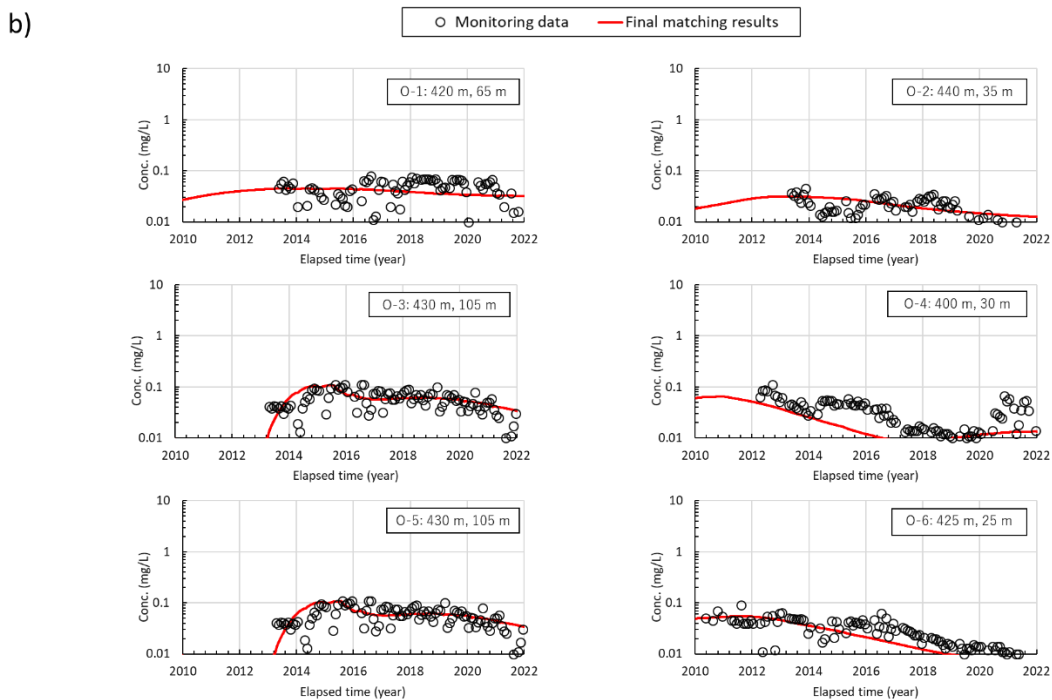
Figure A4 a) simulation of 1,4-dioxaone contaminants in H-area b) the final matching results with historical monitoring data in H-area

Figure A5 a) simulation of 1,4-dioxaone contaminants in J-area b) the final matching results with historical monitoring data in J-area

Figure A6 a) simulation of 1,4-dioxaone contaminants in E,K-area b) the final matching results with historical monitoring data in E,K-area
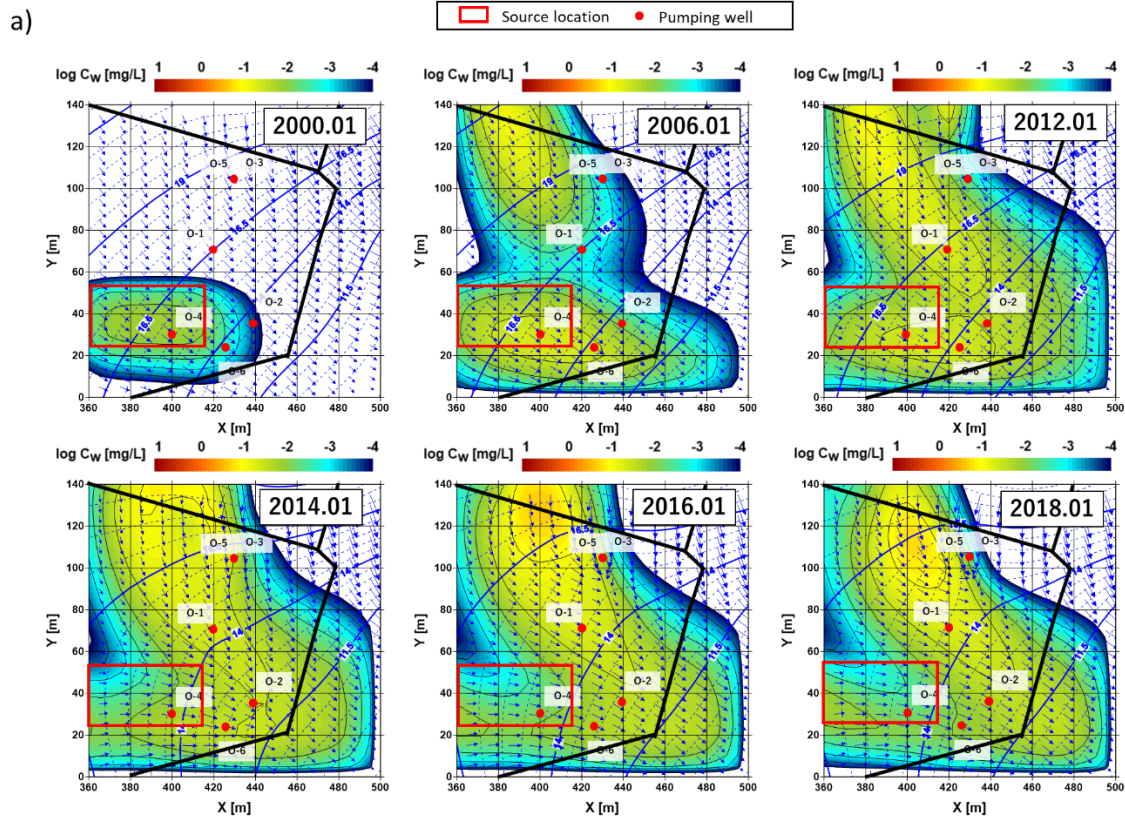
Figure A7 a) simulation of 1,4-dioxaone contaminants in O-area b) the final matching results with historical monitoring data in O-area
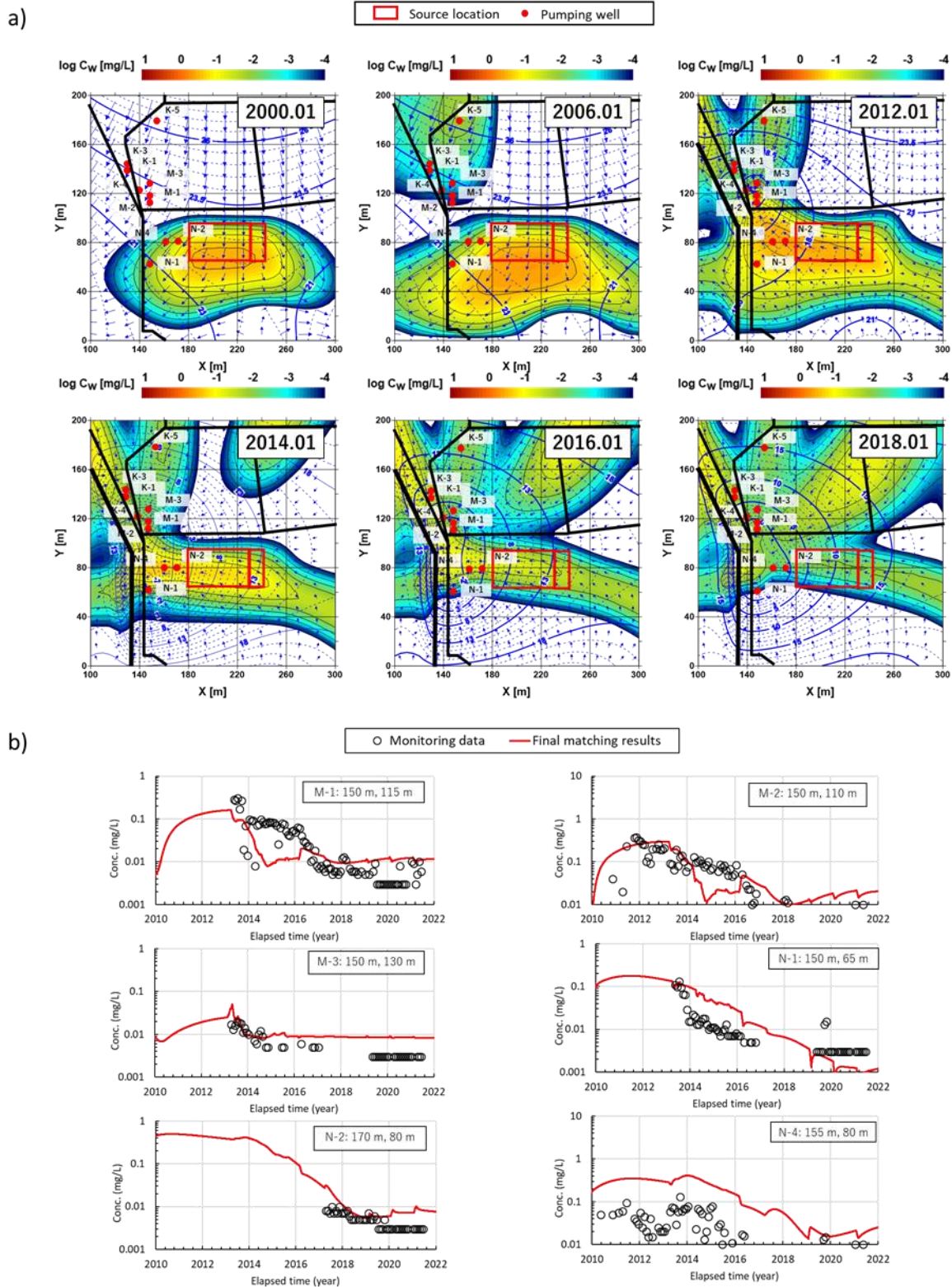
Figure A8 a) simulation of 1,4-dioxaone contaminants in M,N-area b) the final matching results with historical monitoring data in M,N-area

Achievement list

Journal papers

Pongritsakda, T., Nakamura, K., Wang, J., Watanabe, N., Takeshi, K., Prediction and Remediation of Groundwater Pollution in a Dynamic and Complex Hydrologic Environment of an Illegal Waste Dumping Site. *Applied Sciences*, 11(19), 9229.

Pongritsakda, T., Sakamoto, Y., Wang, J., Kawabe, Y., Sirivithayapakorn, S., Komai, T., Watanabe, N., Prediction of 1,4- Dioxane migration in groundwater and evaluation of remediation measures in an illegal dumping site using a 2D-numerical model. *Sustainability*, 15, 3930.

Conference proceeding

Pongritsakda, T., Nakamura, K., Wang, J., Langa, C., Shiratori T., Watanabe, N., Sirivithayaphakorn, S., and Komai T., Applying the 2D and 3D numerical simulation results of the 1,4-dioxane plume distribution to design the groundwater remediation active treatment". Geo-environment and geo-technics, 32, 103-108 (2021).

Conference presentation

Pongritsakda, T., Sirivithayapakorn, S., Shiratori, T., and Komai, T., Analysis of potential sources with heavy metals in a landfill site using preliminary data, A case study in Thailand. EGU 21 conference (April 2021)

Pongritsakda, T.,Nakamura, K.,Wang, J., Langa, C., Shiratori, T., Watanabe, N., and Komai, T., Applying the 2D and 3D numerical simulation results of the 1,4-dioxane plume distribution to design the groundwater   remediation active treatment., 31st Social Geology Symposium (November 2021)

Pongritsakda, T., Sirivithayapakorn, S., Nakamura, K., Sakamoto, Y., Watanabe, N., and Komai, T., "Pump and Treat method for 1,4-Dioxane groundwater contamination under complex hydrogeological conditions at an illegal waste dumping site" Internatioal Clean Up Conference, Adelaide 2022 (September, 2022)

Acknowledgements

I would like to express my sincere gratitude and appreciation to all those who have contributed to the successful completion of this project. Without their support, dedication, and expertise, this accomplishment would not have been possible.

First and foremost, I extend my heartfelt thanks to my supervisor, Prof. Noriaki Watanabe for his guidance, patience, and encouragement throughout the entire process. Their invaluable insights and constructive feedback have greatly shaped the outcome of this work.

I would also like to acknowledge the contributions of my colleagues and fellow team members who collaborated closely with me. Their commitment, hard work, and willingness to go the extra mile have been instrumental in achieving our shared goals.

Furthermore, I am deeply indebted to the participants who generously gave their time and insights, enabling us to gather the necessary data for this study. Their involvement and cooperation have significantly enriched the quality of our findings.

I am grateful to Jiajie Wang and Takeshi Komai for their assistance in proofreading and editing the final manuscript, ensuring its clarity and coherence. Their meticulous attention to detail and constructive suggestions have elevated the overall quality of this work. In addition, I would appreciate the kind support from Yasuhide Sakamoto to help me on the model development and all suggestion and comments on my doctoral thesis.

Lastly, I want to express my profound appreciation to my family and friends for their unwavering support, understanding, and encouragement throughout this journey. Their love and belief in my abilities have been a constant source of inspiration, motivating me to overcome challenges and strive for excellence.

In conclusion, I am humbled by the collective effort and support of all those mentioned above. Their contributions have been invaluable in shaping this project and making it a success. I am truly grateful for their involvement and would like to extend my deepest thanks to each and every one of them.